Directed chemical communication in artificial eukaryotic cells

---

Dissertation

zur Erlangung des akademischen Grades
doctor rerum naturalium
(Dr. rer. nat.)
in der Wissenschaftsdisziplin Physikalischen Chemie
von
Sunidhi C Shetty

eingereicht an der
Mathematisch-Naturwissenschaftlichen Fakultät
Institut für Chemie
der Universität Potsdam
und
der Max-Planck-Institut für Kolloid- und Grenzflächenforschung

Datum der Disputation: 23. August 2021

Hauptbetreuer: J. Prof. Dr. Salvatore Chiantia
Betreuer: Dr. Tom Robinson
Gutachter: Dr. Jean-Christophe Baret

Published online on the
Publication Server of the University of Potsdam:
https://doi.org/10.25932/publishup-53364
https://nbn-resolving.org/urn:nbn:de:kobv:517-opus4-533642

Abstract

Eukaryotic cells can be regarded as complex microreactors capable of performing various biochemical reactions in parallel which are necessary to sustain life. An essential prerequisite for these complex metabolic reactions to occur is the evolution of lipid membrane-bound organelles enabling compartmentalization of reactions and biomolecules. This allows for a spatiotemporal control over the metabolic reactions within the cellular system. Intracellular organization arising due to compartmentalization is a key feature of all living cells and has inspired synthetic biologists to engineer such systems with bottom-up approaches.

Artificial cells provide an ideal platform to isolate and study specific reactions without the interference from the complex network of biomolecules present in biological cells. To mimic the hierarchical architecture of eukaryotic cells, multi-compartment assemblies with nested liposomal structures also referred to as multi-vesicular vesicles (MVVs) have been widely adopted. Most of the previously reported multi-compartment systems adopt bulk methodologies which suffer from low yield and poor control over size. Microfluidic strategies help circumvent these issues and facilitate a high-throughput and robust technique to assemble MVVs of uniform size distribution.

In this thesis, firstly, the bulk methodologies are explored to build MVVs and implement a synthetic signalling cascade. Next, a polydimethylsiloxane (PDMS)-based microfluidic platform is introduced to build MVVs and the significance of PEGylated lipids for the successful encapsulation of inner compartments to generate stable multi-compartment systems is highlighted.

Next, a novel two-inlet channel PDMS-based microfluidic device to create MVVs encompassing a three-step enzymatic reaction cascade is presented. A directed reaction pathway comprising of the enzymes α-glucosidase (α-Glc), glucose oxidase (GOx), and horseradish peroxidase (HRP) spanning across three compartments via reconstitution of size-selective membrane proteins is described. Furthermore, owing to the monodispersity of our MVVs due to microfluidic strategies, this platform is employed to study the effect of compartmentalization on reaction kinetics.

Further integration of cell-free expression module into the MVVs would allow for gene-mediated signal transduction within artificial eukaryotic cells. Therefore, the chemically inducible cell-free expression of a membrane protein alpha-hemolysin and its further reconstitution into liposomes is carried out.

In conclusion, the present thesis aims to build artificial eukaryotic cells to achieve size-selective chemical communication that also show potential for applications as micro reactors and as vehicles for drug delivery.

Zusammenfassung

Eukaryontische Zellen können als komplexe Mikroreaktoren betrachtet werden, die in der Lage sind, verschiedene biochemische Reaktionen parallel durchzuführen, die für die Aufrechterhaltung des Lebens notwendig sind. Eine wesentliche Voraussetzung für die Durchführung dieser komplexen Stoffwechselreaktionen ist die Entwicklung von Organellen mit Lipidmembranen, die eine Kompartimentierung von Reaktionen und Biomolekülen ermöglichen. Dies ermöglicht eine räumlich-zeitliche Kontrolle über die Stoffwechselreaktionen innerhalb des zellulären Systems. Die durch die Kompartimentierung entstehende intrazelluläre Organisation ist ein Schlüsselmerkmal aller lebenden Zellen und hat synthetische Biologen dazu inspiriert, solche Systeme mit Bottom-up-Ansätzen zu entwickeln.

Künstliche Zellen bieten eine ideale Plattform, um spezifische Reaktionen zu isolieren und zu untersuchen, ohne dass das komplexe Netzwerk von Biomolekülen, das in biologischen Zellen vorhanden ist, stört. Um die hierarchische Architektur eukaryontischer Zellen zu imitieren, haben sich Multikompartiment-Anordnungen mit verschachtelten liposomalen Strukturen, die auch als multivesikuläre Vesikel (MVV) bezeichnet werden, durchgesetzt. Die meisten der bisher vorgestellten Multikompartiment-Systeme basieren auf Bulk-Methoden, die eine geringe Ausbeute und eine schlechte Kontrolle über die Größe aufweisen. Mikrofluidische Strategien helfen, diese Probleme zu umgehen und ermöglichen eine robuste Technik mit hohem Durchsatz, um MVVs mit einheitlicher Größenverteilung herzustellen.

In dieser Dissertation werden zunächst die Bulk-Methoden zum Aufbau von MVVs und zur Implementierung einer synthetischen Signalkaskade untersucht. Anschließend wird eine auf Polydimethylsiloxan (PDMS) basierende mikrofluidische Plattform zur Herstellung von MVVs vorgestellt und die Bedeutung von PEGylierten Lipiden für die erfolgreiche Verkapselung der inneren Kompartimente zur Erzeugung stabiler Multikompartiment-Systeme hervorgehoben.

Es wird ein neuartiges mikrofluidisches Gerät mit zwei Einlasskanälen auf PDMS-Basis zur Herstellung von MVVs vorgestellt, das eine dreistufige enzymatische Reaktionskaskade umfasst. Es wird ein gerichteter Reaktionsweg beschrieben, der die Enzyme α-Glucosidase (α-Glc), Glucoseoxidase (GOx) und Meerrettichperoxidase (HRP) umfasst und sich über drei Kompartimente erstreckt, die durch die Rekonstitution von größenselektiven Membranproteinen entstehen. Aufgrund der Monodispersität unserer MVVs durch mikrofluidische Strategien nutze ich diese Plattform außerdem, um die Auswirkungen der Kompartimentierung auf die Reaktionskinetik zu untersuchen.

Eine weitere Integration von zellfreien Expressionsmodulen in MVVs würde eine genvermittelte Signaltransduktion in künstlichen eukaryotischen Zellen ermöglichen. Daher wird die chemisch induzierbare zellfreie Expression eines Membranproteins alpha-Hämolysin und seine weitere Rekonstitution in Liposomen durchgeführt.

Zusammenfassend lässt sich sagen, dass die vorliegende Arbeit darauf abzielt, künstliche eukaryotische Zellen zu bauen, um eine größenselektive chemische Kommunikation zu erreichen, und das Potenzial für Anwendungen als Mikroreaktoren und als Vehikel für die Verabreichung von Medikamenten aufweisen.

Acknowledgements

I would like to acknowledge the time and effort of those who have supported me throughout the course of my research project.

To begin with, I would like to thank Dr. Tom Robinson, who provided me with an opportunity to work in his lab. He has always been a constant source of support and encouragement and has always been open to new ideas. I am grateful that my time in his lab has helped me discover myself as a researcher. I would also like to thank Prof. Salvatore Chiantia for always being there for discussions and giving fruitful insights.

My thesis would not have been possible without the support of my wonderful colleagues. Special thanks to Naresh for helping me with microfluidics and for all the fruitful discussions and good advice. A big thank you to Tina for the numerous times you helped me in the lab and always being available to answer my queries, I know there were quite too many! Thanks to Tabea for always lending me an ear and providing me with excellent suggestions (scientific or otherwise).

I would also like to thank all my colleagues at MPIKG who provided me a congenial workplace environment. A special mention to my amazing office mates, Julia, Swapnil and Richard who always came to my rescue with their fantastic Deutschsprache skills. A huge shoutout to the two wonderful people, Mareike and Niharika, who diligently went over my thesis and helped me with making edits and corrections. And ofcourse, Rikhia and Pallavi, I would be up for another PhD only and only if you guys join me in the journey. You made the journey a lovable one.

I express my gratitude to my family: my mom and dad for always encouraging me, Vicky and Plavita for lifting me up whenever the going gets tough and Deb. Without all of your continued support and love, none of this would have been possible. Thank you Deb for being by my side always - during happy as well as troubling times. Looking forward to spending more of these days together.

Last, but not the least, I thank the almighty, without whom, nothing would have been possible.

To mom and dad

Declaration

Die Vorliegende Arbeit entstand im Zeitraum zwischen Dezember 2017 und August 2021 am Max-Planck-Institut für Kolloid- und Grenzflächenforschung in der Abteilung für Theorie und Biosysteme. Ich, Sunidhi C Shetty, erkläre hiermit, dass die vorliegende Arbeit an keiner anderen Hochschule eingereicht sowie selbstständig von mir angefertigt wurde. Ebenso wurden nur die hier angegebenen Hilfsmittel und Literaturen verwendet wurden. Teile der in Kapitel 4 vorgestellten Arbeit wurden auf dem Preprint-Server ChemRxiv veröffentlicht.

Shetty S, Yandrapalli N, Pinkwart K, Krafft D, Vidakovic-Koch Tanja, Ivanov I, Robinson T, et al. Directed Signaling Cascades in Monodisperse Artificial Eukaryotic Cells. ChemRxiv. Cambridge: Cambridge Open Engage; 2021; This content is a preprint and has not been peer-reviewed.

The present work was carried out and written during December 2017 and August 2021 at the Max Planck Institute of Colloids and Interfaces in the department of Theory and Biosystems. I, Sunidhi C Shetty, hereby declare that neither I nor anybody else has submitted this thesis to any other university. I have produced this work independently, using only literature and other aids as described and listed here. Parts of work presented in the Chapter 4 has been published in preprint server ChemRxiv.

Shetty S, Yandrapalli N, Pinkwart K, Krafft D, Vidakovic-Koch Tanja, Ivanov I, Robinson T, et al. Directed Signaling Cascades in Monodisperse Artificial Eukaryotic Cells. ChemRxiv. Cambridge: Cambridge Open Engage; 2021; This content is a preprint and has not been peer-reviewed.

List of Abbreviations

LACA	Last archaeal common ancestor
FECA	First eukaryotic common ancestor
LECA	Last common ancestor of all eukaryotes
RuBisCO	Ribulose-1,5-bisphosphate carboxylase/oxygenase
GV	Giant vesicles
SUV	Small unilamellar vesicles
LUV	Large unilamellar vesicles
GUV	Giant unilamellar vesicles
MLV	Multilamellar vesicles
MVV	Multivesicular vesicles
W/O	Water-in-oil
ITO	Indium tin-oxide
DNA	Deoxyribonucleic acid
PCR	Polymerase chain reaction
μTAS	Micro-Total Analysis System
Re	Reynold's number
Ca	Capillary number
W/O/W	Water-in-oil-in-water
GOx	Glucose oxidase
HRP	Horseradish peroxidase
CCD	Charge-coupled device
PMT	Photomultiplier tube
POPC	1-Palmitoyl-2-oleoyl-sn-glycero-3-phosphocholine
DOPC	1,2-Dioleoyl-sn-glycero-3-phosphocholine
DOPG	1,2-Dioleoyl-sn-glycero-3-phospho-rac-(1-glycerol)
DPhPC	1,2-Diphytanoyl-sn-glycero-3-phosphocholine
Chol	Cholesterol
NBD-PE	1,2-Dioleoyl-sn-glycero-3-phosphoethanolamine-N-(7-nitro-2-1,3-benzoxadiazol-4-yl)
Atto 633-DOPE	1,2-Dioleoyl-sn-glycero-3-phosphoethanol-amine labeled with Atto 633
BSA	Bovine serum albumin
PBS	Phosphate-buffered saline
Atto 390-DOPE	1,2-Dioleoyl-sn-glycero-3-phosphoethanol-amine labeled with Atto 390
α-Glc	α-glucosidase
PDMS	Polydimethylsiloxane
PDADMAC	Poly(diallyldimethylammonium chloride
PSS	Poly(sodium 4-styrenesulfonate

IA	Inner aqueous solution
OA	Outer aqueous solution
PEG	Polyethylene glycol
PVA	Polyvinyl alcohol
H_2O_2	Hydrogen peroxide
AUR	Amplex ultra red
AR	Amplex red
αHL	α-hemolysin
LO	Lipid oil
RSD	Relative standard deviation
OmpF	Outer membrane protein F
DLS	Dynamic light scattering
DiD	1,1'-dioctadecyl-3,3,3',3'-tetramethylindodicarbocyanine
mRNA	Messenger ribonucleic acid
CFES	Cell-free expression system
ATP	Adenosine 5'-triphosphate
GFP	Green fluorescent protein
EsaR	esaO-binding repressor protein
3OC6HSL	N-(3-oxohexanoyl)-L-homoserine lactone
RFP	Red fluorescent protein
$DiIC_{18}$	1,1′-dioctadecyl-3,3,3′,3′ tetramethylindocarbocyanine
GPCR	G-protein coupled receptor
PDB	Protein data bank

List of Figures

Contents

Chapter 1

Introduction

1.1 Introduction

This chapter describes the origin of cells, their classification and their evolution into more complex structures. The importance of compartmentalization is outlined along with the need to build artificial cells. The different methodologies to generate artificial cells and the limitations of each method are described. Furthermore, the origins and fundamental principles of microfluidics are elucidated. The chemical signaling transduction, an important functional aspect of a cell that has been reconstituted in artificial cells is presented. Finally, the principles of fluorescence and confocal microscopy are introduced.

1.1.1 Cells

History The often-quoted physicist Richard Feynman said, 'nature's imagination is so much greater than man's, she's never going to let us relax.' This statement can perfectly describe the incredibly complex and interconnected systems that constitute cells. Cells are considered as building blocks of all known life forms and act as extremely efficient micro-reactors. In order to have deeper insights about their highly complex structure and function, one needs to gain a better understanding about fundamental physical and chemical processes in living systems.

The discovery of cell dates back to 1665 when it was first observed by Robert Hooke wherein, he described the microscopic structure of different samples such as peacock feathers, bluish molds, hair, a flea, mites, cork, etc. He observed tiny box like structures while looking at the cork under the microscope and called them as cells since they resembled the rooms of Christian Monks in the Monasteries (Fig 1.1) [1].This led to the official formation of classical cell theory by Schwann and Schleiden in 1839. They concluded that all organisms are made up of cells and that they are the basic and elementary

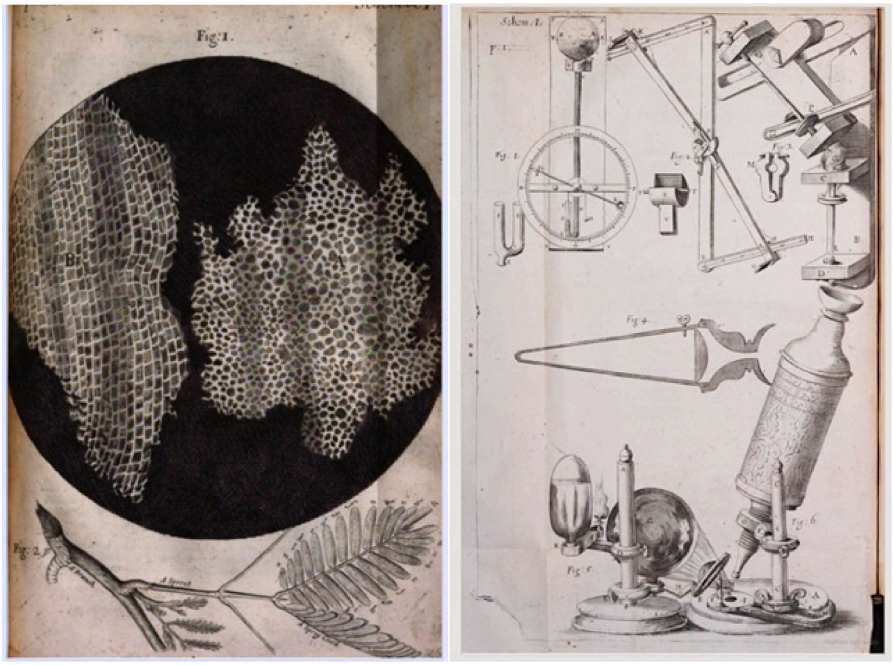

Figure 1.1: Cellular structure of cork according to Hooke (left) and the device setup drawings used (right) by Robert Hooke (reproduced from Micrographia, 1665).

unit of all life forms. Furthermore, Rudolf Virchow concluded that all cells come from previous cells which defines the aspects of classical cell theory [2].

Modern cell theory incorporated the new discoveries and findings of the twentieth century and concluded that all cells carry hereditary information in DNA which is passed from cell to cell during division, all cells belonging to the similar species have both structurally and chemically same composition, and energy flow in terms of metabolism occurs in cells. The similarity of the cell's structural elements indicates its role as ancestral unit of life, which was then succeeded by multi-cellular organisms [3]. The study of structural similarities and differences between different types of cells such as prokaryotic and eukaryotic cells gives an insight into the evolutionary development of all life forms.

The origin of eukaryotic cells Cells are classified mainly into prokaryotic and eukaryotic cells (Fig 1.2). Fundamentally, eukaryotic cells have larger genomes, complex structural features such as a membrane bound nucleus and a dynamic cytoskeleton which prokaryotic cells do not possess [4]. However, more recently exclusive characteristics of eukaryotic cells such as, larger sizes or multiple genomes [5], and cell engulfment due to phagocytosis-like processes [6] have been discovered in prokaryotes as well [7].

The origin of eukaryotic cells have been hypothesized by different theories, the most widely accepted theory is the endosymbiont hypothesis theory [8]. The theory defines that a eukaryote emerged due to the engulfment of alpha-

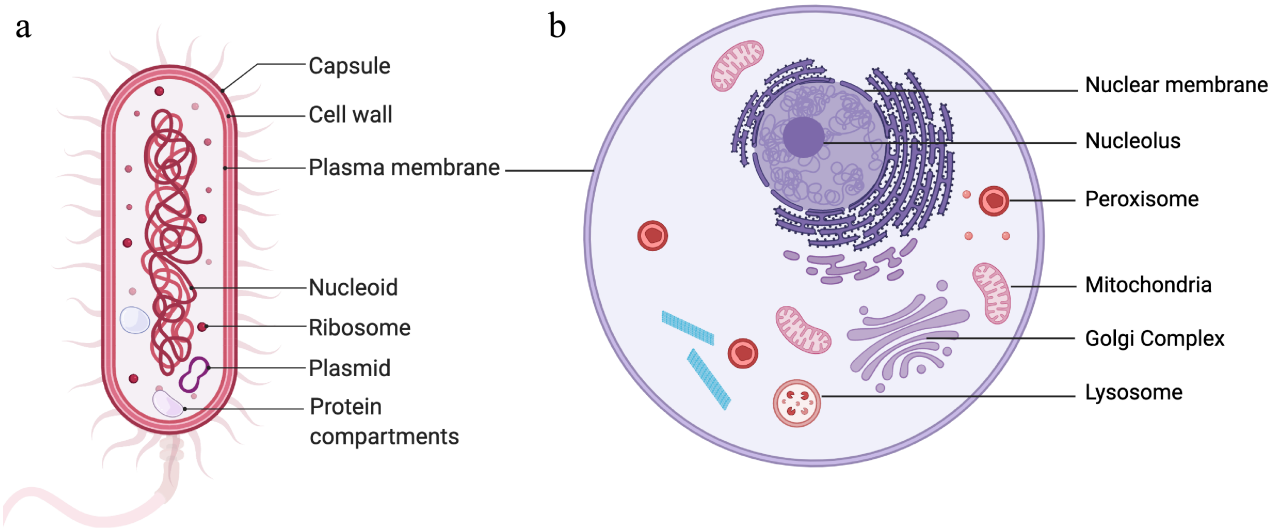

Figure 1.2: a) Prokaryotic cell versus b) eukaryotic cell (created with BioRender.com).

proteobacteria by an ancient archaebacteria. Metagenomic studies describe that the host related to Asgard-archaea, which was discovered more recently, contained homologs of many of the eukaryotic proteins which are involved in formation of a dynamic cytoskeleton as well as membrane trafficking [9].

The mitochondrial endosymbiont descended from prokaryotic bacterial ancestor shared with a subgroup of alpha-proteobacteria as shown by comparative genomics data [10]. Upon encapsulation of mitochondria by Archaean host, there was an increase in the complexity resulting in formation of endomembrane system, transcription regulation network and complex signaling to form the first eukaryotic cell [11]. The increase in complexity has been attributed to the increase in energy provided by the incorporation of mitochondrion that led to multicellular life of eukaryotes. It also led to the 200,000-fold increase in gene expression going from prokaryotic to a complex eukaryotic cell [12]. The complex-host related to Asgard-archaea contained several homologs of eukaryotic signature proteins to enable primitive-phagocytosis required for the host to engulf the bacterial endosymbiont [13]. The eukaryotic cells thus formed consisted fully differentiated multi-compartmentalized internal structures capable of carrying out different functions (Fig 1.3). Many of the complex reaction processes are carried out in membrane-bound structures called organelles. Much like the cell which contains a membrane to separate the inner environment from the outer environment, most organelles also have a distinctive lipid bilayer to separate the inside from the outside. This resulted in the evolution of higher order structures with an intracellular compartmentalization which is an essential prerequisite for different metabolic reactions in eukaryotic cells.

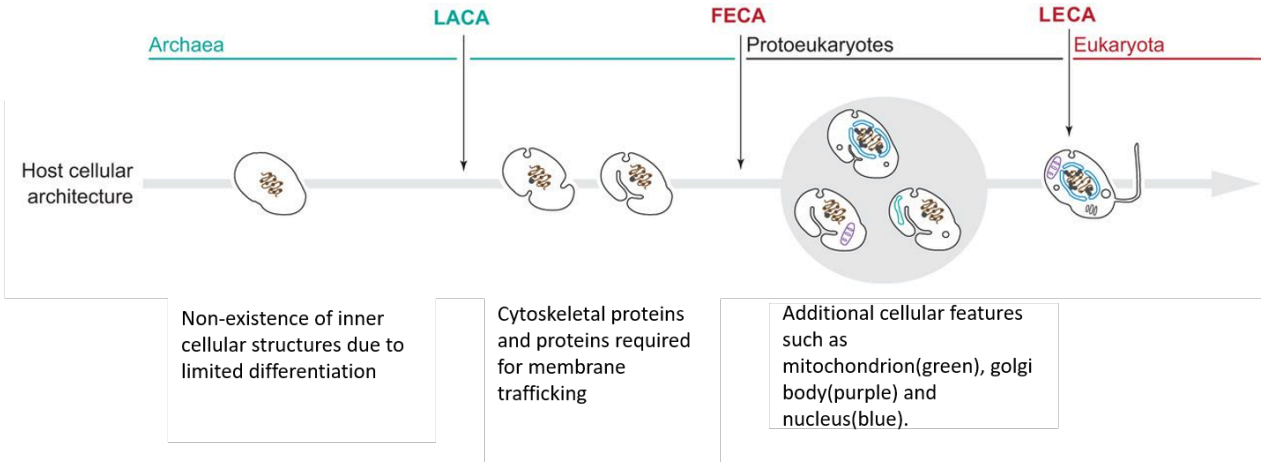

Figure 1.3: Eukaryogenesis. The two transitional periods – the first period shown to occur between the last archaeal common ancestor (LACA) and the first eukaryotic common ancestor (FECA). The second transition occurs between the FECA and the additional cellular features that was acquired by last common ancestor of all eukaryotes (LECA). (Adapted from Dacks et.al 2016) [7].

Compartmentalization and its importance Cells require subcellular spatial organization to regulate various metabolic processes in order to sustain vital life functions [14]. Several theories also support that compartmentalization played an instrumental role in the origin of life [15]. Compartmentalization plays an integral role to limit the diffusion of molecules in a confined space and to increase the local concentration of enzymes and substrates to have a higher turnover rate. Moreover, it also protects cells from the build-up of toxic intermediates and allows for the availability of molecules for multiple competing reactions [16]. Both prokaryotic and eukaryotic life forms overcome many such challenges with the help of intracellular spatial organization. In eukaryotic cells, the emergence of hierarchical architecture with membrane-bound compartments, also known as organelles, help in regulation of metabolic processes. While eukaryotes contain endomembrane systems, most prokaryotes contain proteinaceous microcompartments that segregate internal spaces of the cells to perform specialized functions. These microcompartments act as organelles capable of sequestration of specific enzymes to enhance their catalytic efficiency [17]. The co-localization of enzymes surrounded by a barrier not only increases turnover rate of the enzymes but also protects the enzymes from the interference of outer bulk cellular mechanism. Cyanobacteria and many other autotrophic prokaryotes have 'carbon-concentrating mechanism' with the help of carboxysomes. These microcompartments increase the levels of carbon dioxide (CO_2) to help alleviate the slow turnover rates of ribulose-1,5-bisphosphate carboxylase/oxygenase (RuBisCO) enzyme [18]. Many such bacterial sub-compartments have been discovered in approximately 400 microbial genomes including ethanolamine utilization microcompartment [19] and

1,2-propanediol utilization microcompartment [20] that help protect cells from toxic intermediates. Another nature's strategy of compartmentalization are the large multi-enzyme complexes, as it places the enzymes close together for a given pathway which aids substrate channeling [21]. Some examples found in nature are tryptophan synthase [22], polyketide synthase [23], and cellulosome [24], which work towards increasing the reaction kinetics of the reaction by overcoming the loss of intermediates as well as reducing multiple-competing reactions.

Eukaryotic cells however comprise of multiple sub-compartments (organelles) which are both membraneless and membrane-bound in nature. Multi-compartmentalization allows for the spatial organization and separation of biomolecules and processes in different compartments which also provide the cells with spatio-temporal control over their metabolic reactions [16]. They can perform multiple chemically incompatible enzymatic reactions simultaneously as they are separated in different sub-compartments/organelles. For example, peroxisomes which are able to encapsulate oxidative reactions that give rise to hydrogen peroxide (H_2O_2), a toxic intermediate lethal to a cell [25]. Confinement in eukaryotes also helps in the segregation of reaction pathways that involve multiple enzymes and multiple cellular compartments. For example, the citric acid cycle, which takes place in mitochondria and also interacts with other cytosolic enzymes [26].

To understand and deeply investigate the complex cellular structure and its functions, researchers have designed experiments to probe different aspects of cells with the help of model systems such as minimal cells. Although *in vivo* studies provide more insights on the overall complexity in the living organisms, the isolation of individual components is extremely difficult and furthermore there is a large interference arising from other cellular entities and reaction networks. Therefore, the results might not be easily interpretable and lead to more questions than answers.

Synthetic biology offers a platform to understand the complex machinery by combining the tools of cell biology and engineering to design and develop biological systems [27]. It not only provides tools to re-design and fabricate existing biological systems but also to engineer novel systems with advanced features and functions. The two fundamental approaches to build minimal cells are the top-down approach and the bottom-up approach (Fig 1.4). The first approach deals with the elimination of cellular components that are not deemed essential for the cell to survive. This has led to the formulation of a minimal genome for the cell to function or even totally replacing it with a synthetic genome [28].The minimal cell thus generated consists of minimum set of genes to regulate cellular functions and it was shown that approximately 265-350 genes were essential [29]. It was later hypothesized with a theoretical

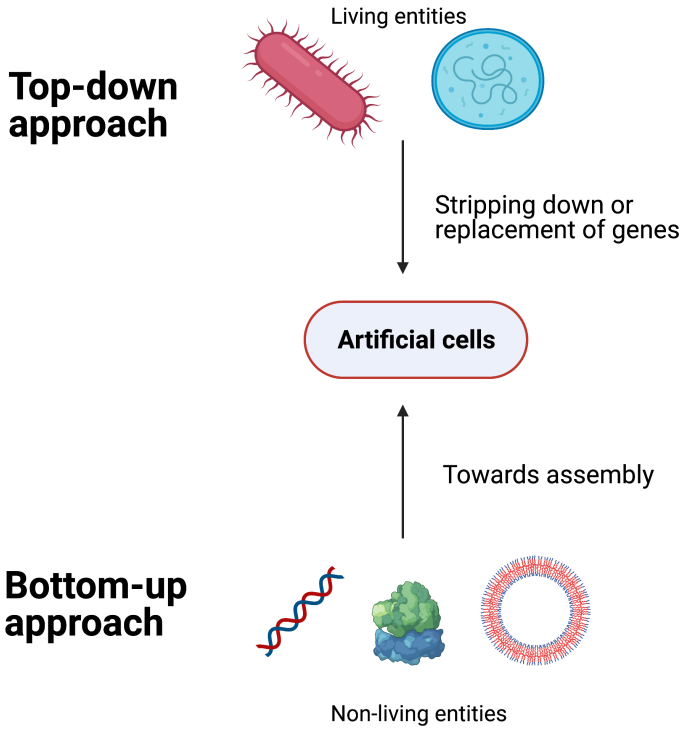

Figure 1.4: Approaches for construction of artificial cell (created with biorender.com).

knockdown of the genome that mapping out the genes responsible for transcription, translation and membrane biosynthesis would require a minimum of 150 genes [30], a number less than proposed in Gil et.al which was 206 protein-coding genes required for a minimal genome [31]. The top-down approaches, however, have bottlenecks such as high mortality rates and inherent toxicity of host cells. The alternate route to build minimal cells is the bottom-up approach. This approach involves creating bio mimics such as artificial cells that utilize non-living entities as starting material to achieve molecular complexity [32] instead of stripping down genes from an existing organism. Bottom-up approaches help gain insights about the origin of life and help to bridge the gap between non-living and living matter [33]. These artificial cells work as substitutes for natural cells by imitating certain properties of a cell which is described more in detail in the next section.

1.2 Artificial cells

Biomimicry to create synthetic constructs of natural cells are proving advantageous to not just contribute towards understanding cellular complexity but also towards generating autonomous cell-like systems with applications in drug delivery, drug screening, bioreactors *etc.* [34, 35]. Artificial cells are defined as

cell-like structures that emulate some of the key features of a biological cell. Constructing artificial cells is considered one of the pillars of bottom-up synthetic biology. The minimum requirements for a cell to be considered 'alive' is when it can self-maintain, self-reproduce and evolve [36]. Construction of even the simplest form of a living cell is an extremely challenging task and it requires significant effort in this field. Therefore, many researchers focus on tackling this arduous goal of generating complex cellular biomimetics by dividing it into smaller, achievable goals. All biological cells share five common hallmarks of life namely compartmentalization, growth and division, information processing, energy transduction and adaptability [37]. Although biomimetic systems for each of these hallmarks have been described and reported, constructing an artificial cell containing all these hallmarks remain a challenge. Current efforts are being carried out to converge diverse approaches from different fields to create an artificial living system [38].

It must be noted that minimal cells and artificial cells are used interchangeably in most literature, but they do not necessarily mean the same. A minimal cell is defined as an entity which requires minimum set of features to be called living for *eg.*, self-maintenance, self-reproduction and to be able to evolve. Whereas an artificial cell is not built to be regarded as alive or minimal in that sense, rather it is designed to be a platform for various biomedical and biotechnological applications. Although, be it minimal cell, protocell, artificial cell or a synthetic cell, they all share one common key feature, that they are chemical micro-compartments with spatial-organization displaying cell-like behavior. Artificial cells generated using bottom-up approach are more robust, simple and controllable systems. Some of the basic features are information processing elements, a membrane which acts as a mediator for communication with external environment, and energy generation components for cellular growth and evolution.

1.2.1 Bottom-up artificial cell models

To build artificial cells, the design and construction of several membrane-bound compartments such as lipid vesicles, proteinosomes [39, 40], polymerosomes [41, 42], colloidosomes [43] and membraneless compartments such as coacervate microdroplets [44] have been reported. However, lipid vesicles are most commonly used model system as they are biocompatible in nature and therefore can act as a membrane model in various biophysical studies. Usually lipid based vesicles are classified into small unilamellar vesicles (SUVs), large unilamellar vesicles (LUVs), giant unilamellar vesicles (GUVs), multilamellar vesicles (MLVs) and multivesicular vesicles (MVVs) as shown in Fig 1.5. Liposomes have been used for several decades as drug delivery systems and for drug

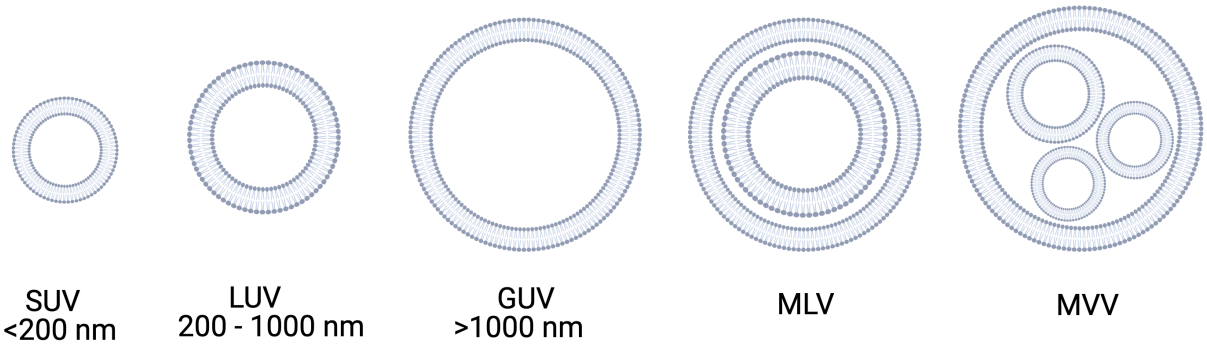

Figure 1.5: Classification of lipid vesicles based on their size and lamellarity.

screening [45]. While GUVs are often used as protocellular models (which are thought to be precursors of origin of life), it has also been reported as a perfect candidate for minimal cell constructs. Moreover, the size of GUVs which are in the range of micrometer reflects that of real cells, and therefore can be imaged using standard microscopy techniques (described in section 1.5). Numerous studies have shown both non-enzymatic as well as enzymatic reactions within them making it the most attractive platform to carry out biochemical studies [46].

Another attractive platform to mimic biological cells are polymersomes, a family of vesicular structures which are self-assembled from block co-polymers [41, 42]. These bio-mimics possess most of the features of lipid vesicles with higher stability and low permeability although it is not as bio-compatible as its liposomal counterpart. Hybrid cell constructs which can be viewed as a mix of co-polymers and liposomes are considered as advanced vesicular structures which have wide range of applications to understand lipid-raft mechanisms [47] or as templating agents [48]. In this thesis, the focus will be imparted on the construction of GUVs and MVVs and their use as a model system for further studies. GUVs are well-studied models and contain large dimensions typical of a cell size (couple of microns). They can be easily observed and manipulated that allows for direct observations and furthermore to study different phenomenon at single cell level.

1.2.2 Preparation methods for GUVs

Different preparation methodologies have been reported based on the various parameters such as lipid type, type of the aqueous medium and temperature. In principle, the two main ways to produce GUVs are described as follows – 1) swelling methods to produce vesicles and 2) use of oil/organic phase to first form water-in-oil (W/O) droplets and then transform these droplets into GUVs (Fig 1.6). Typical swelling methods involve spreading of lipid solution

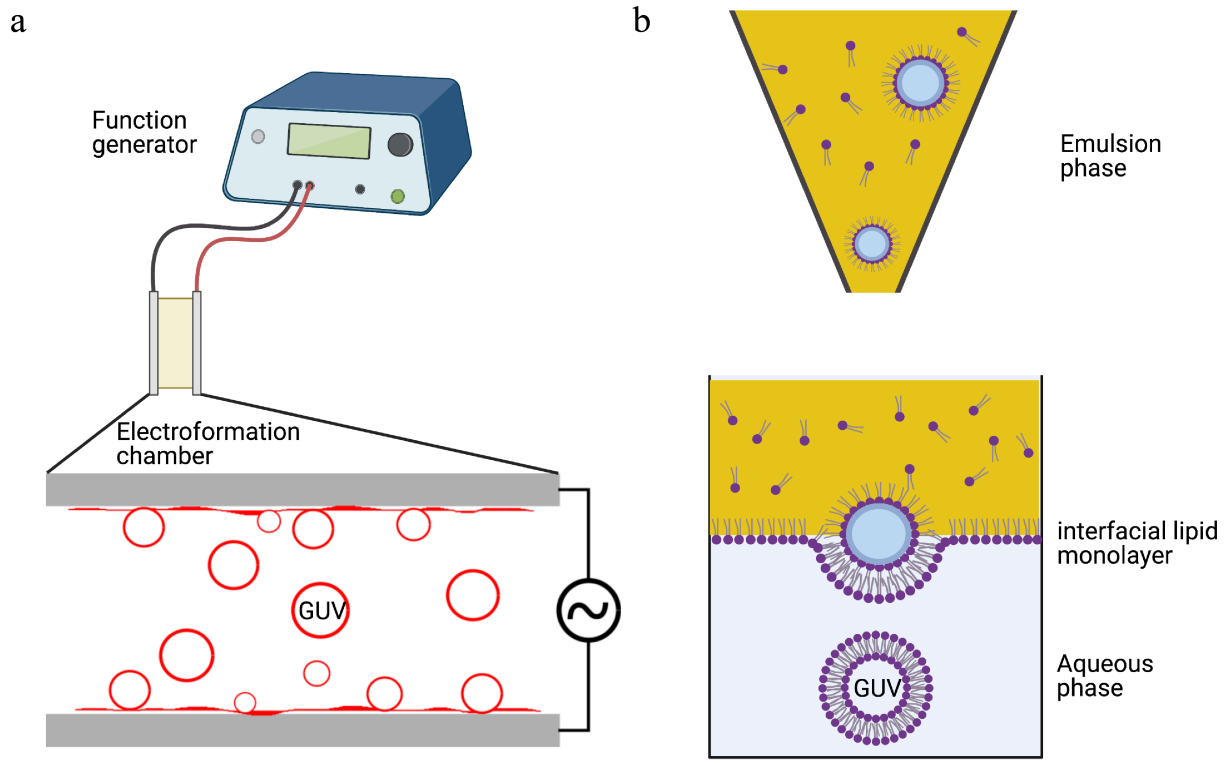

Figure 1.6: Strategies for GUV formation. (a) Electroformation. (b) Emulsion phase transfer method (created with biorender.com).

on a solid substrate (e.g., glass), followed by rehydration with the help of aqueous buffer. These normally yield multilamellar vesicles [49] and do not have control over its lamellarity. Alternatively, the hydration of the lipid film can be influenced by an externally applied electric field and therefore the lipids are deposited on an electrically conductive surface [50]. This conductive surface is usually an indium tin-oxide (ITO) coated glass or a platinum wire that is used as an electrode [51, 52]. Other electrodes that have been reported are made up of steel [53], titanium [54], or silicon substrates [55]. One can produce high yields of GUVs, and moreover the size distribution of GUVs can be controlled by the variation in strength of AC field applied [56]. A main disadvantage of this methodology is the formation of oxidation products when the lipid mix contains polyunsaturated chains. Moreover, the encapsulation of biomolecules such as proteins or deoxyribonucleic acid (DNA) to build minimal cells remains a challenge. The emulsion phase transfer method provides the advantage of efficient encapsulation of bio-molecules as well as encapsulates low sample volumes both of which are highly desirable. The procedure contains mainly two steps, the first step involves the formation of W/O droplets containing single (mono)layer of lipids, the second step involves the wrapping of second layer of lipids to create vesicular structure by driving the droplets through oil-water interface and therefore the two leaflets of the membrane are formed independently [57]. The density gradient between inner aqueous solu-

tion and outer aqueous solution acts as a major contributing factor to generate GUVs. The droplet transfer can be facilitated by adding a centrifugal force for high yield and rapid generation of vesicles. This method has shown great potential in encapsulating DNA [58], cells [59] and also smaller GUVs [60]. The main disadvantage of this technique is the polydispersity, the residual oil in the membrane of the GUVs and low control over the yield of the GUVs. Therefore, to improve the monodispersity of GUVs, many researchers are turning towards microfluidic approaches which is discussed more in detail in the next section. In the end, one should choose a suitable strategy to form GUVs based on the type of the experiment to be performed.

1.3 Microfluidics

1.3.1 Background

Microfluidics deals with handling of fluids in systems with depth and height scale between 100 nm and 100 μm and has witnessed a great deal of interest in the last couple of decades [61]. The first miniaturized analytical device was fabrication of a gas chromatograph which was etched on a silicon wafer with micro-meter sized channels for industrial applications [62]. Presently, this device is widely regarded as the first "Lab on a chip" device or as "micro-Total Analysis System" (μTAS). In 1990s, a system was described that integrated all the processing steps such as sample preparation, transportation and detection in a single micro device. All of these steps were automated and was introduced as μTAS [63]. Also, it was hypothesized that multiple channels could be fabricated into a single device allowing for the simultaneous processing of several samples. This paved the way towards advanced technologies and resulted in a range of applications in various fields such as single cell analysis [64], high throughput polymerase chain reaction (PCR) [65], nanoparticle synthesis [66], enzyme screening [67], glucose sensors [68].

1.3.2 Principles

Microfluidics involves design of systems that control and manipulate small amount of fluids at microscale using channels with micro-meter sized dimensions [69]. To understand the relevance of microfluidic systems, we need to understand that the behavior of fluids at microscale differs from macroscopic scale. To describe a fluid regime , Reynold's number (Re) [70] is used, which is ratio of the inertial forces to the viscous forces of fluidic system given by Eq 1.1:

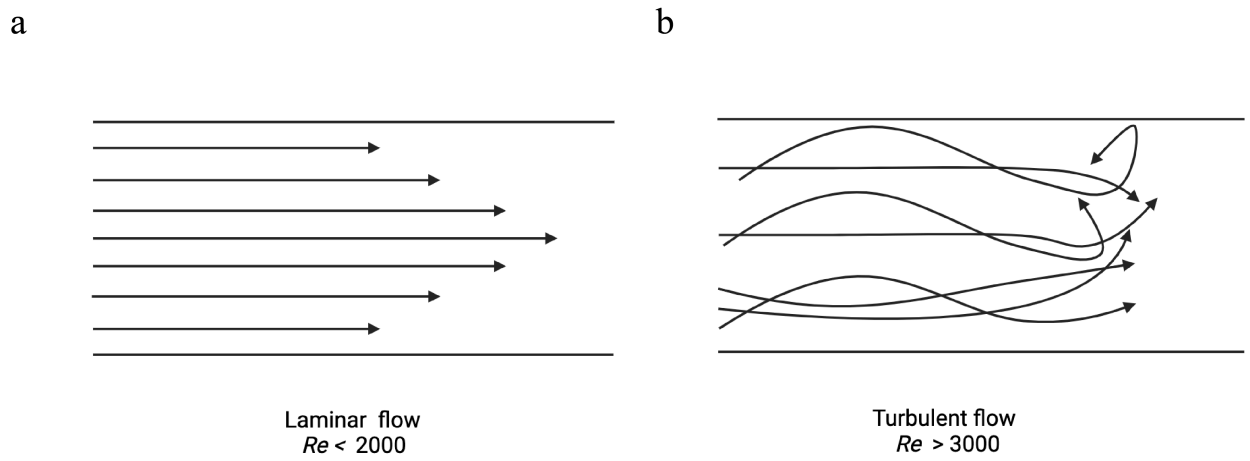

Figure 1.7: Schematic showing (a)laminar and (b) turbulent fluid regimes

$$Re = \frac{Viscous forces}{interfacial forces} = \frac{\rho v L}{\mu} \tag{1.1}$$

Here, ρ is the density of the fluid $[kg\ m^{-3}]$, v is the velocity $[m\ s^{-1}]$, L is the characteristic length $[m]$ and μ is the dynamic viscosity $[Pa\ s]$.

From the equation, we can understand that as Re is proportional to the characteristic length of the system, at microscale, Re is also reduced to a low value and when the Re falls below 2000, the system enters the laminar flow regime. At low Re, inertial forces dominate over viscous forces and give rise to highly predictable kinetics in contrast to turbulent flow regime with high Re number ($Re > 3000$) [71] as shown in Fig 1.7. In most microfluidics devices, the Reynold's number Re is at a very low value [72]. Also, surface forces like shear stress and surface tension dominate over volumetric forces like gravity which becomes less significant at microscale. Therefore, when the flow inside the channel is laminar, the fluid streams in a microchannel flow in parallel, and the mixing is only due to diffusion. When the dimensions of the systems are greatly reduced, the diffusion time taken by molecules are decreased in microfluidic devices. This results in high control over fluids in space and time and researchers have taken advantage of these effects to perform biological and chemical studies. Moreover, since these devices have reduced sizes, it requires small sample volumes and is advantageous for the studies with precious sample molecules [73] and offers possibility of allowing multiple measurements to run in parallel.

1.3.3 Droplet microfluidics

One of the most significant sub-categories of microfluidics is droplet-based microfluidics, also referred to as digital microfluidics. It deals with generating

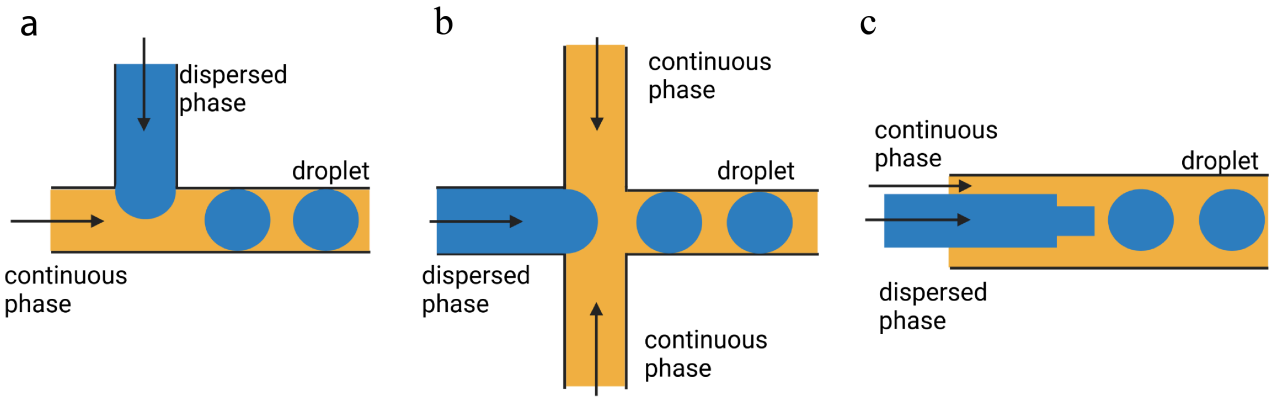

Figure 1.8: Droplet generation geometries. Three most popular geometries are (a) T-junction (b) flow-focusing and (c) co-flow design geometry.

discrete volumes with the use of immiscible phases. This method deals with producing and handling large numbers of highly monodisperse droplets in microdevices. It allows precise control over droplet volumes, generation frequency and stability [74]. The presence of two immiscible phases is required for this technique. The aqueous phase which acts as the droplet body and the carrier phase which is hydrophobic in nature. The formation of droplets is highly reproducible and is based on flow rates and channel geometry. Also, physical properties of both the immiscible phases influence droplet generation. It is expressed by the dimensionless capillary number Ca (Eq 1.2) [75] which is given as ratio of the viscous forces to the interfacial forces between two fluids. Parameters such as flow rates and composition of fluids must be tuned to attain a stable formation of droplets for each device geometry.

$$Ca = \frac{Viscous forces}{interfacial forces} = \frac{\eta\mu}{\gamma} \tag{1.2}$$

Where η is the dynamic viscosity of the liquid $[Pa\ s]$, μ is the fluid velocity $[m\ s^{-1}]$ and γ is the surface tension $[N\ m^{-1}]$.

For the high-throughput generation of different droplets- three types of microfluidic devices are generally utilized: T-junction, flow-focusing, and coflowing devices [76]. T-junction design was one of the first reported geometry to generate droplets using the microfluidic devices [77]. The design is made up of two channels that intersect perpendicular to each other. The dispersed phase merges into the main channel that contains the continuous phase. As the fluid flow continues, the shear forces caused due to the continuous phase and the pressure gradient elongate the dispersed phase and thin the neck to break into a droplet as shown in Fig 1.8a. At low to intermediate Ca , stable droplet formation is achieved with T-junction geometry [78].

Flow-focusing junction design consist of three channels intersecting into

a main channel with a downstream orifice as shown in Fig 1.8b. Here the continuous and dispersed phase are forced through the narrow region and the symmetric shearing of the dispersed phase by the continuous phase result in monodisperse and stable formation of droplets [79, 80]. The sizes of the formed droplets can be decreased by increasing the flow rates of aqueous (dispersed) phase and the frequency can be controlled by the flow rate of continuous phase.

Co-flow design consists of both continuous and dispersed phase flow together in parallel direction as shown in Fig 1.8c. Here the dispersed phase is introduced into a coflowing continuous phase *via* a tapered capillary. At the end of capillary, the droplet formed breaks off when the size of the droplet reaches such that drag force due to coflowing exceeds the interfacial tension [81]. Here the sizes of the droplets can be adjusted in a precise manner based on pressure and flowrates [74].

In this thesis, the focus would be on the use of flow-focusing device consisting double cross-junctions to form water-in-oil-in-water (W/O/W) droplets to create double emulsion templates which can render GUVs after undergoing dewetting. The generation of GUVs and MVVs using this device would be explained more in detail in Chapter 2.

1.4 Communication in artificial cells

Cellular signaling is vital for survival of all life forms. The interactions among organelles and cells are extremely important for the cells to be able to sense and adapt to the surrounding environment [82]. Compartmentalization has been shown to play an important role to spatially segregate biomolecules as well as to avoid incompatible side reactions [83, 84]. Also, confinement is important for the separation of reaction pathways spanning across different subcellular compartments such as endosomes, peroxisomes or mitochondria [85]. Living cells can communicate with their neighboring cells by sending out diffusible signaling molecules and thus perform information transduction. Although studying these transduction mechanisms *in vivo* is challenging and studying each individual pathway without the interference of other molecules is extremely difficult. Therefore, lipid-based vesicles are fabricated using bottom-up approaches to have cell-like morphology to investigate and mimic biological cellular functions in synthetic cellular systems [86]. Several attempts are being carried out to mimic complex reaction cascades and fabricate synthetic cell-cell communication systems [87, 88]. Most artificial cell systems mimic signaling by implementing transport of molecular signals through lipid membranes [89–91]. These cell-mimicking synthetic cell systems are becoming more and more complex in their structure and several studies have been reported to show multi-compartment systems as ideal candidates to mimic hierarchical archi-

tecture of eukaryotic cells. The bottom-up approaches to build these synthetic cell systems and reconstitute enzymatic reaction networks offer the advantage of having control over the design and composition of the system. Also, it allows us to individually study different pathways by isolating them in different compartments. The multi-compartment systems are useful not only to study enzyme reaction networks but also to build artificial cells in the context of synthetic biology [38].

Many studies have been carried out to build complex hierarchical structures to reflect eukaryotic cells and their functional aspects. The multi-compartmentalized structures containing an inner compartment in an outer compartment using liposomes [89], polymersomes [92] and capsosomes [93] have been reported [94–96]. The first ever reported multi-compartment structure termed as vesosomes was achieved by the entrapment of SUVs in GUVs [97]. Vesosomes have been assembled from cochleate cylinders [98] derived from fusion of unilamellar liposomes and using interdigitation method [99]. Other hierarchical assemblies have also been reported with the help of lipid hydration method, wherein outer vesicles ranged between 1-10 μm and inner vesicles around 100 nm and temperature-triggered enzymatic reactions within them were demonstrated [100]. The more commonly used methodology to form multi-compartmentalized structures is the emulsion phase transfer method and its principle has been described in the section 1.2.2. Here, the droplets containing preformed proteoliposomes [89, 101], or intermediate sized-GUVs [60] are driven through water-oil interface to generate nested liposomal structures. Although this method is relatively straightforward and can be used to have different composition for inner and outer compartments, it relies on the density of the solutions and has low reproducibility and control over their size. Another depicted strategy is a layer-by-layer assembly to form complex multi-compartment structures [102], however with this method the yield was low and the population was polydisperse in nature. Chemical cascade signaling within nested liposomal structures has been reported using electroformation method [103]. Here, the LUVs containing the enzyme glucose oxidase (GOx) was co-encapsulated with another enzyme horseradish peroxidase (HRP) and substrate Amplex Red (AR) and the entire network was initiated with the reconstitution of melittin pore protein which would allow the glucose molecule into the artificial cell to trigger the cascade communication. Another example showed temperature controlled release of substrate molecules which resulted in enzyme catalyzed conversion into fluorescence product [104].

While these bulk approaches show promising results for the fabrication of multi-compartment systems they suffer from low yield, lack of control over size and reproducibility and not fully reliable for the analysis of several parallel biochemical reactions. Therefore, scientists are turning towards microfluidic ap-

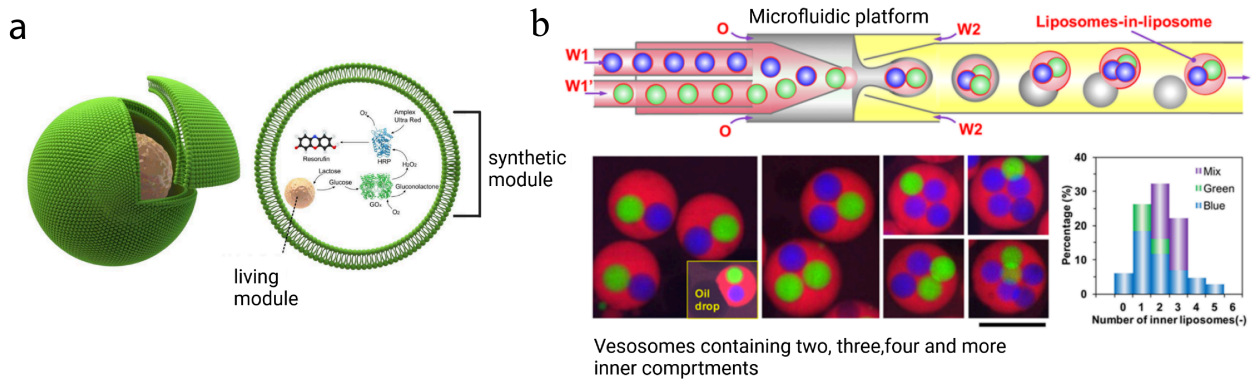

Figure 1.9: Microfluidic approaches to generate microfluidic based multi-compartmentalized artificial cells. (a) Schematic of hybrid cell with an encapsulated cell that further acts as an organelle, which processes feedstock to trigger further processing of synthetic enzymatic reaction cascade (Adapted from Elani et.al 2018 [59]). (b) Schematic of microfluidic formation of multi-compartment with distinct inner liposomes and the corresponding confocal images along with their size distributions (Adapted from Deng et.al 2016 [105]).

proaches to overcome these challenges. Droplet-based microfluidic approaches are extensively used to create artificial cell models as they offer several advantages including high-throughput, uniform size distribution and requirement of low sample volume [74]. Such a microfluidic based strategy was applied to generate multi-vesicular droplets with a two-step enzymatic reaction within them [90]. A hybrid system involving encapsulation of living cells within vesicles using a microfluidic device was also demonstrated [59]. Here, the cells encapsulated acted as a bioreactor and carried out one step of reaction cascade and synthetic enzymatic machinery carried out the subsequent steps of the cascade network. Although such approaches open up the possibility of using living cells as functional modules, they require non-physiological conditions with high sugar concentrations to drive the final bulk gravity-driven formation of the compartmentalized systems (Fig 1.9a). Another approach showed generation of MVVs with a control over the number of inner compartments along with their encapsulated content using co-flow devices (Fig 1.9b) [105]. This approach showed an advanced level of control but does not fully represent complex enzymatic cascades. Moreover, these approaches have not been used to directly compare the effects of different hierarchical levels of compartmentalization on enzymatic pathways which is reported in this thesis.

1.5 Fluorescence Microscopy

The most widely used imaging technique to investigate biological samples as well as biomimetic vesicles is fluorescence microscopy [106]. Fluorescent molecules absorb light of a specific wavelength and emit light of longer wave-

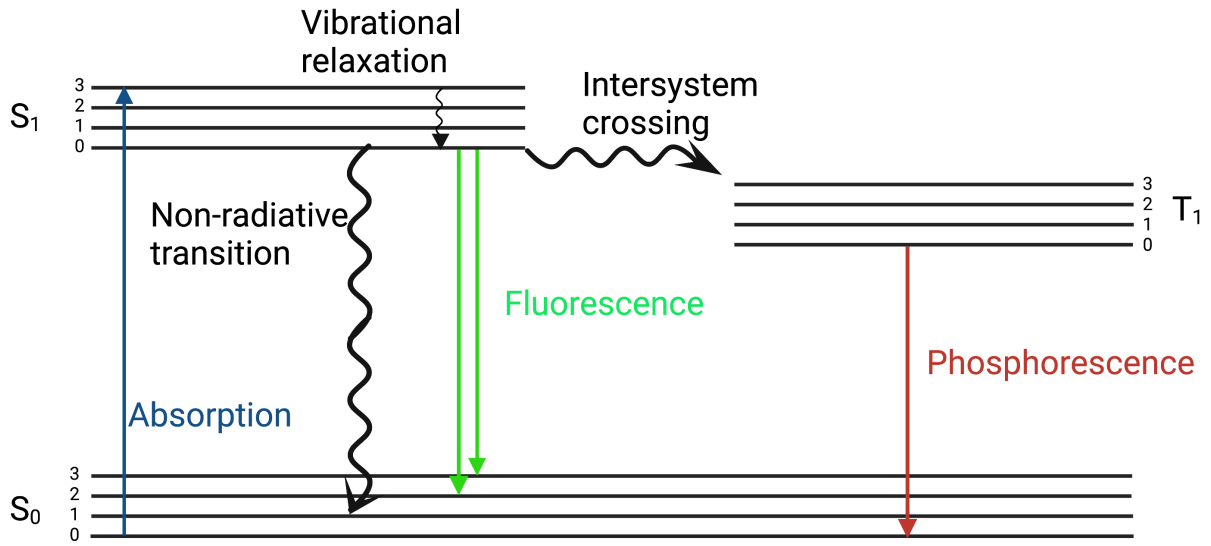

Figure 1.10: Jablonski diagram where S_0 and S_1 are singlet ground and first electronic state respectively and T_1 is the first triplet state.

lengths. This effect is defined as Stokes shift. Fluorescent molecules (also referred to as fluorophores or fluorescent dyes) are engineered to bind to a specific molecule or react to a specific stimulus and are termed as fluorescence probes. Such fluorescent probes can be used to detect GUV membranes or a specific reaction byproduct inside the lumen.

To better understand the fundamental principles of fluorescence microscopy, we need to first understand how the process of fluorescence works. Fluorescence is based on the change in the excitation states of the fluorophore upon uptake and release of photons as shown in Jablonski diagrams [107] (Fig 1.10). Absorption of a photon by a fluorophore's electron changes its quantum state from ground state (S_0) to higher energy electronic state (S_1). Due to non-radiative relaxation by internal conversion, the electron then loses its vibrational energy to the surrounding environment and returns to lowest S_1. From this state, the electron then returns to S_0 ground state by emission of photon by a process called as fluorescence and the fluorescence lifetime is typically in the order of nanoseconds ($10^{-9}s$).

The intersystem crossing from excited singlet state to excited triplet state T_1 could also occur. The relaxation from T_1 to S_0 ground state results in emission of photon results in phosphorescence. Typically, its lifetime is in the order of milliseconds ($10^{-6}s$) and longer than the fluorescence process. To study a fluorophore, one of the most used property is the fluorescence intensity which can be defined by the number of photons emitted by a fluorophore. Also, each fluorophore has a characteristic emission spectrum, and the energy of the emitted photon is always lower than the excitation photon.

The most common fluorescence microscopy is the wide-field epifluorescence

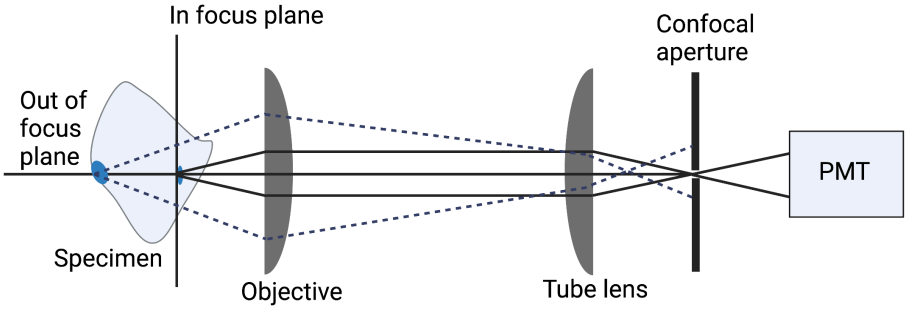

Figure 1.11: Schematic of a confocal microscope where the scanning spot is at the center of in-focus plane. The emitted light from the in-focus plane (solid lines) is focused into the PMT through the confocal aperture or the pinhole. The light emitted from the out of focus plane (dashed blue line) are rejected by the pinhole as shown (adapted from Conchello et.al [108]).

microscope. In this setup, the excitation light incident on the sample and the emitted light passes through the same objective. The emitted light from the specimen passes through the dichroic mirror to filter all other wavelengths apart from that of fluorescence of the sample. A charge - coupled device (CCD) or the more sensitive electron multiplying charge-coupled device sensors are employed as fluorescence detectors. The specimen is generally placed on a microscope slide and positioned on the sample holder. One of the main disadvantages of wide-field fluorescence microscopy is the illumination of the entire specimen resulting in the detection from out of focus planes, and blurred images.

Elimination of out of focus light and a better spatial resolution can be achieved by confocal microscopy [108]. Here, the images are built up by scanning the laser point over the sample. The detector aperture or a pinhole with a circular opening at the conjugate plane to the image collects the emitted light and sends it to the detector photomultiplier tube, PMT (Fig 1.11). This stops the unwanted scattered light and therefore improves the image contrast of the fluorescent samples to produce a precisely focused clear image with a good resolution. In this thesis, confocal laser scanning microscope was used for the inspection of GUVs and MVVs which is described more in detail in Chapter 2.

Aims

The scope of this thesis was to implement a directed chemical communication network within multi-compartmentalized systems that can act as advanced drug-delivery systems, biosensors and as artificial eukaryotic cells in the field of synthetic cell research. In this thesis, the goal was to construct artificial eukaryotic cells and use this platform to study the effect of confinement on biochemical reactions. The aims are divided into following objectives:

- To employ bulk methodologies such as the emulsion phase transfer method and the thin-film hydration method to construct multi-compartmentalized systems. The feasibility of forming multi-vesicular vesicles (MVVs) using bulk methodologies is tested. Furthermore, the optimization of a synthetic enzyme cascade network within MVVs is carried out.

- To use a microfluidic approach to build multi-compartment structures and explore its advantages over bulk methodologies. The formation of monodisperse MVVs with high and uniform encapsulation of inner compartments *i.e.* large unilamellar vesicles (LUVs) is demonstrated.

- To develop a novel two-inlet microfluidic platform to build MVVs that co-encapsulate two different populations of inner compartments (*i.e.*, LUVs) within an outer compartment (*i.e.*, GUVs). The three-enzyme reaction pathway is directed spatially by functionalizing size-selective membrane proteins into the membranes of specific compartments. Finally, the effect of compartmentalization on the overall kinetics of the synthetic enzyme cascade network is studied. The direct comparisons between bulk and compartmentalized systems with increasing order of complexities are implemented.

- The optimization of the cell-free expression of the pore protein, alpha hemolysin, as a step towards building gene-mediated chemical communication network in artificial eukaryotic cells.

Chapter 2

Materials and Methods

This chapter describes the general materials and methods that are used in the entire thesis including instrumental setups, microfluidic chip fabrication, general microscopy settings and protein reconstitution. For any specific variation on these methods, please refer to the relevant chapters.

2.1 Materials

All phospholipids 1-palmitoyl-2-oleoyl-sn-glycero-3-phosphocholine (POPC), 1,2-dioleoyl-sn-glycero-3-phosphocholine (DOPC), 1,2-Dioleoyl-sn-glycero-3-phospho-rac-(1-glycerol) sodium salt (DOPG), 1,2-diphytanoyl-sn-glycero-3-phosphocholine (DPhPC), cholesterol (ovine wool, $>$ 98%) (Chol) and fluorescence-labeled 1,2- dioleoyl-sn-glycero-3-phosphoethanolamine-N-(7-nitro-2-1,3- benzoxadiazol-4-yl) (NBD-PE) were purchased from Avanti Polar Lipids. 1,1'-dioctadecyl-3,3,3',3'-tetramethylindodicarbocyanine(DiD) and Dioctadecyl-3,3,3 Tetramethylindocarbocyanine Perchlorate(DiIC18) were purchased from Thermo fisher Scientific Inc. 1,2-Dioleoyl-sn-glycero-3-phosphoethanol-amine labeled with Atto 633 (Atto 633-DOPE), phosphate-buffered saline (PBS buffer), bovine serum albumin(BSA), stachyose, α-hemolysin, GOx and α-glucosidase(α-Glc) were purchased from Sigma Aldrich. 1,2-Dioleoyl-sn-glycero-3-phosphoethanol-amine labeled with Atto 390 (Atto 390-DOPE) was purchased from Atto-Tec. Amplex Ultra Red was ordered from Thermofisher Scientific. PD-10 columns were purchased from GE Healthcare. Horseradish peroxidase was purchased from Serva. Protein LoBind Eppendorf Tubes and Safe-Lock Tubes were purchased from Eppendorf AG. Osmometer measuring vessels for an Osmomat 3000 were purchased from Gonotec. Polydimethylsiloxane (PDMS) and curing agent were obtained as SYLGARD®184 silicone elastomer kit from Dow Corning. 1H,1H,2H,2H-Perfluorodecyltrichlorosilane was purchased from abcr GmbH. Poly(diallyldimethylammonium chloride (PDADMAC) and poly(sodium 4-

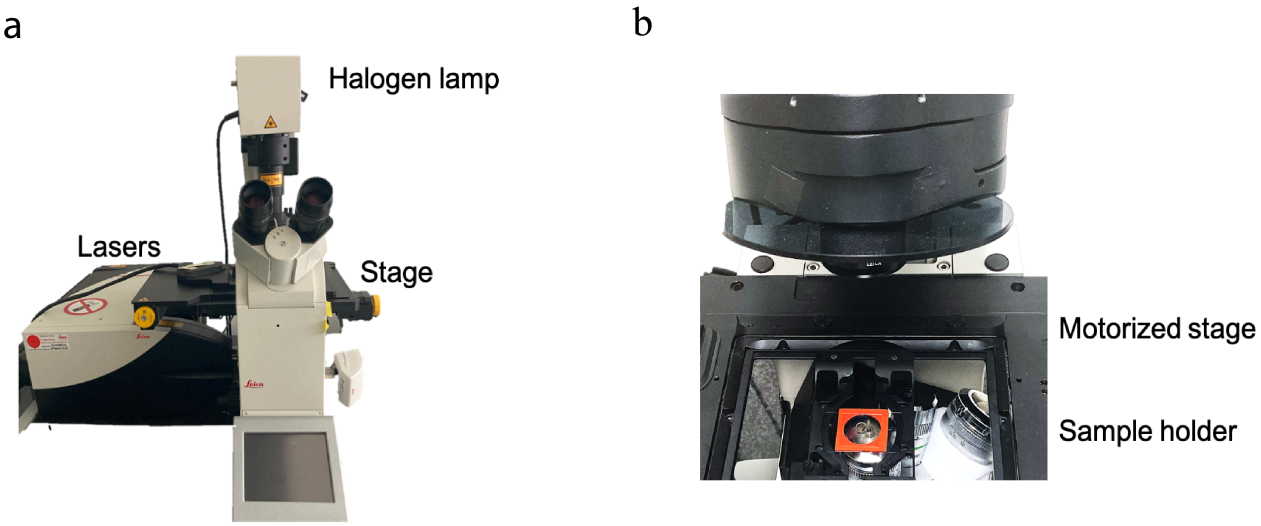

Figure 2.1: Confocal microscope set-up. (a) Leica SP8 microscope with lasers to obtain confocal fluorescence images of sample as well as transmitted light images. The detection of the lasers' reflected light is *via* photomultiplier tubes, or the hybrid detector equipped with a motorized stage. (b) The stage is able to move in x-y-z which is shown with a mounted sample.

styrenesulfonate (PSS) were obtained from Sigma Aldrich. SU8 2050 and SU8 developer solution were from Microchem Inc. Silicon wafers were purchased from Siegert Wafers.

2.2 Methods

2.2.1 Confocal Microscopy

Fluorescence in the GUVs and MVVs was imaged with a confocal microscope (SP8 DMi8, Leica). For detection and imaging purposes, a 63x/ 1.2 water immersion objective or a 20x / 0.40 air objective was used (Fig 2.1). Sequential scanning was used to obtain images with Atto-633 dye excited with 638 nm laser and fluorescence was detected between 650-720 nm. Resorufin signal was obtained using a 552 nm laser and was detected between 583-616 nm. Excitation of NBD-PE dye was performed with a 488 nm excitation laser and the signal was obtained between 499-542 nm. For excitation of Atto-390, the 405 nm excitation was used, and fluorescence was detected at 415-476 nm. Time series were recorded, and images were taken at 7.7 seconds per frame. The quantification of fluorescence signals were carried out with FIJI and a custom written code in Python.

2.2.2 Microfluidic chip fabrication

Microfluidic devices are fabricated using polydimethylsiloxane (PDMS) with the help of soft lithography process. Soft lithography can be defined as a set of techniques based on embossing channels in a thin slab of polymer such as PDMS and allowing it to cure. The design of desired microfluidic chip is drawn using the software AutoCAD. Master moulds of 4" are fabricated using silicon wafers which were purchased from Siegert wafer (Aachen, Germany). Briefly, master forms were produced on a silicon wafer with photoresist SU8 2050 (Microchem Inc.) to a height of 80 µm using standard photolithographic techniques. Following the spin-coating (model no. WS-650MZ-23NPPB, Laurell Tech. Corp) process, a pre-baking step was performed at 65 °C for 3 min and 95 °C for 9 min followed by exposure to UV-light (UV-KUB 3 Kloe, France) for 8 sec through a film mask of required design. Here, film masks with suitable single and double inlet designs were patterned onto SU8 spin coated silicon wafer followed by a post baking step at 65 °C for 2 min and 95 °C for 7 min. The development process of SU8 was performed by washing the wafer gently in a developer solution (Microchem Inc.) for 3 minutes. A hard-bake step was then performed at 200 °C for 30 min and finally the master moulds were silanised overnight with 50 µL of 1H,1H,2H,2H-perfluorodecyltrichlorosilane in a dessicator to prevent adhesion of PDMS to the moulds. Subsequently, the master moulds are ready to use (Fig 2.2a,c).

PDMS-microfluidic chips were fabricated by using heat curing method. PDMS and a curing agent (crosslinker) is mixed at a ratio 10:1 and then degassed to remove any air bubbles for 30 min in a dessicator. Then the mixture was poured onto the master mould silicon wafer and cured at 90 °C for 3 hours. PDMS was then detached from the master mould and diced into individual chips. The inlets and outlets were punched using a 1 mm biopsy puncher (Kai Europe GmbH). Following which the PDMS chips were bonded to plasma cleaned glass coverslips (600 mbar for 1 min, Plasma Cleaner PDC-002-CE, Harrick Plasma) as shown in Fig 2.2b,d. These chips were heated for 2 hours at 60 °C to help with the bonding process after the plasma treatment.

For the efficient production of double emulsion, the surface of the outer channel (from OA inlet to outlet, refer to Chapter 4) of the microfluidic device needs to be hydrophilic in nature. Since the PDMS is hydrophobic in nature, it is not wettable by aqueous solution, and this results in inhibition in the formation of W/O/W double emulsion. Therefore, for the outer aqueous solution (OA) to be able to wet the channels, it was treated with a series of chemical reagents. At first, the second cross junction was flushed with HCl:H_2O_2 (1:2) for 30 sec. This rendered the surface of the channel to be negatively charged followed by flushing it with a positively charged polymeric solution (2 wt.%

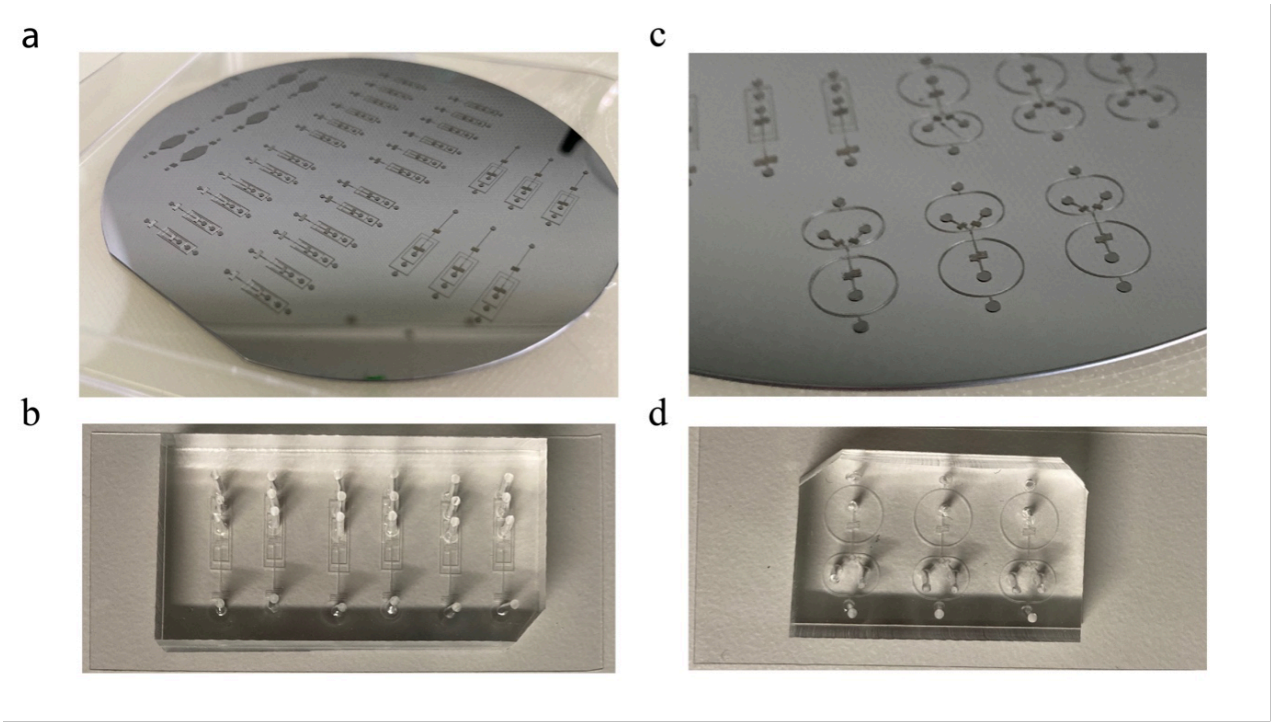

Figure 2.2: Microfluidic chip formation. (a) Master mould for the one-inlet microfluidic device. (b) Final fabricated one-inlet microfluidic chip bonded to a glass coverslip with six copies of the same design for experimental repeats. (c) Master mould for the two-inlet microfluidic device. (d) Two-inlet microfluidic chip bonded to a glass coverslip with three copies of the same design.

PDADMAC) for 2 min. Then it was flushed with a negatively charged polymeric solution (5 wt.% PSS) for 2 min imparting hydrophilic nature to the outer channel. After every step, MilliQ water was flushed for 30 sec, to remove any excess reagents from the outlet to the outer aqueous inlet. The surface treated microfluidic chip was ready to be used immediately thereafter.

2.2.3 Microfluidic formation of compartment systems

Giant vesicles were generated using a microfluidic chip design (refer to Chapter 3 and 4) with two consecutive cross-junctions in a flow-focusing configuration that generates W/O/W double emulsion droplets and imaged using a high-speed camera fitted to Olympus microscope (Fig 2.3). The inner aqueous solution (IA) containing either enzymes, LUVs or both (in 1X PBS buffer) was pumped through the first cross junction to be sheared into aqueous droplets using 1- octanol with a 5 mg/mL of total lipid mix concentration. After which the oil phase containing the W/O droplets was further sheared to form double emulsion at the second cross junction by the OA. These double emulsion templates, after the spontaneous dewetting process, result in GUVs/MVVs (refer to Chapter 3 for more details). In case of the two-inlet microfluidic device,

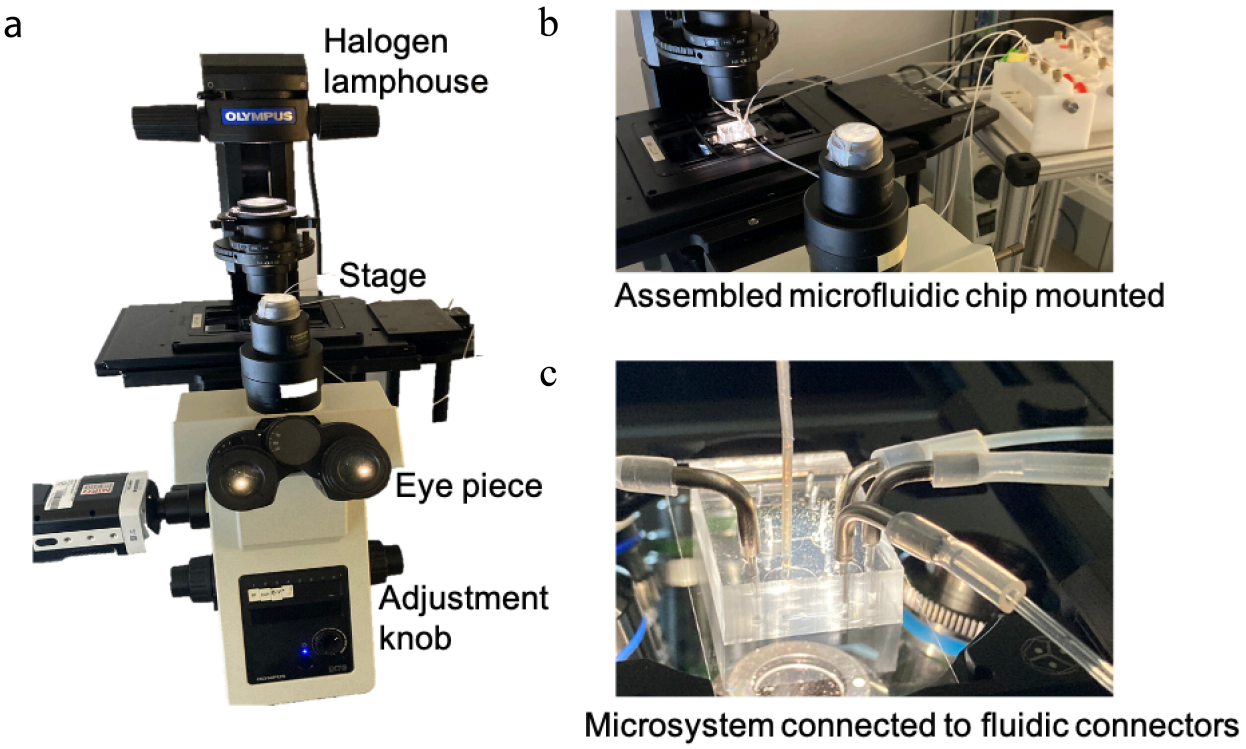

Figure 2.3: Microfluidic set-up. a) Olympus IX73 microscope fitted with highspeed CCD camera (b) Microsystem connected to the pressure pump (MFCS-EZ, Fluigent Inc) and (c) Microsystem connected to the liquid supply in the fluidic inlets and fluidic outlet.

both inlets were flushed in with two different LUV populations in PBS buffer to form three-compartment systems which will be described more in detail in Chapter 4. In the case of two compartmentalized systems, one set of LUVs in PBS buffer plus enzyme solution was used as the IA solution whereas for the one-compartmentalized system, the enzyme solution itself was used as the IA solution.

2.2.4 Bulk approaches for the formation of vesicles

Phase transfer method The emulsion-based phase transfer method is a methodology to produce GUVs that can encapsulate proteins, enzymes, salts and even smaller GUVs. As described before, the main principle behind this method is the density gradient between the aqueous solution of the inner and outer phase which is generally provided by sucrose and glucose. In this thesis, a glucose free environment was required to regulate the activity of specific enzymes discussed more in detail in Chapter 3.

A lipid mixture of desired composition was first prepared at a stock concentration of 8 mM. 75 µL of the lipid mixture was then transferred into a clean 5 mL glass tube followed by the evaporation of chloroform under argon flow for 10 min and then placed under vacuum for 1 hour to form a dried lipid

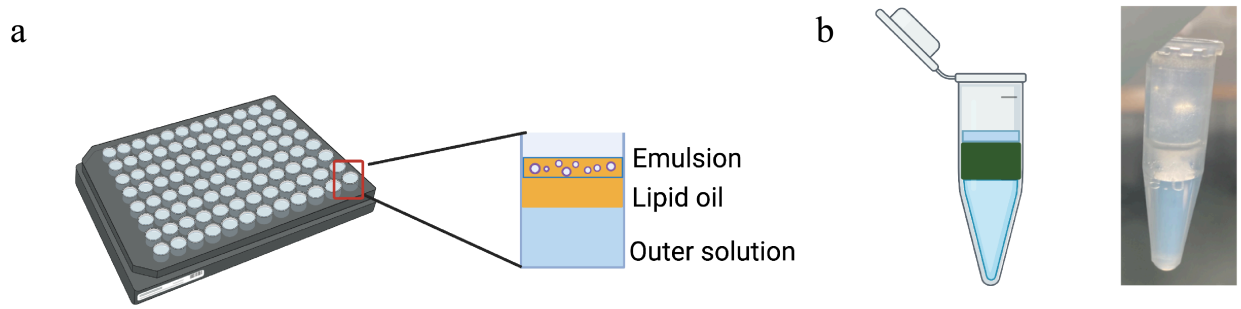

Figure 2.4: Emulsion phase transfer method to form vesicles. (a) Schematic of an emulsion phase transfer method with a microtitre plate and (b) Eppendorf tube to form phase-transfer GUVs and an image depicting the setup (on left).

film. The lipid film was then dissolved in 1500 µl of mineral oil (SIGMA, Life Science), yielding a final concentration of 400 µM. This mixture was further sonicated at 37 °C in water bath (160 W power) for 1 hour and vortexed to ensure the complete dissolution of the lipid. The procedure was carried out in a casein- or BSA-coated 96 well plate by addition of 50 µL of the outer solution of interest (Fig 2.4a). On top of this outer solution, 20 µL of the prepared lipid oil solution was carefully added and it was allowed to rest for at least 30 min to form the interfacial lipid layer. The droplet emulsion was prepared by addition of 5 µl of the inner buffer to 250 µL of the lipid-mineral oil solution in a 1.5 mL Eppendorf tube. The emulsion was formed by sequential rubbing of the Eppendorf tube over an Eppendorf rack resulting in the formation of fine droplets which could be detected by the haziness of the solution. Immediately after which, 50 µL of the emulsion was added slowly on top of the formed interfacial lipid layer. Centrifugation (Rotina420R, Hettich) was performed at 250 rpm for 3 min. This method was also carried out in an Eppendorf tube (Fig 2.4b) with the same procedure as in microtiter plates but with 200 µL of outer solution and 100 µL of lipid-mineral oil solution. And centrifugation was performed at 100 rcf for 10 min. Emulsion phase transfer method with an Eppendorf tube was performed for ease of harvesting of GUVs for further encapsulation to create MVVs (see Chapter 3).

Electroformation: Glass plates from Präzisions Glas & Optik (50 mm x 50 mm) containing a copper tape and coated with ITO were cleaned with ethanol and water and then with a flow of nitrogen. In order to activate the coating and to even out the ITO surface the glass plates were heated on a heater for 15 min at 90 °C. 10 µL of the lipid stock solution were added to one glass plate and 15 µL to the other glass plate and the lipid solution was spread over the glass with the help of a syringe tip to yield a homogenous lipid film. The solvent was then evaporated under vacuum for 1 hour. A Teflon spacer was

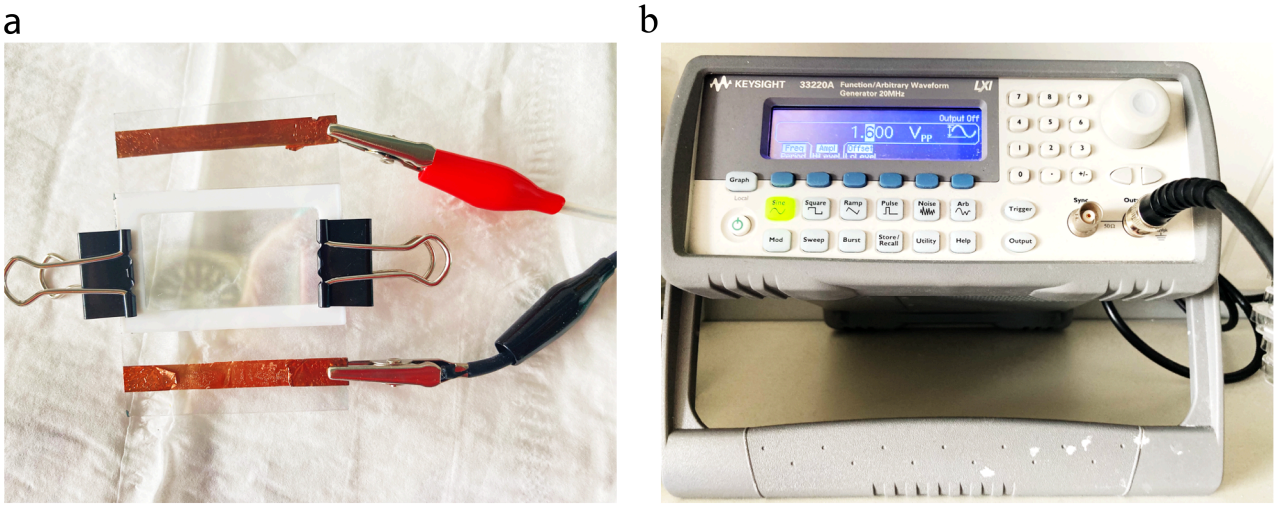

Figure 2.5: Electroformation method to form GUVs. (a) Assembled electroformation chamber connected to electrodes. (b) Function generator to generate Vpp = 1.6 V and at frequency of 10 Hz.

placed between the two glass slides to build up the chamber (Fig 2.5a). For electric swelling, an electric field was applied by an A.C. at a frequency of 10 Hz and a voltage of 1.6 Vpp was applied for 2 hours (Waveform Generator, Keysight Technologies, 33220A) and sucrose solution was used for hydration (Fig 2.5b). The glass plates were unplugged and lightly tapped on both the sides to detach the GUVs and carefully collected with a 2 mL Eppendorf tube for further analysis.

Thin-film rehydration and swelling: LUVs were formed using the thin-film hydration and extrusion method [109]. A lipid mix of concentration 5 mg/mL was dried in a 5 mL glass vial under argon and placed under vacuum for 2 hours. The dried lipid film was then rehydrated with a rehydration buffer (either PBS or enzyme solution) to a final concentration of 5 mM to form MLVs. Here, additional freeze-thawing step was performed for three times with liquid nitrogen to generate more unilamellar vesicles. The lipid vesicle solution was then extruded 11 times with a 400 nm membrane filter to form LUVs of uniform size distribution as shown in Fig 2.6.

2.2.5 Fluorescence dyes

Fluorescence dyes or fluorophores are molecules that absorb light of specific wavelength and emit at a higher wavelength. These fluorophores can be categorized into biological fluorophores (for e.g. green fluorescent protein, red fluorescent protein), organic dyes (for e.g. fluorescein, calcein) and quantum dots. Based on the sample to be monitored and analyzed, one can choose the preferred fluorophore. Organic dyes in general offer higher photostability

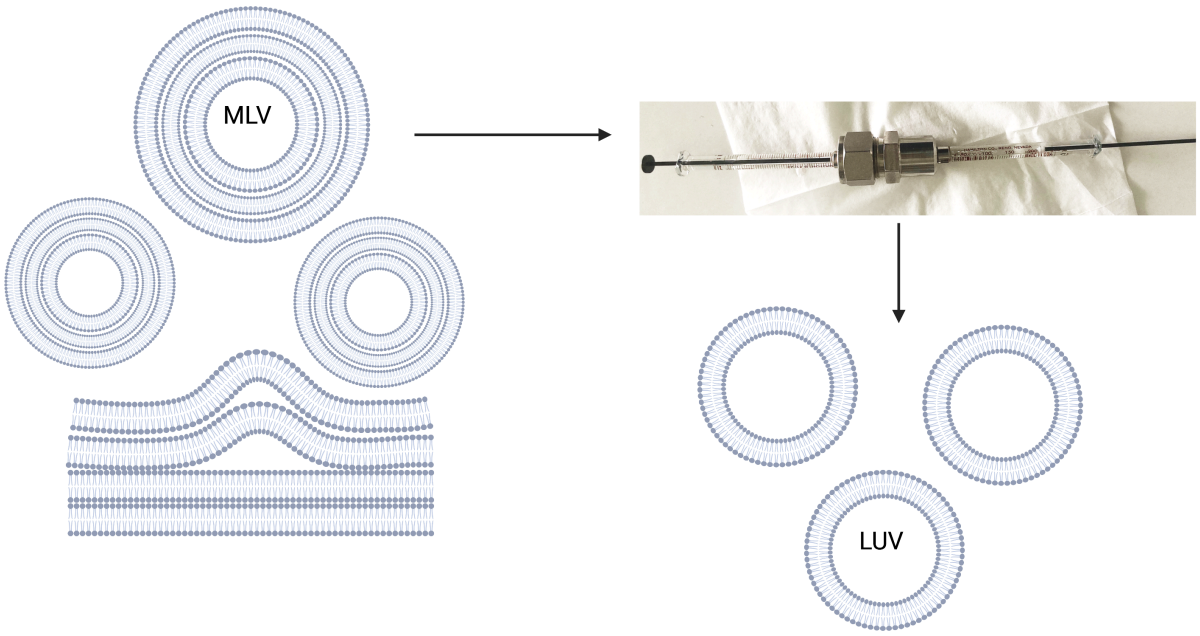

Figure 2.6: Thin-film lipid rehydration method followed by extrusion with polycarbonate membrane to form LUVs.

and brightness compared to fluorescent proteins [110]. To investigate and detect vesicles (*i.e.*, GUVs/LUVs/MVVs), lipophilic fluorescent dyes such as DiD and $DiIC_{18}$ with absorbance wavelength of 644 nm and 544 nm were employed. Apart from that, fluorescently labelled lipids with different emission and excitation wavelengths were incorporated in lipid composition mix. The fluorescently labeled lipids, 2-Dioleoyl-sn-glycero-3-phosphoethanol-amine (DOPE) labeled with NBD, Atto 390 and Atto 633 with absorbance wavelengths of (λ_{abs}) of 460 nm, 390 nm and 633 nm respectively are incorporated to visually confirm the proper formation of multi-compartment vesicles as well as for the analysis of formed membranes.

2.2.6 Measuring osmolarity of solutions with Osmomat 3000

The osmolarity of the solution was measured with a cryoscopic osmometer, Osmomat 3000 (Gonotec, Berlin, Germany) by freezing point depression. The total osmolality of aqueous solutions is determined by comparative measurements of the freezing points of pure water and of different solutions. 50 µL of sample solution was required to measure the osmolarities of different solutions. The osmometer was calibrated using calibration standard solutions (100, 300, 500, 850 mOsmol kg^{-1}) were purchased from Gonotec, Berlin, Germany.

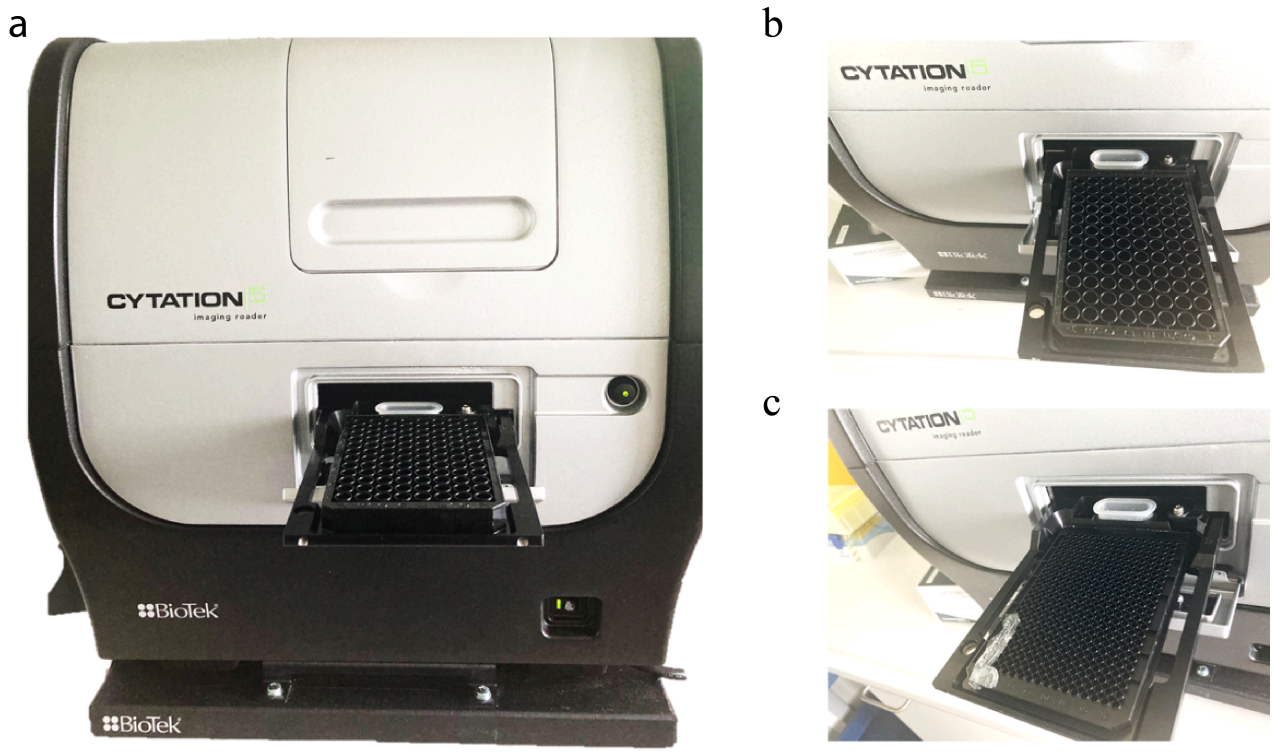

Figure 2.7: Fluorescence spectroscopy. (a) Cytation 5 plate reader mounted with a 96-well plate (b) above and 384- well plate (c) below.

2.2.7 Bulk fluorescence measurements

Bulk fluorescence measurements were performed using Cytation 5 Imaging plate reader (BioTek) with a 96-well plate (Corning) at a fixed excitation and emission wavelength for detecting fluorescent molecules with a bandwidth of 10 nm and an integration time of 100 ms (Fig 2.7). Gen 5 software allows automated processing with multi-mode instrument operations and provides quantitative measurements. The plate reader optics has a quad monochromator design with variable bandwidth which can be set between 9 to 50 nm with 1 nm increment. The read modes consist of kinetic, endpoint and spectral scanning which have been used for different experiments in this thesis.

Chapter 3

Formation of multi-compartmentalized systems

This chapter describes the optimization of a synthetic enzyme cascade network followed by the formation of hierarchical structures with bulk techniques. First, the optimization of different parameters to generate the compartment systems using the emulsion phase transfer method is detailed. Next, the importance of microfluidics to build multi-compartment structures is reported and its advantages over other methodologies to form monodisperse population of GUVs/MVVs is highlighted.

3.1 Synthetic signaling pathway within multi-compartment systems

To construct a signaling pathway mimicking those found in eukaryotic cells, a synthetic reaction cascade was implemented based around a three-enzyme reaction pathway as shown in Fig 3.1. The oxidase/peroxidase system is a very well characterized reaction which is used here as a part of the model reaction cascade. The first enzyme α-Glc works in cohort with GOx and HRP to constitute a three-enzyme reaction pathway. The relatively large tetrasaccharide molecule, stachyose is broken down into smaller glucose molecules by α-Glc. Enzyme GOx catalyzes the oxidation of glucose to gluconolactone with the generation of H_2O_2. Then finally enzyme HRP oxidizes Amplex Ultra Red (AUR) into fluorescent resorufin in the presence of H_2O_2.

The fluorogenic dye Amplex Red (AR) is more commonly used employed to detect the release of H_2O_2 from biological cells and also to assess biochemical

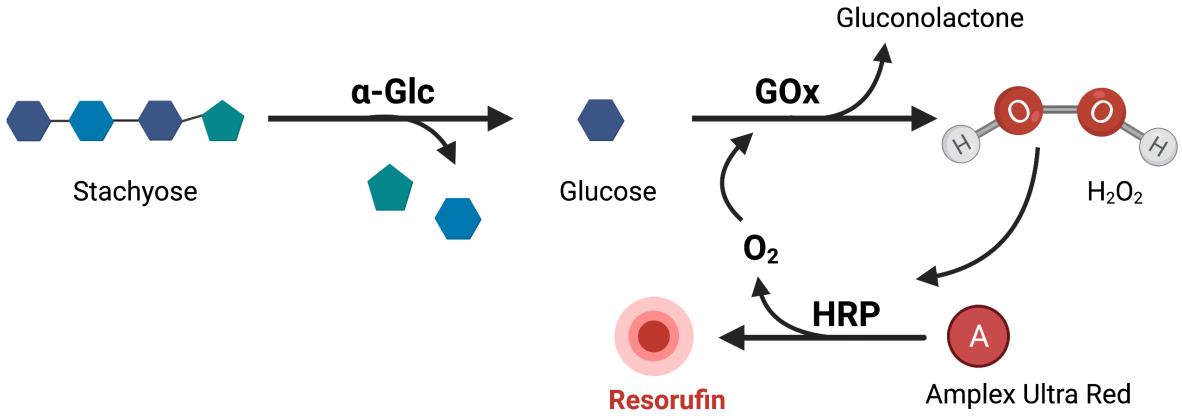

Figure 3.1: Biomimetic three-enzyme cascade reaction containing "α-*Glc-GOx-HRP*" working in tandem to form the final resorufin product.

reactions coupled to oxidases [111]. It has also been extensively used to monitor reactions in nano- and micro-volume confined systems [112]. However, the reaction product of AR is pH dependent which limits its sensitivity. Therefore, in our studies a similar fluorogenic substrate AUR is employed in the final step of the cascade. AUR is extremely robust across a broader pH range and has enhanced sensitivity compared to AR [113]. To obtain optimal conditions for the enzymatic reaction cascade, a bulk spectroscopy study was carried out by varying concentration of enzymes and substrate AUR in order to be able to observe a dynamic three-enzyme reaction cascade in GUVs/MVVs in significant amounts in a relatively short time scale.

The most widely used strategy to encapsulate biomacromolecules such as proteins, enzymes, DNA and other smaller GUVs is the emulsion phase transfer method. The reported first study which showed the formation of GUVs using this methodology demonstrated a potential application by efficient encapsulation of actin monomers and its polymerization kinetics were studied upon addition of magnesium within the GUVs [114]. This method offers several advantages such as efficient encapsulation of large bio-molecules, formation of liposomes with complex multi-component mixtures [115], ability to tune inner and outer leaflet composition to make asymmetric vesicles and have different inner and outer solutions. Therefore, it acts as a suitable strategy to build advanced synthetic cells with hierarchical architecture.

3.2 Objectives

The objective of this chapter is to construct multi-compartmentalised systems using both bulk methodolgies and microfluidic approaches. The advantages

of the microfluidics over bulk methodologies is explored. The formation of monodisperse MVVs with uniform encapsulation of inner compartments within GUVs is also demonstrated.

3.3 Methods

3.3.1 Generation of GOx-LUVs

LUVs were formed using the thin-film hydration and extrusion method. A lipid mixture (5 mg/mL) containing POPC: NBD-PE in molar ratio 99.9:0.1 and POPC: DOPG: Cholesterol: NBD-PE in a 79.9:10:10:0.1 ratio was dried in a 5 mL glass vial under argon and placed under vacuum for 2 hours. The lipid film was then re-hydrated with a 1X PBS buffer containing 8 U/mL GOx to a final concentration of 5 mM. It was then freeze-thawed three times followed by extrusion 11 times with a 400 nm filter.

3.3.2 Assembly of αHL in GOX-LUVs

GOx encapsulating LUVs (GOx-LUVs) were pre-incubated with a final concentration of 5 μg/mL αHL in 1X PBS buffer for 1 hour at room temperature. GOx-LUVs embedded with αHL pores were flowed through PD-10 columns to remove the unencapsulated enzymes. The eluted volume containing LUVs were collected for further encapsulation.

3.3.3 Microfluidic Generation of Compartmentalized Systems

Double emulsion templating for the formation of microfluidic GUVs is conducted using the procedure previously reported [116]. In brief, enzyme solution or LUVs or both (in 1X PBS buffer) as the IA are pumped through the microfluidic chip (using a pressure pump, MFCS-EZ, Fluigent Inc) to be sheared into uniform-sized W/O droplets at the first junction using a lipid oil of 5 mg/mL concentration in 1-octanol. The W/O droplet suspension was further sheared by pumping PBS buffer as the OA at the second junction to form double emulsion templates which undergo spontaneous dewetting process resulting in GUVs containing LUVs.

3.3.4 Image Analysis using FIJI and Python

The images were processed on FIJI and analyzed using Python to determine sizes of GUVs and detection of fluorescence within GUVs. The plots were

created using GraphPad prism and OriginPro9.

3.4 Results and discussion

3.4.1 Optimization of synthetic signaling cascade in bulk systems

At first, the concentration of HRP was varied (in bulk) to ensure efficient detection of final fluorescence output resorufin as shown in Fig 3.2a. The concentration of HRP were varied between 10 mU/mL - 1 U/mL while keeping the substrate and enzyme concentration constant at 10 μM AUR, 8 U/mL GOx, 2 U/mL α-Glc and 50 mM stachyose in 1X PBS buffer. It was observed that HRP was already in excess for the conditions tested. Next, the concentration of enzyme GOx was varied between 2 U/mL – 32 U/mL while keeping concentrations of HRP at 200 mU/mL and the rest constant (Fig 3.2b) and likewise with enzyme α-Glc with varying concentrations between 0.5 U/mL – 5 U/mL (Fig 3.2d). The substrate AUR concentration was varied between 5 - 50 μM which was also in excess for the conditions tested (Fig 3.2c).

It was observed that the GOx catalyzed conversion of glucose to gluconolactone and H_2O_2 was found to be the rate-limiting step as shown in the rate kinetics. The reaction cascade was optimized such that GOx concentration was one of the critical parameters for tuning enzyme kinetics. It was also observed that when one of the enzymes was omitted in the reaction cascade, there was no formation of resorufin fluorescence which confirmed that all the components are necessary for the entire cascade to be triggered. The optimum reaction conditions were established at 200 mU/mL HRP, 8 U/mL GOx, 2 U/mL α-Glc, 10 μM AUR substrate concentration and the trigger input was maintained at 50 mM stachyose concentration. The next step was to compartmentalize the reaction cascade within one-compartment systems *i.e.* GUVs. Firstly, the well-established emulsion phase transfer method was employed to encapsulate the three- enzyme reaction cascade within a compartment (*i.e.* GUV) and gradually built up to have a spatial and temporal control within the system (*i.e.* MVV).

3.4.2 Optimizing the conditions to build up the three - enzyme cascade within multi-compartment systems

With an aim to create multi-compartment systems (which are referred to as MVVs throughout our thesis), at first, inner and outer aqueous solutions with

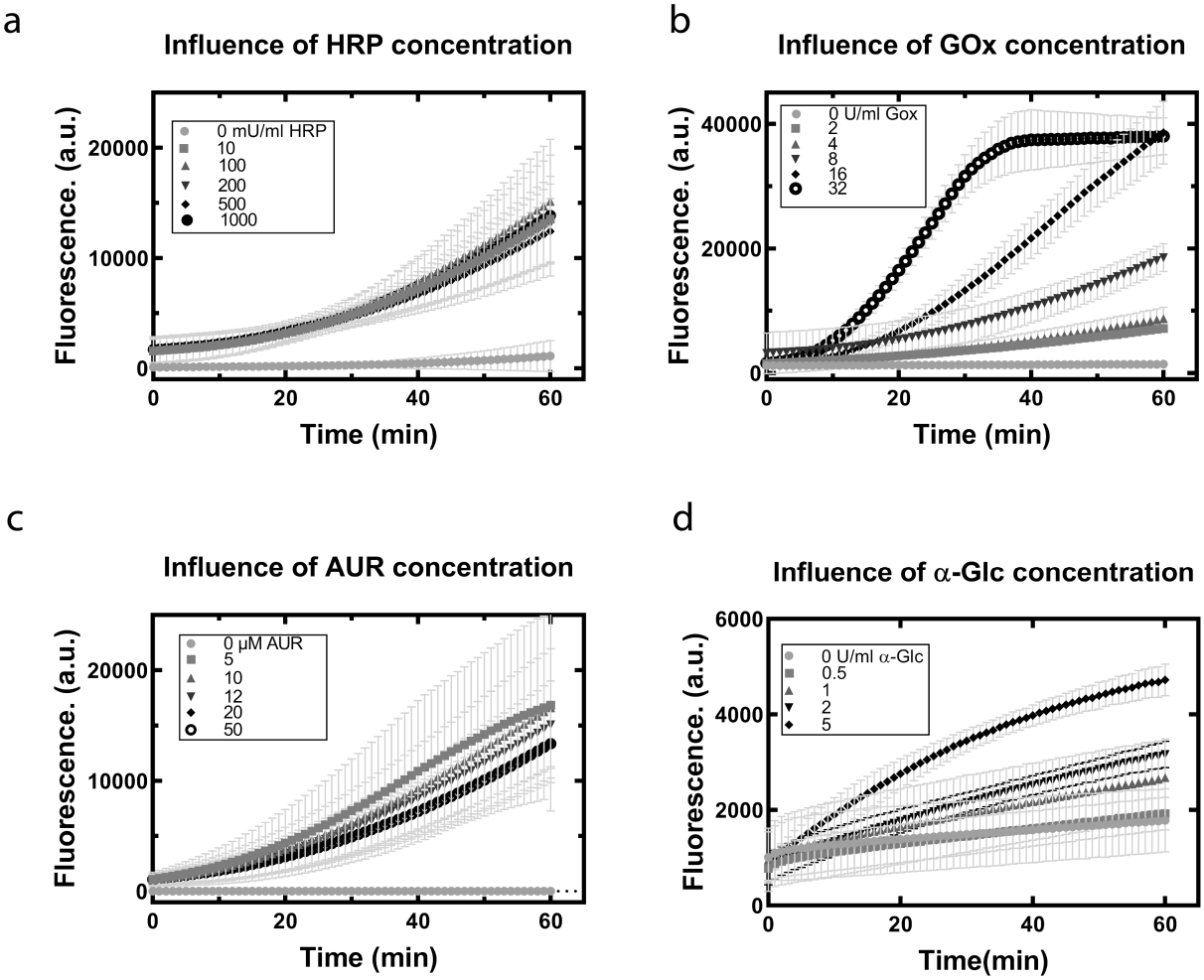

Figure 3.2: Optimization of the three-enzyme reaction cascade in bulk systems using a 96-well plate reader.

different compositions were tested and optimized to generate GUVs. To form a density gradient, which is essential to create GUVs, sucrose and glucose are the most commonly used aqueous phase solutions to maintain iso-osmotic conditions across the bilayer. Therefore, to first establish the basic step of the reaction cascade, detection of H_2O_2 within one-compartment system i.e. GUVs was formed using the emulsion phase transfer method. Here, 200 mU/mL HRP and 50 μM AUR along with 500 mM sucrose and 50 mM sodium phosphate was encapsulated within GUVs at an osmolarity of 840 mOsm. The outer solution containing glucose and sodium phosphate dibasic was adjusted to have the isotonic condition as inside of the GUV which is a prerequisite for the stable formation of GUVs. The oxidation of substrate AUR to form the fluorescent resorufin was triggered by the external addition and subsequent diffusion of final concentration of 50 μM H_2O_2 across the membrane into the GUVs as shown in Fig 3.3a. It has been suggested to avoid high concentrations of H_2O_2 as it has been previously reported that excess amounts of H_2O_2 can cause

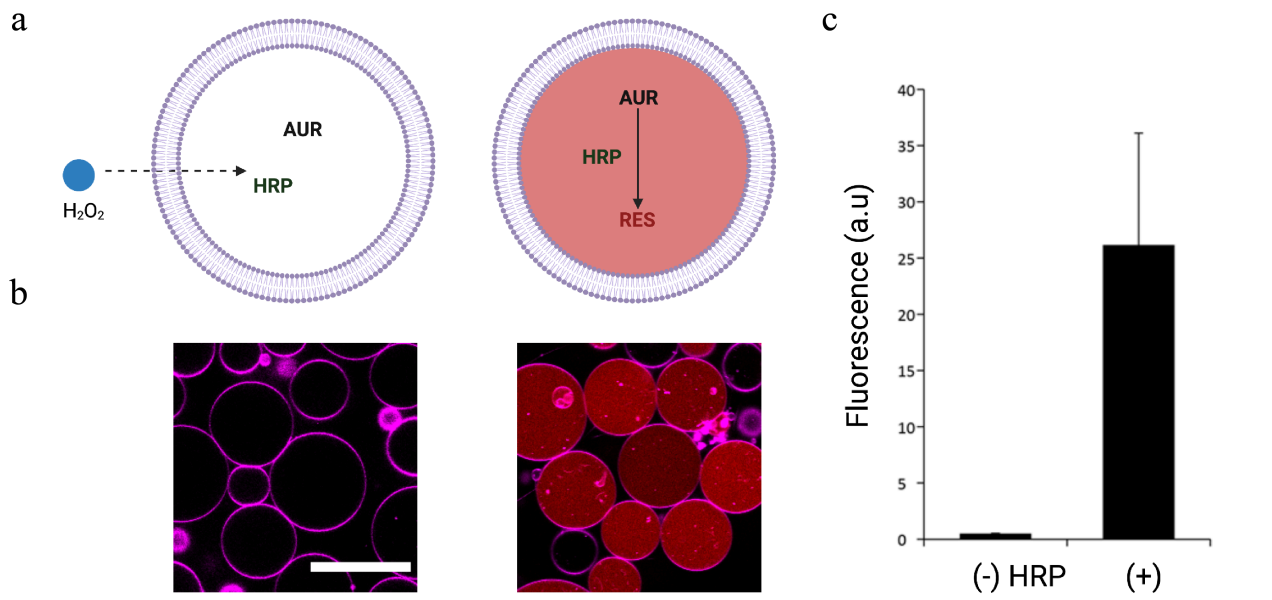

Figure 3.3: One-step enzymatic reaction in one-compartment systems. (a) A schematic of a one-step enzymatic reaction in POPC GUVs labelled with DiD. (b) Confocal images of control and sample containing enzyme HRP in the presence of H_2O_2. Scale bar: 50 μm. (c) Bar plots showing relative fluorescence intensities within GUVs in the presence of H_2O_2 and control experiment in the absence of enzyme HRP. Purple - DiD membrane dye; Red – Resorufin fluorescence signal.

inactivation of enzyme HRP and substrate inhibition (AUR) [117].

The resorufin fluorescence was obtained from within the GUVs using confocal microscopy and quantified (Fig 3.3b). For control experiments, GUVs without HRP were prepared. The endpoint measurements revealed the formation of final product resorufin with the addition of H_2O_2 in the presence of enzyme HRP within the GUVs (Fig 3.3c). This showed the successful triggering of the first step of reaction cascade within GUVs and formed the basis to build on towards the two-step enzyme cascade network.

Next, a two-enzyme cascade reaction was demonstrated with enzyme HRP encapsulated within GUVs and enzyme GOx present in the outer environment. The formation of final output resorufin was externally triggered as shown in Fig 3.4a. GUVs were formed with inner aqueous solution containing 500 mM Sucrose with 50 mM sodium phosphate and the outer solution containing 500 mM glucose and 50 mM sodium phosphate. The enzyme GOx with the concentration of 8 U/mL, was added to the external environment of the GUVs. Glucose, present as the outer aqueous solution of GUVs acted as an input that was oxidized by GOx to generate gluconolactone and H_2O_2. H_2O_2 diffused across the membrane of GUVs, into the lumen of GUVs and catalyzed enzyme HRP to oxidize AUR to form the final product resorufin. The endpoint formation of resorufin was quantified within the GUVs and for the control

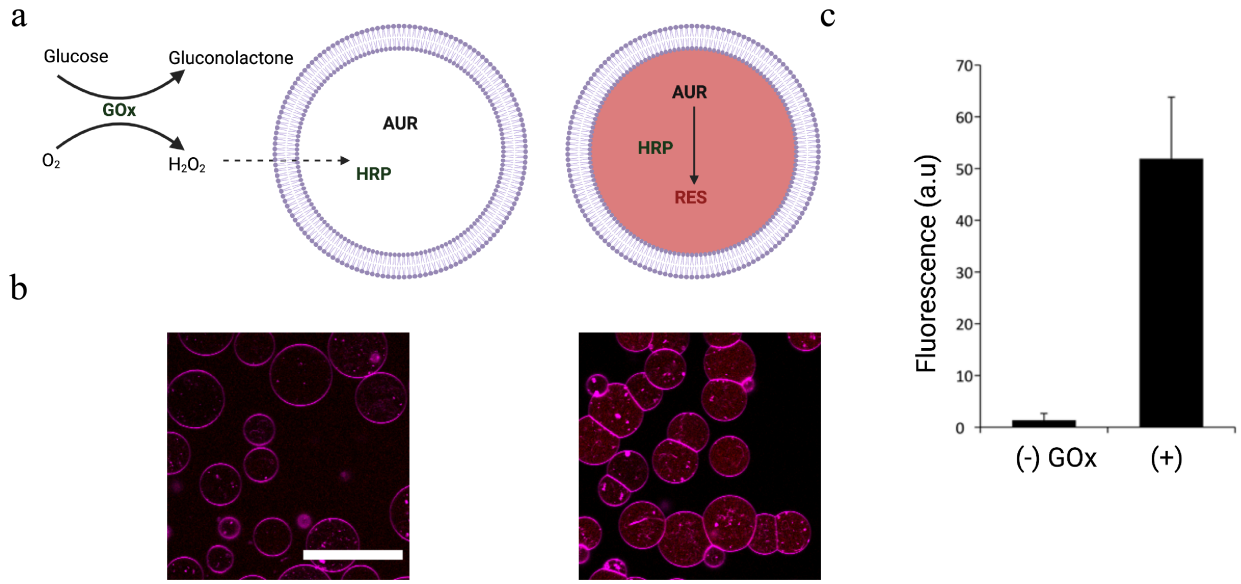

Figure 3.4: A two-step enzymatic reaction shown in and across compartment systems. (a) A schematic of two-step enzyme reaction with enzyme GOx in the external environment and enzyme HRP within POPC GUVs labelled with DiD. (b) Confocal images of control and sample containing enzyme GOx in the presence of glucose. Scale bar: 50 μm. (c) Bar plots showing relative fluorescence intensities within GUVs and control experiment is in the absence of enzyme GOx. Purple - DiD membrane dye; Red - Resorufin fluorescence signal.

experiments, enzyme GOx was omitted from the system (Fig 3.4b,c). The formed resorufin within the GUVs comprising HRP inside the lumen and GOx in the outer environment confirms the successful activation of the two-step enzyme network. Furthermore, it ascertained that both the enzymes, HRP and GOX, worked in cohort and were necessary to form the final product resorufin in one-compartment systems.

The next step was to build MVVs with the enzymes enclosed within different compartments and to externally trigger the reaction cascade within the system. The generation of compartmentalized GUVs was first realized by fabricating one population of GUVs with sufficient yield using first phase transfer and then further encapsulating them within a second population of GUVs using a second phase transfer step as shown in Fig 3.5.

To meet this, at first, glucose needed to be eliminated from the outer aqueous solution containing GOx to only allow the formation of glucose by the catalytic breakdown of stachyose molecules due to the enzyme α-Glc. Therefore, to have the required density gradient, trisaccharide raffinose was chosen as the inner solution and sucrose as the outer solution for the first phase-transfer to form the first set of GUVs. Raffinose was chosen as it was reported previously that it does not interact with HRP and GOx and result in the activation of reaction cascade [118]. The GUVs thus formed, were harvested and subjected to a second phase transfer to further encapsulate them within the outer GUVs

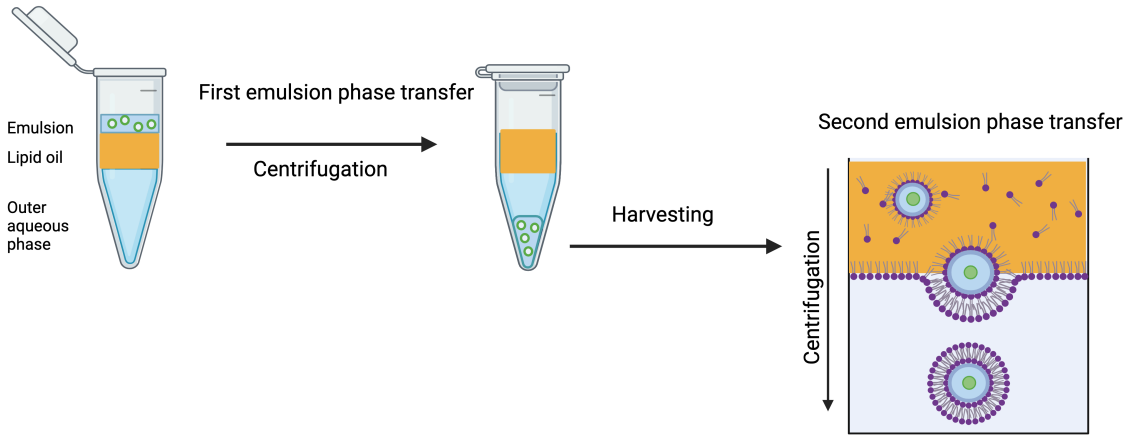

Figure 3.5: Schematic of formation of MVVs using the emulsion phase transfer method. The first phase transfer in Eppendorf tubes, harvesting the formed GUVs and further encapsulation of GUVs within the second set of GUVs using a second phase transfer (Created with biorender.com).

to obtain MVVs.

3.4.3 GUVs in GUVs

The sugar-based density gradient to form multi-compartment systems was maintained at 500 mM raffinose with 50 mM sodium phosphate as the innermost aqueous solution and 500 mM sucrose with 50 mM sodium phosphate as the outer aqueous phase of inner GUVs. This step was carried out using the emulsion phase transfer in Eppendorf tubes, due to the ease of harvesting GUVs, as the oil phase could be easily removed from the transparent tubes compared to the microtiter plate. The harvested GUVs were further encapsulated within the second set of GUVs by having a density gradient with the outermost solution containing 500 mM glucose with 50 mM sodium phosphate as shown in Fig 3.6a. The sucrose-glucose gradient was maintained only for the second phase transfer method as the outer-most environment was devoid of enzyme GOx that could oxidize glucose. The inner compartment contained AUR, HRP and raffinose whereas the outer compartment contained sucrose and GOx and the outermost environment contained glucose. The raffinose/sucrose gradient for inner GUVs and sucrose/glucose gradient for outer GUVs was maintained to render sugar density difference necessary for the emulsion-based phase transfer method to produce multi-compartmentalized GUVs. Confocal images show the MVVs with the first set of POPC GUVs labelled with NBD-PE (green channel) which are further encapsulated within POPC GUVs labelled with Atto 633 (purple channel) as shown in merge image in Fig 3.6b.

However, with this methodology, the yield of the formed multi-

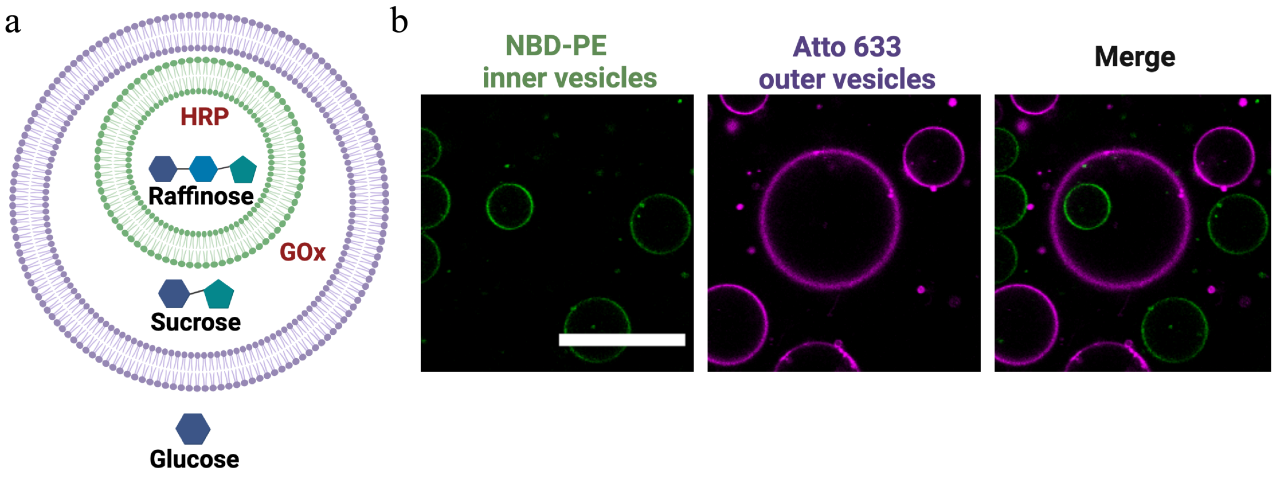

Figure 3.6: Formation of MVVs with the emulsion phase transfer method. (a) Schematic illustration of GUVs encapsulated within GUVs with a density gradient rendered by raffinose, sucrose and glucose. (b) Confocal images of GUVs within GUVs depicting inner GUVs composed of POPC lipids labelled with NBD-PE and outer vesicles composed of POPC lipids labelled with Atto 633 DOPE. Scale bar: 50 μm.

compartment GUVs was inherently low. It was observed that out of 10 GUVs formed per field of view, an average of $<$ 2 MVVs per field of view (246.03 μm x 246.03 μm) were obtained. It was more challenging to attain statistically significant data as this method suffered from poor encapsulation of inner compartments as seen in Fig 3.6b (merge image). Several inner GUVs (green channel) were un-encapsulated within outer vesicles even after the second phase transfer). This is attributed to the larger size diameter of the inner GUVs which do not get encapsulated within the emulsion droplets during the mechanical agitation to form multi-compartmentalized GUVs. To overcome this, another alternative was to enclose smaller vesicles such as LUVs within GUVs which is described in detail in the next section.

3.4.4 LUVs in GUVs

The LUVs were generated using lipid film rehydration technique followed by extrusion using 400 nm membrane filter as described in section 2.2.4. These LUVs were further encapsulated within GUVs using the emulsion phase transfer method. The MVVs thus formed contained one set of LUVs within GUVs as shown in Fig 3.7a. Confocal images show the inner LUVs which are encapsulated within outer GUVs as shown in the Fig 3.7b. The inner LUVs were prepared in 500 mM raffinose with 50 mM sodium phosphate solution. The outer solution contained sucrose and sodium phosphate that was maintained to have isotonic conditions with the inner solution of outer GUVs.

The LUVs were then encapsulated with GOx and further reconstituted

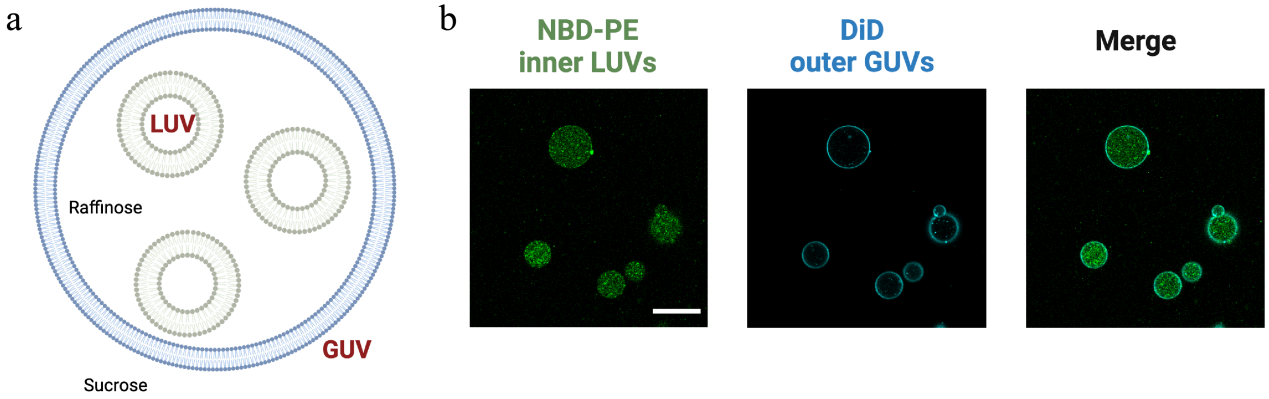

Figure 3.7: Generation of MVVs containing LUVs within GUVs using the emulsion phase transfer method. (a) Schematic illustration of LUVs enclosed within GUVs having a raffinose-sucrose density gradient. (b) Confocal images of LUVs within GUVs, here inner LUVs composed of POPC lipids labelled with NBD-PE and outer vesicles composed of POPC lipids labelled with dye DiD and the merge image. Scale bar: 50 μm.

with membrane pores alpha-hemolysin (αHL) as described in the section 3.3. GOx encapsulating LUVs (GOx-LUVs) thus formed were co-encapsulated with enzyme HRP (200 mU/mL) within outer GUVs as shown in Fig 3.8a. In order to have temporal control over the reaction network, the entire cascade was initiated by external addition of αHL and glucose molecules. First, the glucose molecules passed through the outer membrane into the lumen of outer GUV via assembled αHL and then into GOx-LUVs functionalized with αHL pores. Within the LUVs, glucose was oxidized by GOx to generate gluconolactone and H_2O_2 which then freely diffused across the inner LUV membrane into the GUV's lumen where it catalyzed the formation of fluorescent resorufin by HRP enzyme. As shown in Fig 3.8b, the formation of resorufin was monitored over a period of 25 min. Control experiments were carried out with the removal of GOx and no resorufin fluorescence was observed and the corresponding confocal images depict the formation of resorufin at 0 min (time of initiation) and 25 min within the MVVs. Note that the successful functionalization of the membranes with αHL also confirmed the unilamellarity of our GUVs/MVVs.

However, the main disadvantage with this method was the low yield of formed compartmentalized systems. And moreover, several bursting events of inner LUVs were observed as there was presence of fluorescence signal (green channel) of the LUVs on the outer membrane of GUVs as shown in Fig 3.9a,b. Moreover, the size distribution of the formed MVVs was polydisperse in nature which show non-normal distribution as shown in Fig 3.9c which could be curbed with the use of microfluidic devices.

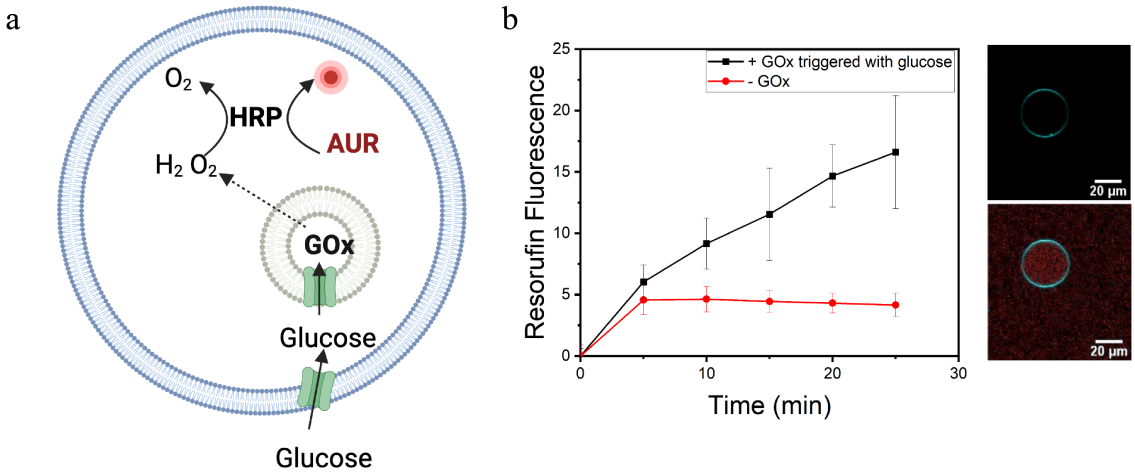

Figure 3.8: Activation of two-step enzyme cascade within MVVs. (a) Schematic illustration of GOx-LUVs functionalized with αHL pores enclosed within outer GUVs containing enzyme HRP (b) Average kinetic traces of the resorufin signal in multi-compartmentalized GUVs (n = 10) and confocal images of MVVs with the formation of resorufin (red fluorescence signal) at 0 min (left) and 25 min (right) when triggered externally with 50 mM glucose. Error bars are taken from the standard error of the mean. Scale bars: 20 μm.

3.4.5 Microfluidic generation

Fabrication Bulk methodologies to produce GUVs such as electroformation, PVA swelling method, phase transfer method have poor control over size of the formed liposomes. Moreover, these approaches lack reproducibility and possess low yield of encapsulated inner compartments which is vital for high throughput processing of biochemical reactions. To circumvent these issues, microfluidic technologies have been employed to produce compartmentalized systems. Microfluidic technology for the creation of artificial cells have been widely reported in the recent years [119, 120]. Droplet-based microfluidics offers high-throughput and good control over fluid volumes, mitigates the loss of expensive biological samples, and therefore is an ideal platform to generate complex artificial cell models [74, 121]. Although, glass-based microfluidic approaches have been shown to successfully form nested liposomal structures, referred to as "vesosomes", the alignment and sealing of the capillaries is extremely difficult and at times needs to be performed manually [122]. Polydimethylsiloxane (PDMS) microfluidics-based approaches were employed as they are easy to fabricate by soft lithography techniques and requires rather inexpensive material. PDMS is a silicon elastomer which has inherent hydrophobicity with a water angle $> 100°$ which accounts for its wettability [123]. It is chemically inert, permeable to gases, compatible with organic solvents, biocompatible, and is optically transparent which makes it an ideal candidate for development of several microfluidic platforms for biomedical applications. Therefore, PDMS based microfluidic devices were employed in this work for

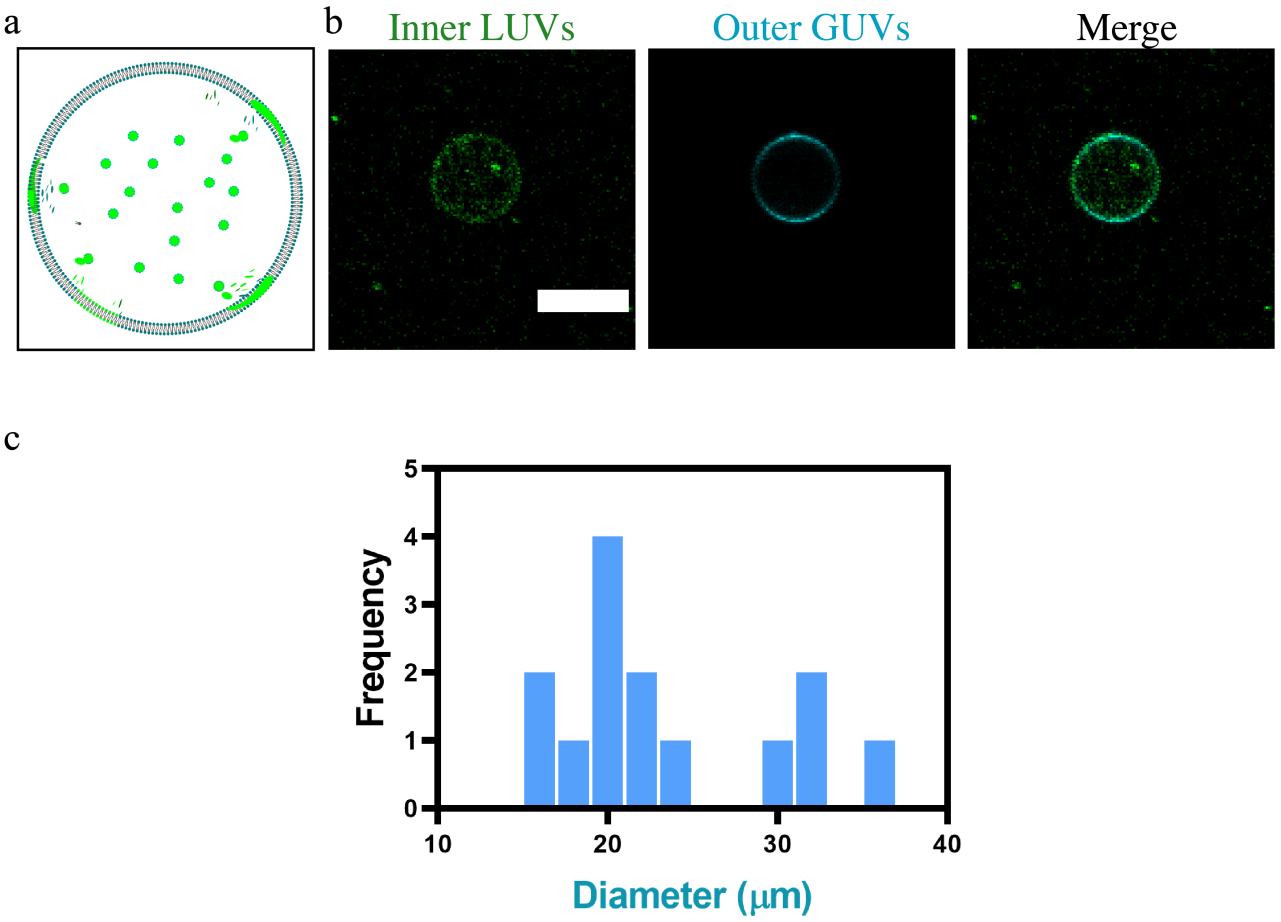

Figure 3.9: Generation of MVVs with the emulsion phase transfer method. (a) Schematic representation of bursting of LUVs and aggregation on the membrane (b) Confocal images of burst inner LUVs (green channel) at the outer GUV membrane, outer GUV (cyan channel), and the merged image (right-most panel). Scale bar: 20 μm.

high-throughput formation of compartmentalized systems

A one-inlet microfluidic device used for the formation of liposomes consists of IA which is sheared by lipid oil (LO) at the first cross-junction. This resulted in formation of W/O droplets which are further sheared by OA at second cross-junction to form W/O/W double emulsion templates (Fig 3.10a). After W/O/W formation, the droplets undergo dewetting spontaneously to minimize the interfacial energies between the three phases (LO, IA and OA). The interfacial energies are defined by a parameter called as spreading co-efficient (S_{ij}), which can determine the dewetting of double emulsion templates. It has been reported that complete dewetting occurs when (S_{ij}) of outer phase $S_{OA} > 0$ where $S_{OA} = \gamma_{IA-LO}$ - γ_{IA-OA} - γ_{OA-LO} where γ is the interfacial tension between two fluids [105].

Fig 3.10b show two serpentine modules that are included in the microfluidic design, one at the first cross-junction, where IA is sheared by LO to form W/O droplets, and the other module is implemented after the second cross-

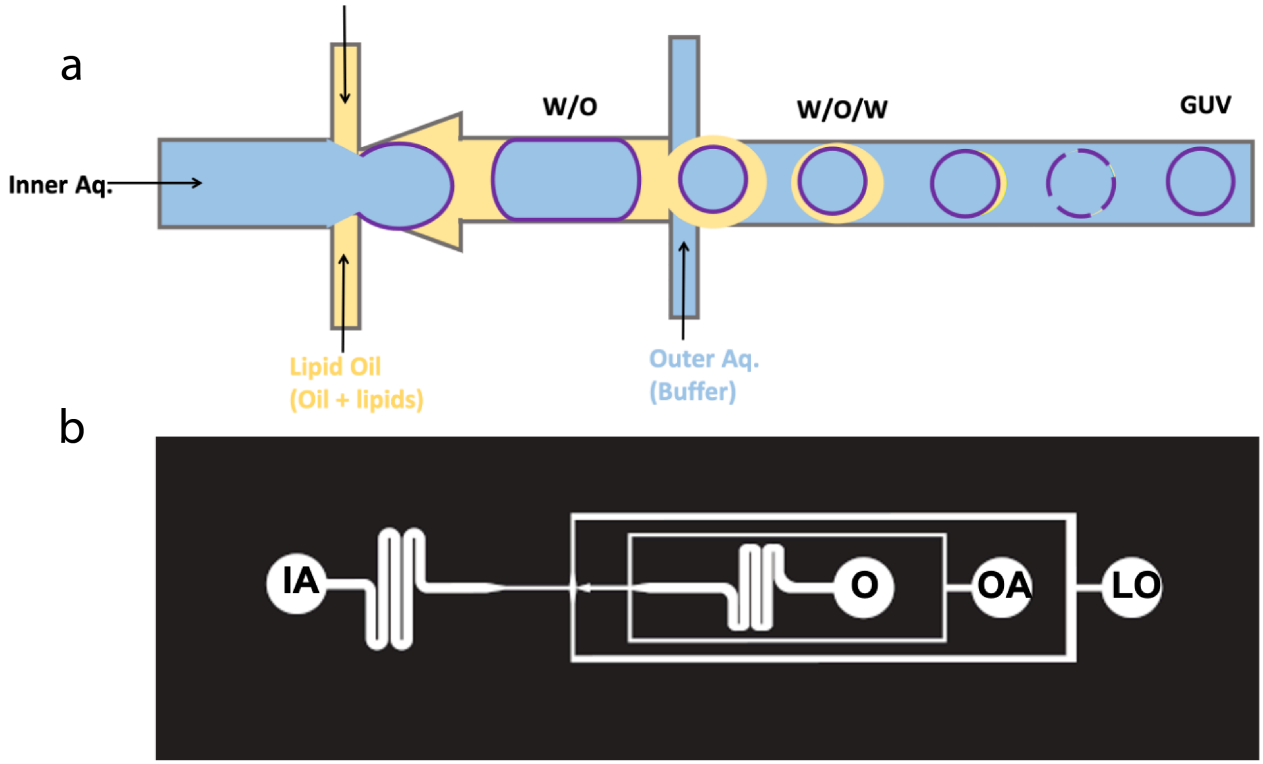

Figure 3.10: One-inlet microfluidic device design to form GUVs. (a) Schematic illustration of formation of GUVs using double cross-junction microfluidic device. (b) Design (mask) of a microfluidic chip used to fabricate monodisperse GUVs with two serpentine modules for better flow stability [116].

junction connected to outlet for collection of vesicles. Here both modules act as fluidic resistors and maintain the flow stability for longer duration. However, the second serpentine module not just maintains the stability of the flow but provides shear force required to remove the excess oil pockets from W/O/W double emulsion templates that finally aid in the formation of stable MVVs.

3.4.6 Addition of PEGylated lipids

Monodisperse GUVs are created using a W/O/W double emulsion technique and multi-compartment systems are formed by encapsulating LUVs in the IA (Fig 3.11a). At first, LUVs were produced using lipid film rehydration technique followed by extrusion using 400 nm membrane filter. The LUVs which were fluorescently labelled were then encapsulated within microfluidic GUVs. At first, the microfluidic chip is functionalized by surface treatment (see section 2.2.2) followed by pumping in OA through the channels and subsequently LO and then IA. The OA helps in wetting of the channels and therefore once all three fluids are introduced into the microfluidic device, the flow rates are tuned to produce MVVs of a desired diameter.

Fig 3.11b shows the production of MVVs by pumping the LUVs prepared

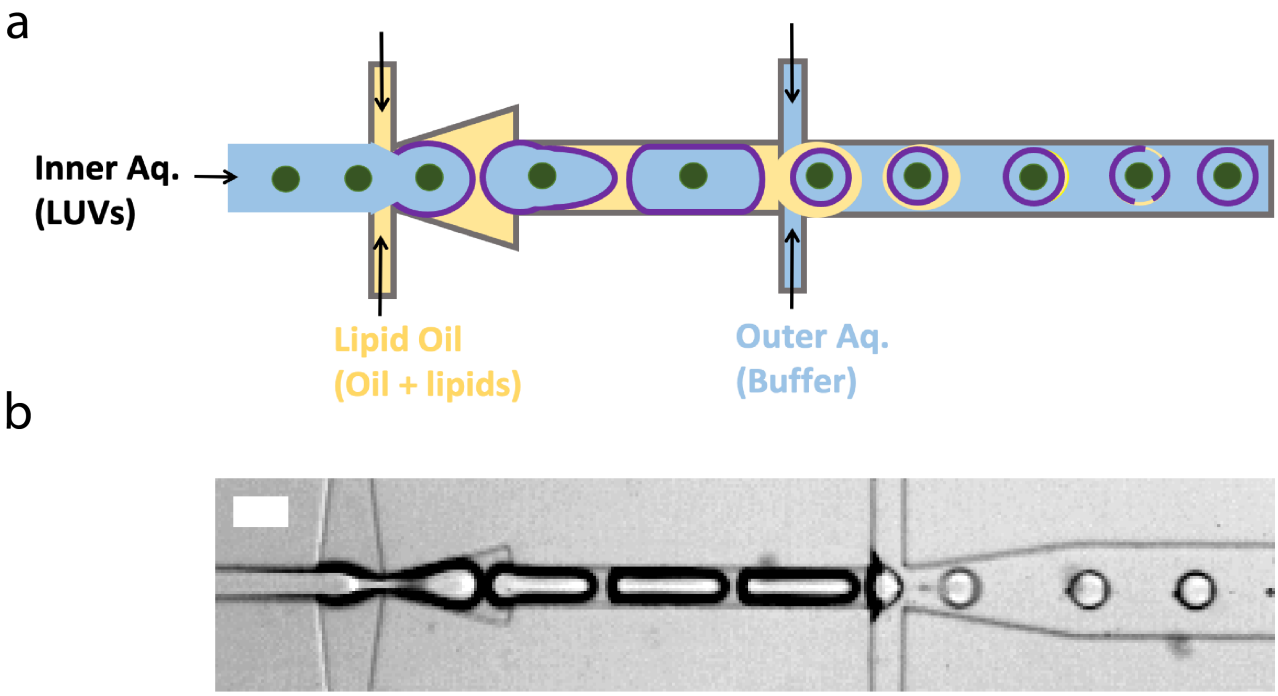

Figure 3.11: Microfluidic assembly of MVVs. (a) Schematic and (b) bright-field image of the microfluidic platform taken with a high-speed camera. Scale bar: 100 μm.

in 1X PBS buffer as IA and 1X PBS buffer as OA and lipid mix containing POPC: DOPG: Cholesterol: mPEG-DSPE (5 mg/ml) in 1-Octanol as LO. The pressures used for the formation of MVVs here was 50 mbar for the IA, 125 mbar for the OA and 50 mbar for the LO. At the second cross-junction, high pressure-induced flow rates are applied which are necessary to shear the W/O droplets to form W/O/W double emulsions. This method allows for the formation of double emulsion with very thin shells of oil phase, therefore low amount of 1-octanol are present in their membranes, which dewets spontaneously to form final multi-compartmentalized vesicles. The high lipid concentration (5 mg/mL) that is maintained for LO facilitates faster assembly of monolayer at the interfaces and therefore mitigates the need for surfactant to stabilize the MVVs.

In the initial set of experiments, a membrane composition of POPC: Cholesterol: DOPG labelled with NBD-PE lipids was employed for inner LUVs and outer GUVs comprised a membrane composition of POPC: Cholesterol: DOPG doped with Atto 633-PE lipids. The inclusion of cholesterol was to enable better integration of membrane pores such as αHL [124]. DOPG is a negatively charged lipid and having this in the composition in both LUVs and GUVs helps to avoid any fusion events of inner compartments with outer GUV membrane by electrostatic repulsions. Following encapsulation of thus formed LUVs within GUVs, several bursting and aggregation events of LUVs were observed at the inner leaflet as depicted in Fig 3.12. The green fluorescence

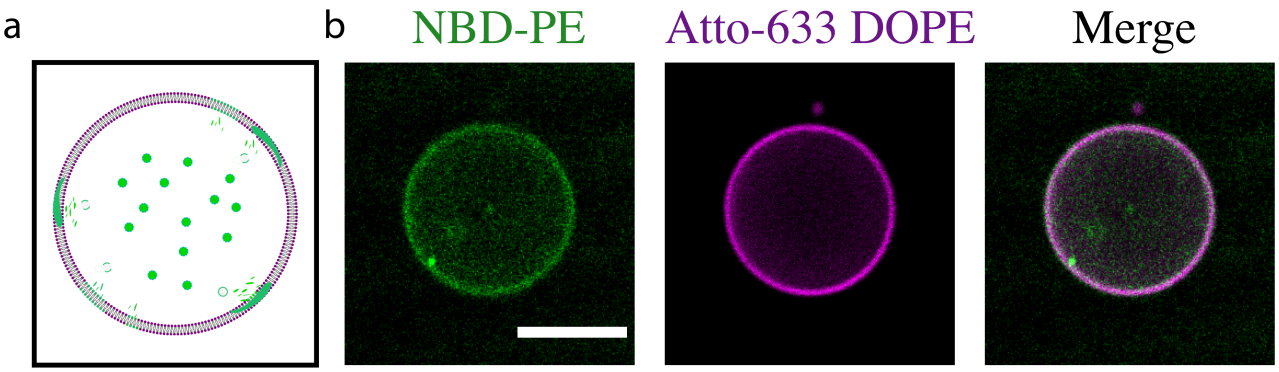

Figure 3.12: Generation of MVVs in the absence of PEGylated lipids. (a) Schematic representation of bursting of LUVs and aggregation on the membrane (b) Confocal images of burst inner LUVs (green channel) at the outer GUV membrane, outer GUV (purple channel), and the merged image (left-most panel). Scale bar: 50 μm.

signal in the outer environment shows the unencapsulated inner LUVs.

To mitigate this issue, the membrane lipid composition was altered to include PEGylated lipids to avoid bursting events. PEGylated lipids exhibit amphiphilic properties, and the inert PEG moiety blocked any interaction between opposing membranes. Traditionally, this strategy has been used for clinical purposes in liposomal preparations to increase the vesicle lifetimes in circulation [125]. PEG-lipid conjugates have also shown a significant steric barrier activity and stabilization against fusion and aggregation of LUVs [126], and this property has been explored here in this thesis for uniform encapsulation of inner LUVs in outer GUVs. It has been previously reported that incorporation of PEGylated lipids in the lipid formulations is beneficial for future *in vivo* applications [127]. Therefore, the addition of 1 mol% DSPE-PEG lipids led to successful encapsulation of LUVs within outer GUVs without any rupture as shown in Fig 3.13. The confocal merged image (Fig 3.13b) shows the absence of green fluorescence signal at the membrane of the GUVs which

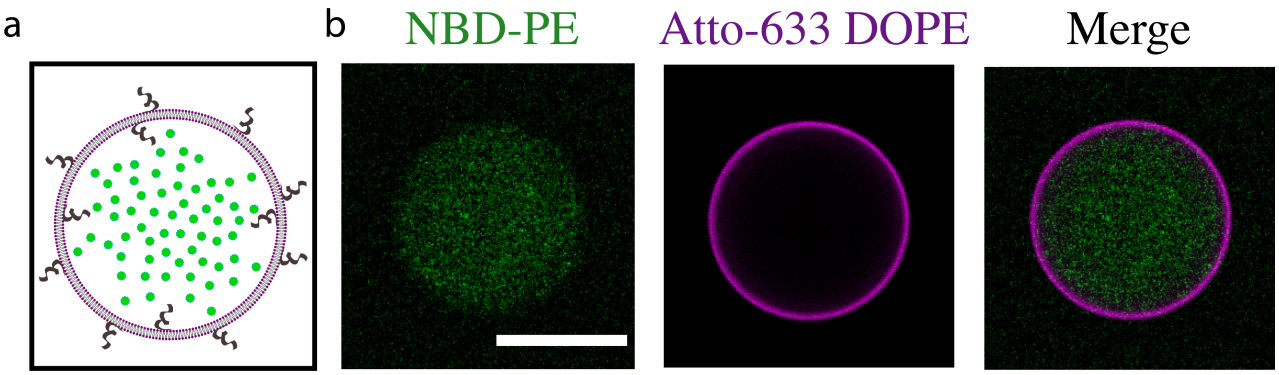

Figure 3.13: Generation of MVVs with the addition of PEGylated lipids. (a) Schematic representation of inner LUVs encapsulated within outer GUVs. (b) Confocal images of burst inner LUVs (green channel) at the outer GUV membrane, outer GUV (purple channel), and the merged image (right-most panel). Scale bar: 50 μm.

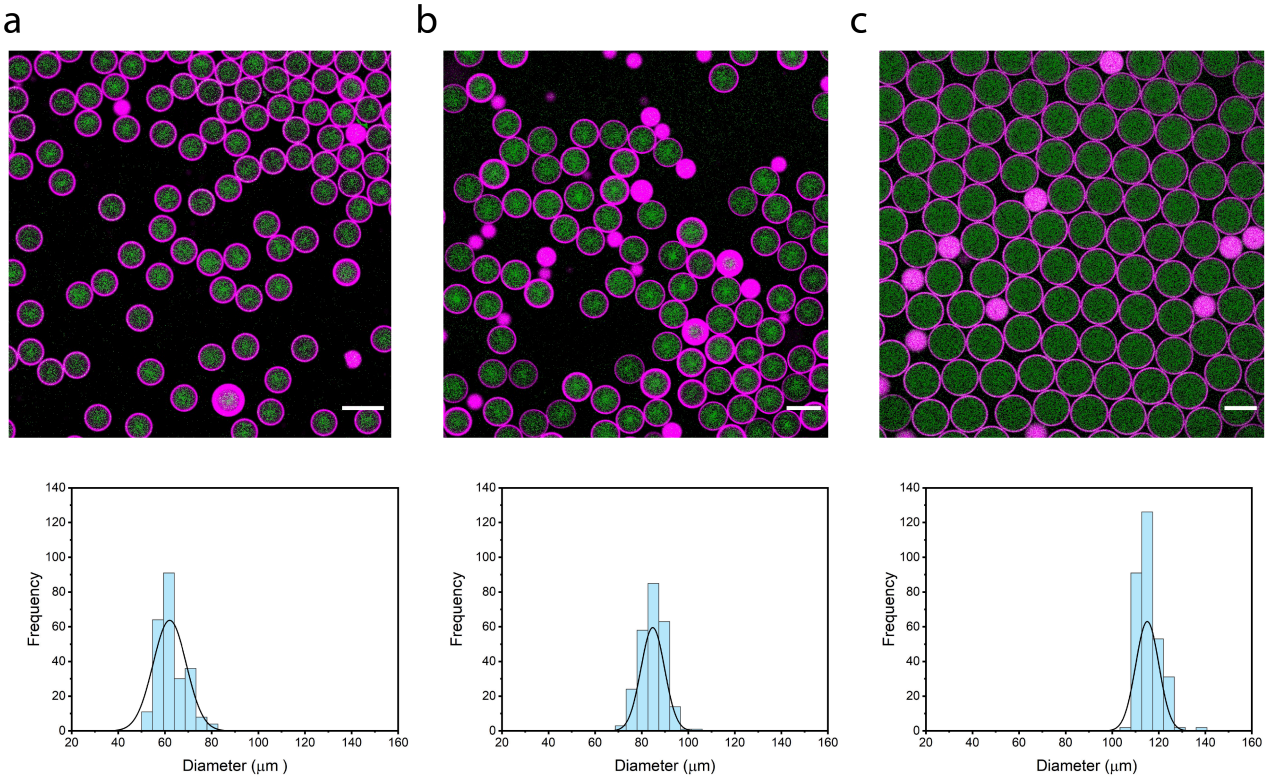

Figure 3.14: Size distribution of MVVs produced with one-inlet microfluidic device. Inner LUVs (green) encapsulated within outer GUVs (purple). Mean size diameter of (a) 62.02 ± 7.07 μm with an RSD of 11 %. (b) 84.74 ± 5.01 μm with an RSD of 6 % (c) 115.05 ± 4.94 μm with an RSD of 4 %. Scale bar: 100 μm.

confirmed no loss of inner compartments *via* LUV bursting. The absence of green fluorescence in the exterior of GUVs further confirmed successful high encapsulation of LUVs within GUVs. This emphasized the importance of employing PEGylated lipids in multi-compartmentalized systems as it allows lossless encapsulation.

3.4.7 Formation of monodisperse MVVs with tunable sizes

The inner LUVs are encapsulated within the outer GUVs using a one-inlet microfluidic device as described in Fig 3.11. The monodisperse population of MVVs was achieved with tunable size diameters. This was achieved by changing the ratio of pressure-induced flow rates at the IA, LO and OA. In Fig 3.14a, a mean size diameter of 62.02 ± 7.07 μm MVVs with a relative standard deviation (RSD) of 11 % was obtained by applying pressures of 98 mbar at the IA, 140 mbar at the OA and 115 mbar at the LO. In Fig 3.14b, a mean size diameter of 84.74 ± 5.01 μm MVVs with an RSD of 6 % was obtained by applying pressures of 65 mbar at the IA, 110 mbar at the OA and

95 mbar at the LO. In Figure 32c, a mean size diameter of 115.05 ± 4.94 μm MVVs with an RSD of 4 % was obtained by applying pressures of 70 mbar at the IA, 96 mbar at the OA and 79 mbar at the LO. Larger RSD values for smaller MVVs was attributed to the low control over the formation of double emulsion templates at the second cross-junction due to high flow rates required to form smaller diameter size MVVs [116]. The corresponding histogram plots show a narrow size distribution of MVVs with size diameters which are readily tunable.

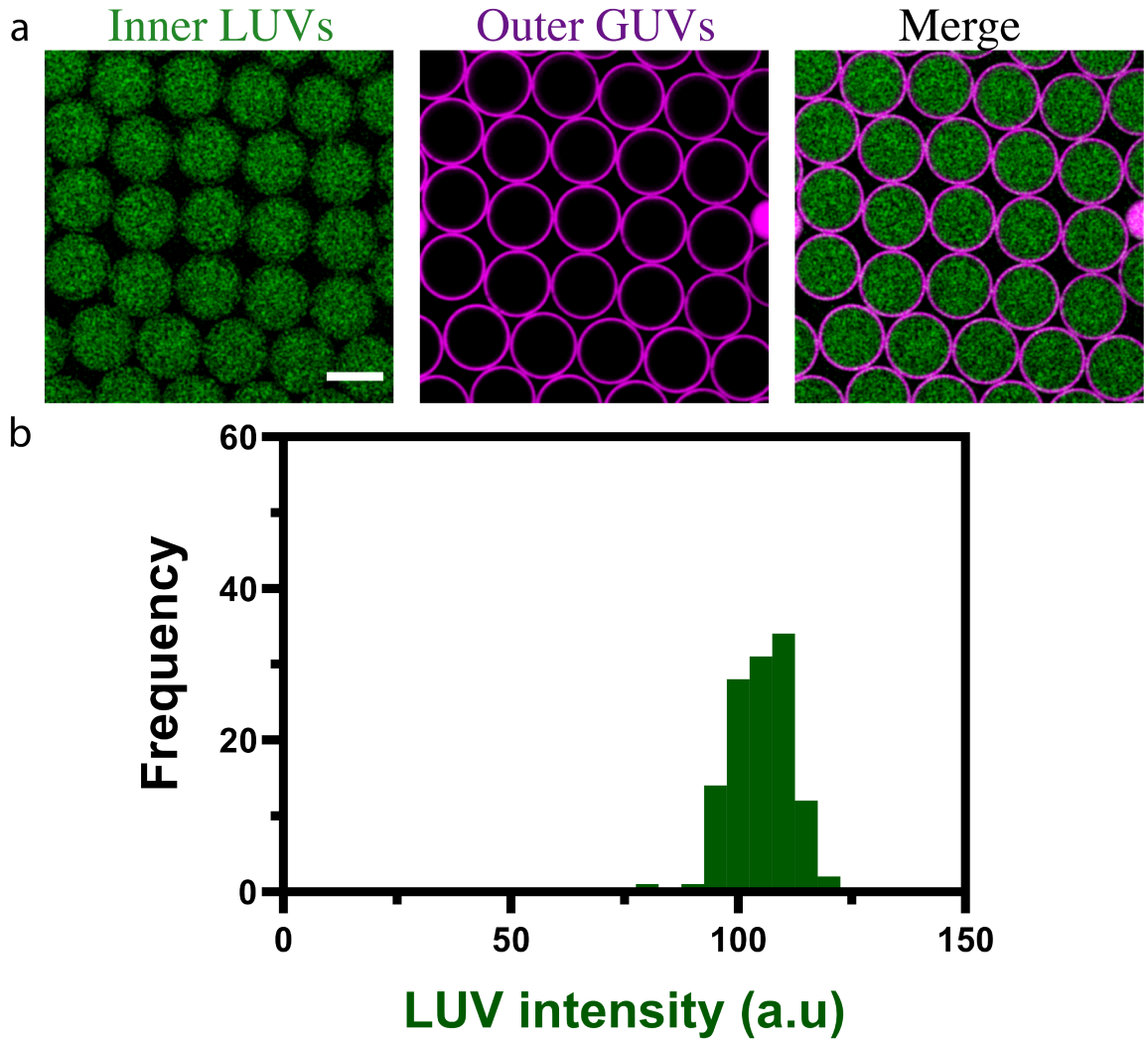

Figure 3.15: Uniform encapsulation of inner LUVs in MVVs.(a) Confocal fluorescence image of the monodisperse GUVs (purple) with inner LUVs (green). Scale bar: 100 μm. (b) Histograms showing the mean intensities of the inner LUVs (n = 123).

Therefore, microfluidic approaches allow for high-throughput formation of lipid vesicles of varying diameters which can be used as monodisperse artificial cell models. It also allows for faster analysis of large populations of multi-compartment systems of precise composition. The encapsulated LUVs maintained their integrity with high and uniform encapsulation of inner compartments within the monodisperse MVVs. The advantage of the monodispersity

of MVVs was that one could readily compare the effects of compartmentalization with increasing complexities in compartment systems. The enzyme and substrate concentrations can be adjusted to remain equal across all compartment systems as they would have same volumes owing to the monodispersity and uniformity of the microfluidic GUVs/MVVs compared to the bulk methodologies shown in Fig 3.9 that formed polydisperse population of MVVs.

3.4.8 Uniform encapsulation of LUVs in GUVs

Another key advantage of microfluidics was the uniform encapsulation of inner compartments within outer GUVs. Fig 3.15a show the confocal images of inner LUVs with uniform green fluorescence signal throughout the population of MVVs thus having an added advantage of high/uniform encapsulation along with the monodispersity. The multi-compartment systems were obtained with uniform encapsulation of LUVs as shown in the histogram plot (Fig 3.15b). Homogenous encapsulation of inner LUVs was attained with a uniform mean intensity of 104.9 ± 6.4 a.u. and an RSD of 6 % compared to low encapsulation of inner compartments in outer GUVs as observed in bulk methodologies (see section 3.4.3).

The microfluidic device with one-inlet was employed as described previously to create one- and two-compartment systems and in the next chapter a novel two-inlet microfluidic device is introduced to build complex three-compartment systems. And furthermore, previously described three-enzyme cascade reaction was implemented within these systems which is discussed in detail in Chapter 4.

Chapter 4

Directed chemical communication in microfluidic-based artificial cells

This chapter describes the formation of a more complex three-compartment systems using novel microfluidic approaches. In Chapter 3, the advantages of using microfluidic technology for the formation of MVVs over other bulk methodologies was demonstrated. Here, a two-inlet design to form multi-compartmentalized systems which co-encapsulate two different population of inner compartments (*i.e.* LUVs) within outer compartment (*i.e.* GUVs) is introduced. Furthermore, the previously described three-enzyme chemical cascade reaction (section 3.1) was incorporated to span across different inner compartments and the outer microfluidic GUV. The reaction pathways are directed spatially by functionalizing size-selective membrane proteins (namely αHL and OmpF) into the membranes of specific compartments. Finally, direct comparisons are derived between bulk and compartmentalized systems with increasing order of complexities.

4.1 Methods

4.1.1 Reconstitution of OmpF in GOx-LUVs

The reconstitution of outer membrane protein (OmpF) was carried out as mentioned in a previously reported protocol [128]. Purified stock OmpF (5.5 mg/mL) prepared in a 1 % solution of n-octylpolyoxyethylene detergent, was diluted 1:1 in the same detergent and vortexed. 1 μL of this freshly diluted

OmpF solution was added to 199 μL of the LUVs/GUVs solution and incubated at room temperature for an hour. The GUVs with OmpF were further utilized for poration assay of OmpF whereas the LUVs functionalized with OmpF pores were flowed through PD-10 columns to remove the detergent and unencapsulated molecules. GOx-LUVs were prepared according to section 3.3 with a variation by addition of 1 % DPhPC lipids for reconstitution of OmpF pores. The eluted volume containing LUVs were collected for further encapsulation to form multi-compartment systems.

4.1.2 Generation of α-Glc-LUVs

LUVs were formed using the thin-film hydration and extrusion method followed by three times freeze thawing. A lipid mixture (5 mg/mL) containing POPC: DOPG: Cholesterol: DSPE-mPEG: Atto 390 in a 78.9:10:10:1:0.1 ratio was dried in a 5 mL glass vial under argon and placed under vacuum for 2 hours. The lipid film was then rehydrated with a 1X PBS buffer containing 2 U/mL enzyme α-Glc to a final concentration of 5 mM. It was then freeze-thawed three times followed by extrusion 11 times with a 400 nm filter.

4.1.3 Assembly of αHL in α-Glc-LUVs

α-Glc encapsulating LUVs (α-Glc - LUVs) were pre-incubated with a final concentration of 5 μg/mL αHL in 1X PBS buffer at room temperature for 1 hour which can self-assemble to form pores. α-Glc-LUVs embedded with αHL pores were flowed through PD-10 columns to remove the unencapsulated enzymes. The eluted volume containing LUVs were collected for further encapsulation.

4.1.4 Dynamic light scattering to determine size radius of LUVs

LUVs with 400 nm diameter were prepared by extrusion with a membrane filter of 400 nm. The size distribution of the LUVs was determined by dynamic light scattering (DLS) analysis using a Zeta Sizer Nano ZS (Malvern, UK).

4.1.5 Microfluidic generation of compartmentalized systems

Double emulsion templating for the formation of microfluidic GUVs is conducted using the procedure previously reported [116]. In brief, enzyme solution or LUVs or both (in 1X PBS buffer) as the IA are pumped through

the microfluidic chip (using a pressure pump, MFCS-EZ, Fluigent Inc) to be sheared into uniform-sized W/O droplets at the first junction using a lipid oil of 5 mg/mL concentration in 1-octanol. The W/O droplet suspension was further sheared by pumping PBS buffer as the OA at the second junction to form double emulsion templates which undergo spontaneous dewetting process resulting in GUVs containing LUVs. In the case of the two-inlet microfluidic device, both inlets are supplied with two different LUVs in PBS buffer, and enzymes with α-Glc-LUVs as the IA solutions for the formation of the three-compartmentalized system. For the one-compartmentalized system, the enzyme solution was used as the IA solution.

4.1.6 Estimating the enzyme concentrations within MVVs

To keep the enzyme concentrations identical within all the systems used in this study, the concentrations of the LUVs were estimated using Triton X-100 based solubilization assay [129]. Briefly, LUVs produced after extrusion and PD-10 column separation were solubilized using 1% Triton X-100 containing 1X PBS buffer. Using fluorescence spectroscopic measurements, obtained intensities for Atto-390. PE and NBD-PE containing Triton X-100 lipid solutions were compared to that of starting lipid concentrations of 5 mM lipid solutions for lipid concentrations determination. Thus, determined lipid concentrations were used to calculate the concentration of LUVs in the MVVs. Finally, concentrations of the enzymes were calculated from the equation below:

$$C_{\frac{enzymes}{MVV}} = \frac{C_{\frac{enzymes}{LUV}} * n_{LUV} * V_{LUV}}{V_{MVV}} \tag{4.1}$$

where $C_{\frac{enzymes}{MVV}}$ = concentration of enzyme per MVV, $C_{\frac{enzymes}{LUV}}$= concentration of enzyme per LUV, n_{LUV} = number of LUVs enclosed in one GUV, $n_{LUV} = C_{LUV}V_{GUV}$ where C_{LUV} = concentration of LUVs , V_{GUV} = volume of GUV and V_{MVV}= volume of MVV.

Here $C_{\frac{enzymes}{LUV}}$ is 1 μM for GOx and 1.72 μM for α-Glc. And calculated final enzyme concentrations ($C_{\frac{enzymes}{MVV}}$) for GOx was 5.125 nM and α-Glc was 9.16 nM. The same enzyme concentrations were used in one-compartment and bulk systems.

4.1.7 Image Analysis using FIJI and Python

The images were processed on FIJI and analyzed using Python for detection of fluorescence within GUVs. The plots were created using GraphPad prism

and OriginPro9. Apparent time constants are calculated by fitting the kinetic curves to a single exponential function.

4.1.8 Labelling OmpF with fluorescamine

The number of amino acids present in the protein OmpF with free amino groups was calculated using ExPASy tool and 10 % of these amino groups were tagged by using fluorescamine with a final concentration of 0.7 mM. The stock fluorescamine was prepared at 35 mM in acetonitrile. After addition of fluorescamine to OmpF protein solution, it was vortexed immediately and placed at 4 °C for 2 hours.

4.1.9 Poration Assay

DPhPC GUVs labelled with membrane dye DiD (1,1'-dioctadecyl-3,3,3',3'-tetramethylindodicarbocyanine) formed using electroformation were reconstituted with OmpF labelled with fluorescamine. 20 μL of sucrose containing DPhPC GUVs were poured on top of 50 μL isotonic glucose solution and imaged with confocal microscopy. Fluorescein (10 μM) was added externally to detect the functionalization of Ompf pores. The control experiments were carried out in the absence of labelled OmpF protein.

4.2 Objectives

In this chapter, the aim is to build complex three-compartment systems using two-inlet microfluidic platform and to achieve directed chemical communication within them. Furthermore, the three-enzyme reaction network is implemented within one-, two-, and three- compartment systems. The final goal is to study the effects of confinement on enzyme cascade network by performing direct analytical comparisons between bulk, one-, two-, and three-compartment systems.

4.3 Results and Discussion

4.3.1 Chemical communication cascade in a one-compartment system

The three-enzyme reaction cascade previously tested and optimized in bulk was at first implemented within a one-compartment system. The one-inlet microfluidic device (Figure 3.10) was employed to produce a one-compartment

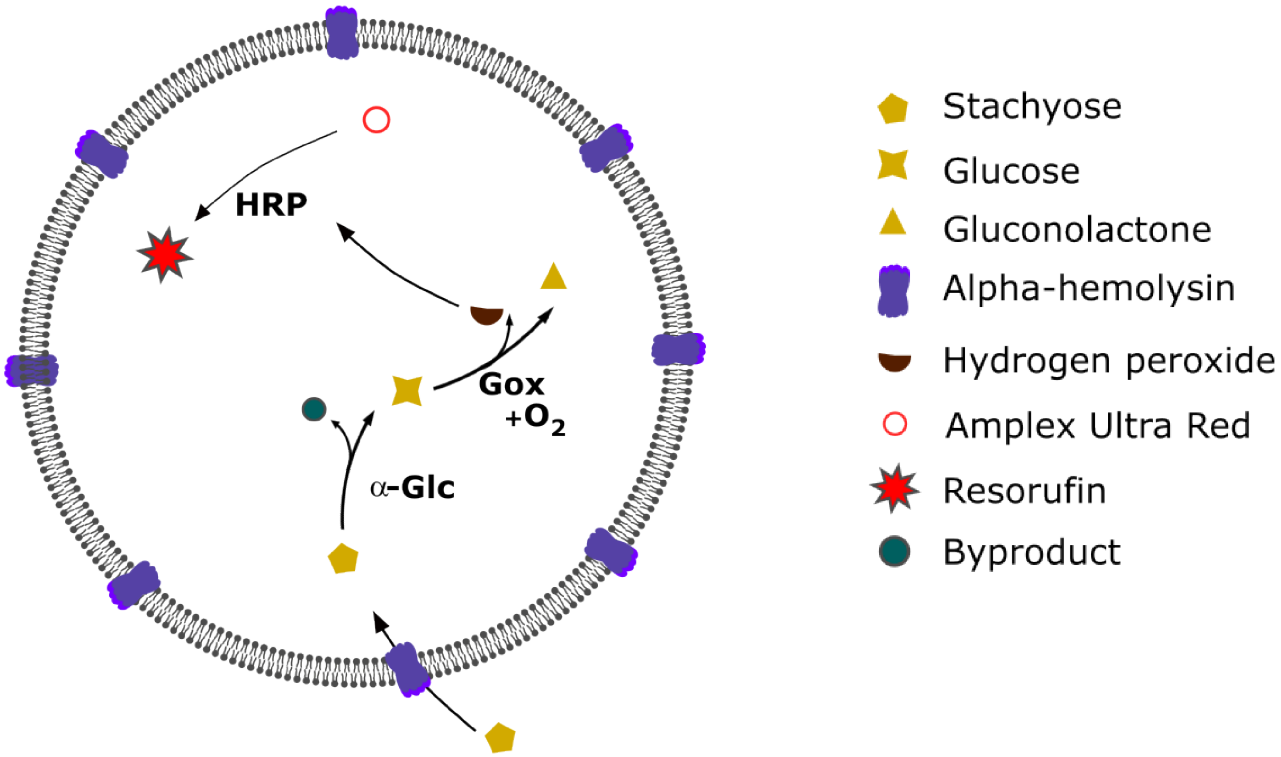

Figure 4.1: Schematic representation of one-compartment system with HRP, GOx, and α-Glc in the lumen of GUVs functionalized with αHL pores.

system containing all three enzymes HRP, GOx and α-Glc respectively. In order to have a temporal control over the reaction network, the trigger molecule stachyose was added externally after the formation of GUVs. The membrane of formed GUVs were functionalized with αHL (20 μg/mL) which was added at the same time as trigger molecule stachyose (50 mM). The protein self-assembles into lipid membrane to form heptameric pores enabling the passage of small molecules such as stachyose into the lumen of GUV [130]. Stachyose then initiated the entire signaling cascade within the GUV wherein three enzymes worked in cohort and rapidly converted the fluorogenic substrate AUR into final fluorescence product resorufin as shown in Fig 4.1.

Confocal microscopy was employed to monitor multiple GUVs simultaneously as depicted in Fig 4.2a over a period of 10 min. The increase in the fluorescence signal from the time point of initiation was observed after which the curve plateaued as shown in Fig 4.2b. Here for the formation of one-compartment systems with a mean size diameter of 75.3 $\pm$ 6.1 μm, pressures of 64 mbar at the IA, 50 mbar at the OA and 74 mbar at the LO was used. Here, an increase in the fluorescence signal post triggering with stachyose (Fig 4.2b, black line) which was higher compared to that measured in the absence of stachyose (red line) as well as in the absence of the enzymes GOx and α-Glc (green line) was observed. Fig 4.2c shows the endpoint measurements of the average fluorescence intensities which was significantly higher when the GUVs

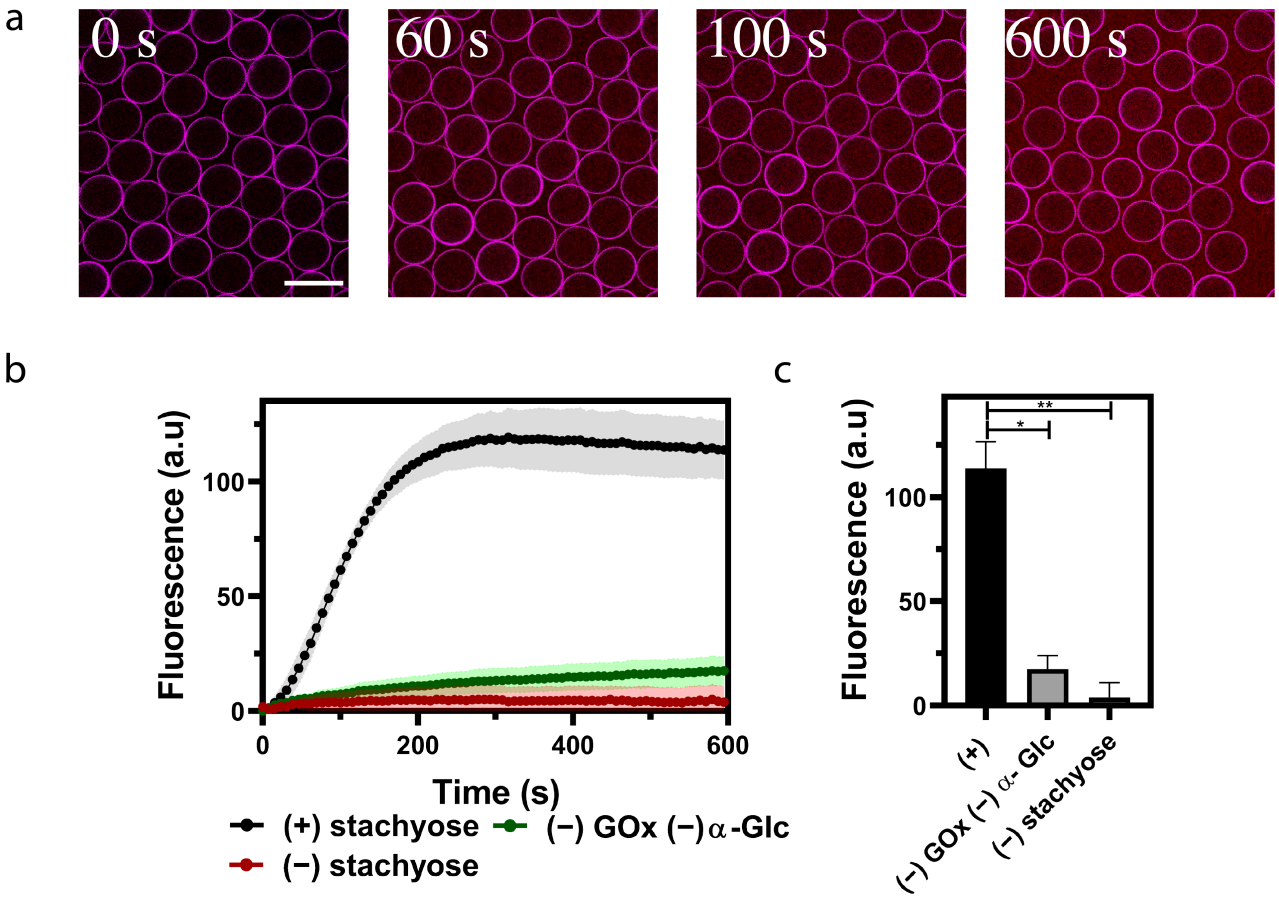

Figure 4.2: Chemical communication cascade in one-compartment systems. (a) Confocal fluorescence time series of multiple homogenous one-compartment GUVs with a mean diameter of 75.3 ± 6.1 μm after triggered externally with stachyose molecules via the αHL pores. (b) Average kinetic traces and (c) endpoints measurements of the resorufin signal ($P < 0.005$, unpaired t-test, $N \geq 2$ for the one-compartment system, - stachyose and - GOx - α-Glc controls respectively, $n \geq 50$). Scale bar: 100 μm.

were triggered with stachyose in comparison with controls (without stachyose and without enzymes respectively). Note that the successful functionalization of the membranes with αHL also confirmed the unilamellarity of our GUVs/MVVs. Owing to the uniform size distribution of the one-compartment systems with the help of one-inlet microfluidic device, high reproducibility in the product formation was observed that resulted in better statistical analysis of one-compartment system compared to bulk methodologies which provide low control over size of formed GUVs.

The formation of resorufin within one-compartment systems confirms the activation of reaction network within microfluidic GUVs. The resorufin signal was also observed outside of the GUVs which could be attributed to the leakage of resorufin molecules after its formation. However, for the analysis, the

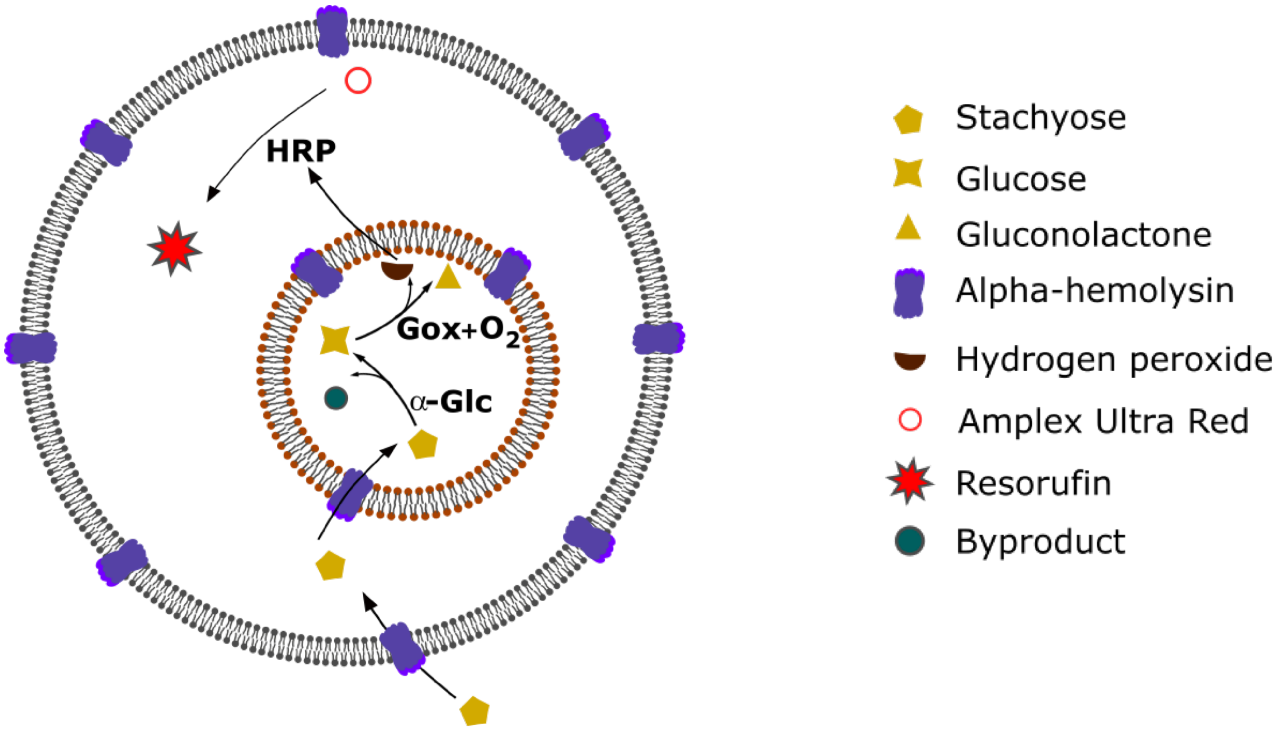

Figure 4.3: Schematic representation of the two-compartment system with HRP in the lumen of outer GUV, and with GOx and α-Glc further encapsulated within a population of LUVs (also embedded with αHL pores).

detection of fluorescence is mainly from within the GUVs in all compartment studies. The slight increase in resorufin signal in control experiments could be attributed to the non-specific oxidation of AUR resulting in low resorufin signal.

4.3.2 Chemical communication cascade in a two-compartment systems

As a second step towards increasing the spatial control, the enzymes were confined within two distinct compartments in a two-compartmentalized system that was fabricated with the one-inlet microfluidic device. Here the three-enzyme pathway was implemented within them as shown in Fig 4.3. Inner LUVs containing GOx and α-Glc were co-encapsulated with enzyme HRP within a GUV.

First, the diameter of our LUVs was investigated using dynamic light scattering (DLS) to measure the dispersion of sizes after passing them through PD-10 columns. This was carried out to check for the integrity of LUVs before encapsulation within multi-compartment systems using microfluidics. LUVs were consistently found to have a mean diameter of 400 nm as shown in Fig 4.4. Note that this was also performed for bulk studies (data not shown in

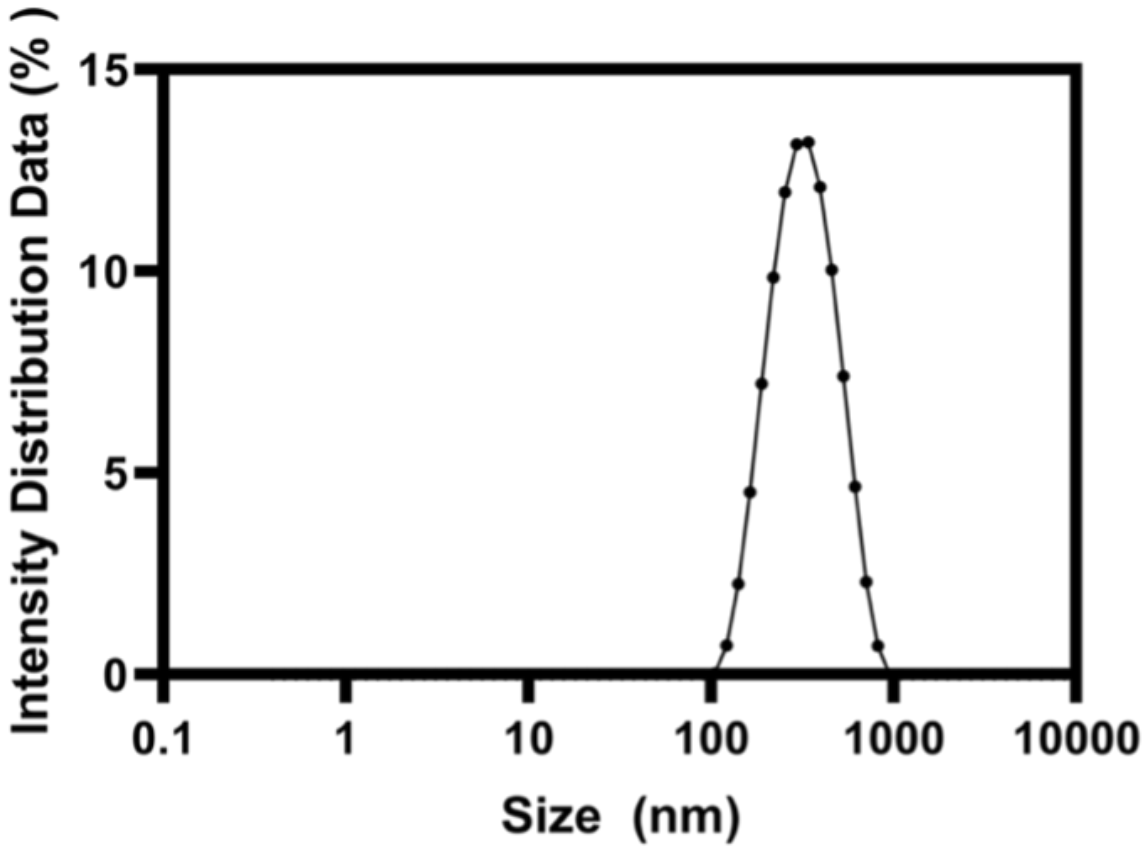

Figure 4.4: DLS data of the inner LUVs sizes which are used for the multi-compartment systems.

Chapter 3 as only microfluidic formation of MVVs was employed for further studies). A normal size distribution of the formed LUVs showed that there was no bursting or aggregation of LUVs since no other corresponding peaks were observed confirming that the LUVs maintained a uniform size distribution.

For the two-compartmentalized systems with a mean size diameter of 70.2 $\pm$ 4.9 μm, the pressures of 65 mbar at the IA, 110 mbar at the OA and 95 mbar at the LO were applied. The inner LUVs labeled with Atto 390-DOPE (first panel), the GUVs labeled with Atto 633-DOPE (second panel), the resorufin channel (third panel) and the merge images (fourth panel) showed an increase in the resorufin fluorescence within them over a period of 10 min (Fig 4.5).

Stachyose molecules entered the GUVs *via* αHL incorporated GUV membranes and then into the inner LUVs *via* αHL and is broken down to form glucose molecules by the catalytic reaction of α-Glc. Glucose is then oxidized by enzyme GOx to generate H_2O_2 and gluconolactone. H_2O_2 then freely diffused across the bilayer of inner LUVs out into the lumen of the GUVs containing HRP and subsequently triggered the formation of the final product resorufin within the lumen of the GUV.

The resorufin fluorescence within MVVs was measured (Fig 4.6a) and the

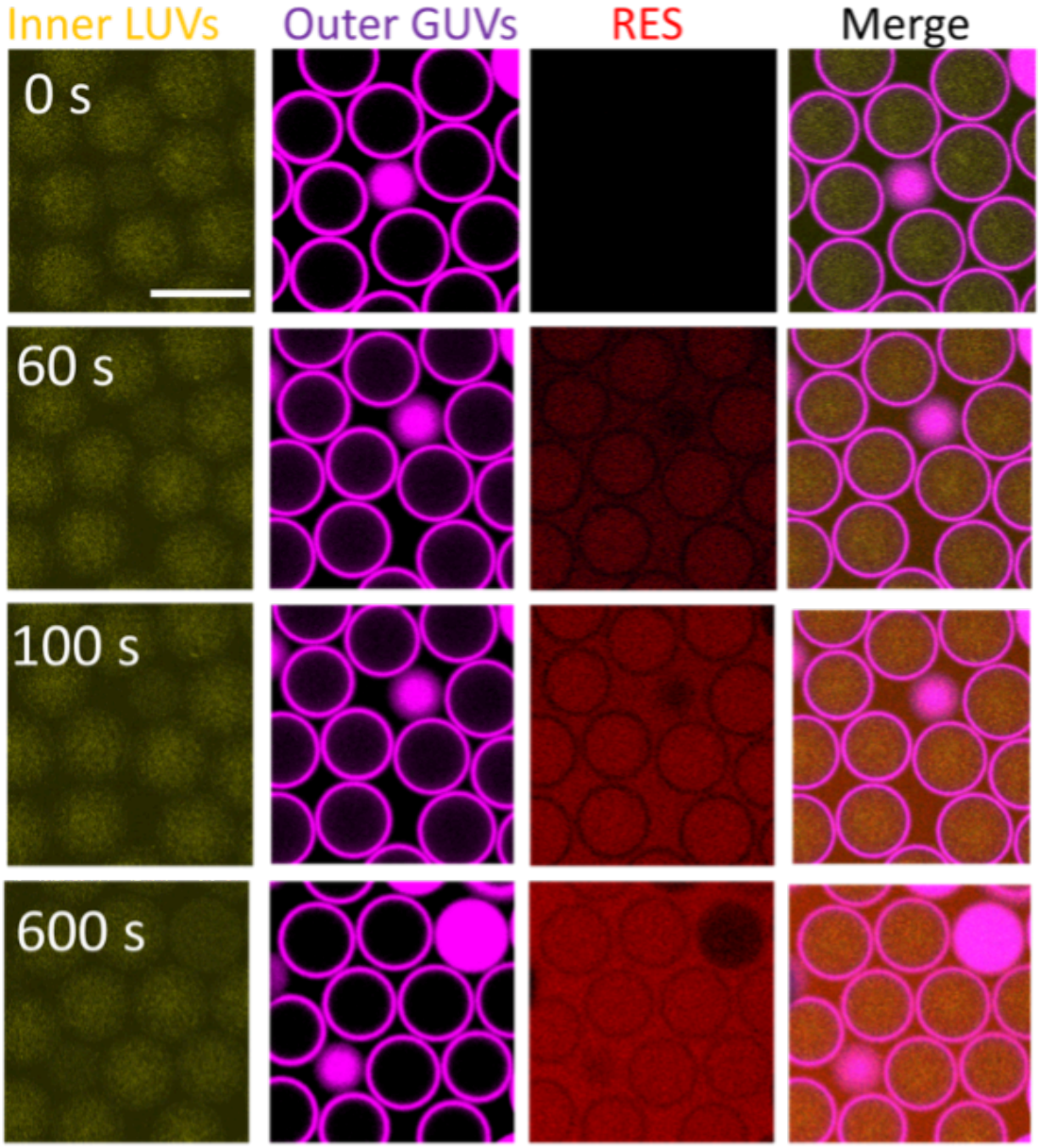

Figure 4.5: Chemical communication cascade in two-compartment systems. Inner LUVs tagged with Atto-390 DOPE lipids (yellow channel), Outer GUVs tagged to Atto-633 DOPE lipids (purple channel), resorufin (red channel), and merge channel. Scale bar: 100 μm.

kinetic measurements revealed an increase in fluorescence intensities when the cascade was initiated with stachyose (black line) in contrast to control experiments, in the absence of stachyose (red line) as well as in the absence of GOx and α-Glc (green line). The endpoint measurement showed a significant increase in resorufin fluorescence intensities as compared to controls (Fig 4.6b).

The inner LUVs also maintained their integrity during the duration of the experiment as shown in the Fig 4.7a. The fluorescence intensity from the LUVs during the duration of experiment remained constant which confirmed

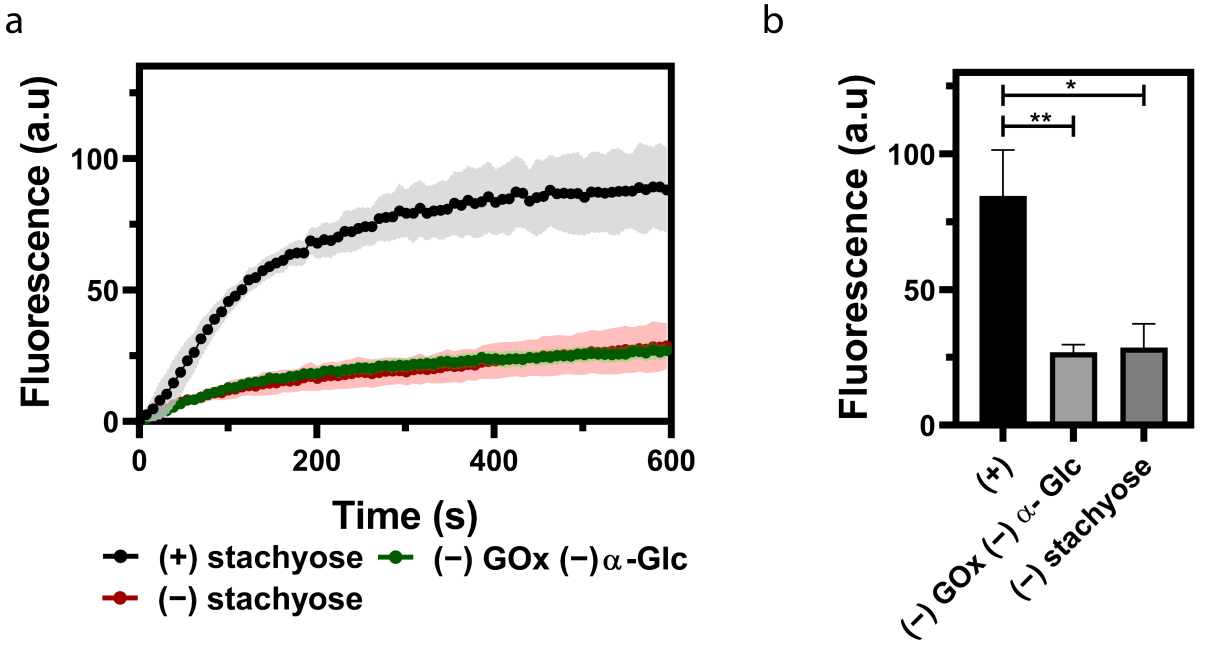

Figure 4.6: Kinetics and endpoints of reaction network in two-compartment systems. (a) Average kinetic traces and (b)endpoints (right) of the resorufin signal ($P < 0.005$, unpaired t-test, $N \geq 2$ for the two-compartment system, - stachyose and - GOx - α-Glc controls respectively, $n \geq 50$). Error bars are taken from the standard error of the mean. Scale bars: 100 μm.

no bursting of LUVs or aggregate formation. This showed there was no leakage of enzymes from within the LUVs into the GUV lumen. Fig 4.7b show confocal images of inner LUVs from the initiation point (0 s) until the end of the experiment (600 s).

The overall rate of the resorufin product formed was observed to be slower in two-compartment system compared to one-compartment system. This could be attributed to the additional number of barriers *i.e.*, LUV membrane in case of two-compartment system. It has been reported that multiple bilayers cause enhanced diffusion resistance for the intermediates such as glucose [131]. This can result in the slowing down of the reaction kinetics in two-compartment system.

4.3.3 Chemical cascade communication in a three-compartment system

The next step was to create a complex hierarchical architecture with three distinct compartments by co-encapsulating two different populations of LUVs within microfluidic GUVs. Here a two-inlet microfluidic device to co-encapsulate two different LUV populations with different membrane composition and internal components is introduced. The two populations of LUVs

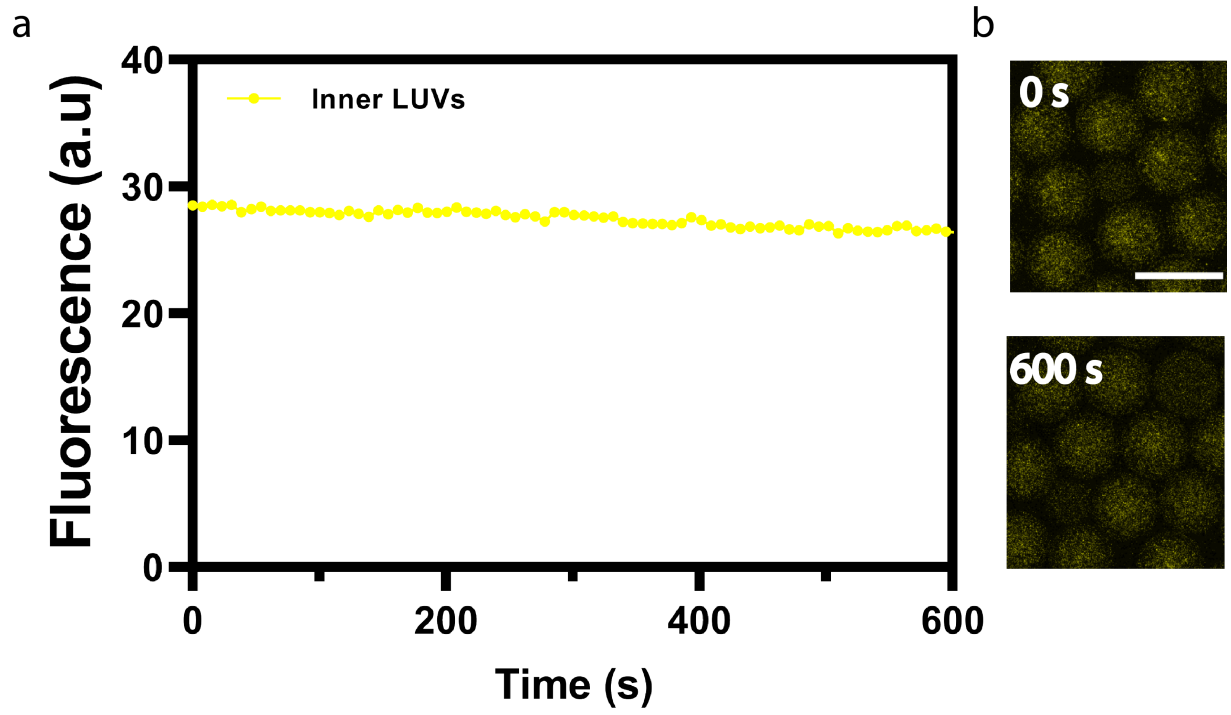

Figure 4.7: Fluorescence intensities of encapsulated inner LUVs within two-compartment system. (a) Intensities of encapsulated inner LUVs fluorescently labeled with Atto 390 DOPE within the two-compartment system during the reaction. (b) Confocal images of inner LUVs at 0 s and 600 s. Error bars are taken from the standard error of the mean (n = 40). Scale bar: 100 μm.

were kept separate before encapsulating them into the W/O droplets formed at the first junction. Following which, it is then sheared at the second junction to form W/O/W double emulsions which spontaneously dewets to form three-compartment GUVs as shown in Fig 4.8. This segregation is to avoid cross-contamination of the LUVs with left-over membrane pores (if any). Moreover, it promoted efficient co-encapsulation of the two inner LUV populations to form distinctive sub-compartments and generated more complex MVVs as one can also tune the flow rates at IA to obtain different ratios of encapsulated inner compartments within the MVVs.

The three-compartment system was established with the goal to have a directed chemical cascade in specific sequence thus having an advanced control over the MVVs. This was achieved by having size-selective membrane pores incorporated into two distinct populations of LUVs, which allow the permeability of certain reactant molecules into specific compartments. Here, membrane protein OmpF was reconstituted within GOx-LUVs and αHL was reconstituted to α-Glc encapsulating LUVs (α-Glc-LUVs). Stachyose, a tetrasaccharide which has a molecular mass of 666.66 Da, can only enter the α-Glc-LUVs *via* αHL pores. The resulting glucose with a molecular mass of 180.15 Da can then pass into the LUVs containing GOx-LUVs *via* OmpF pores, which pre-

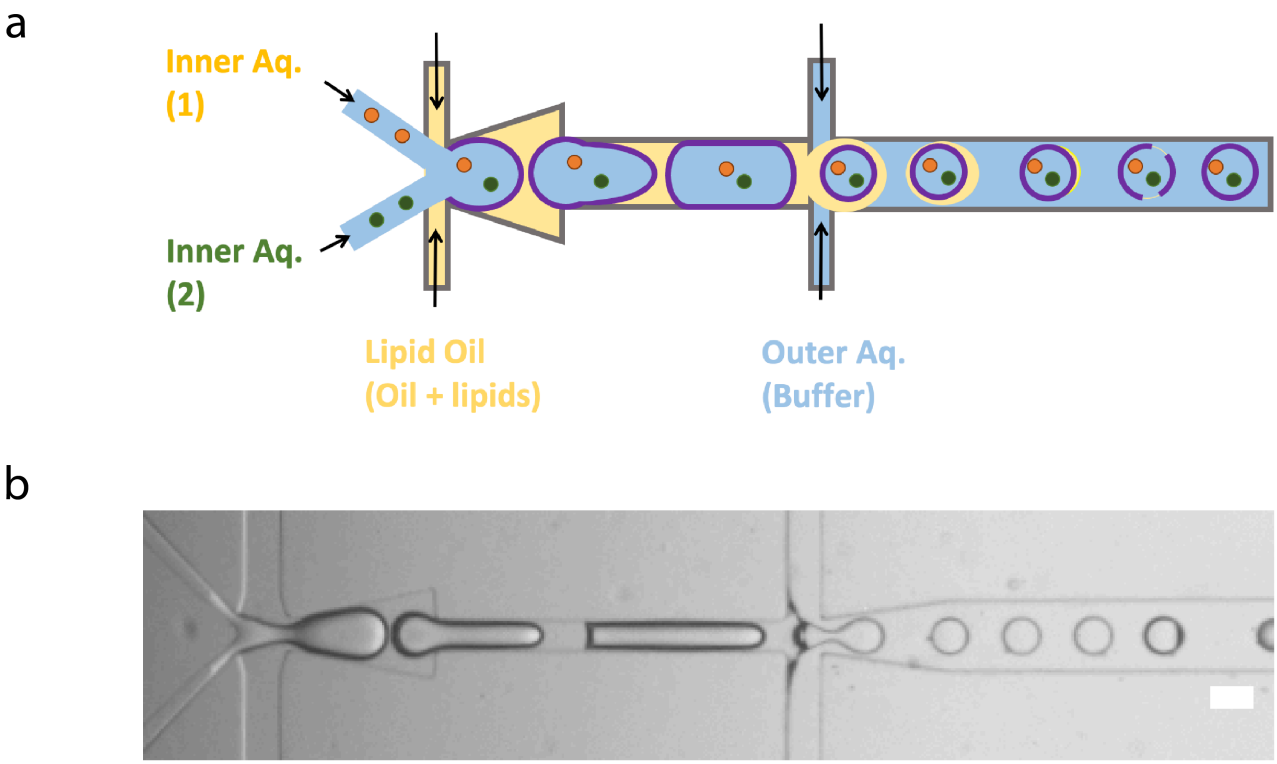

Figure 4.8: A two-inlet microfluidic platform. (a) Scheme and (b) bright-field image of the two-inlet platform encapsulating two distinct LUV populations in the double emulsion templates and subsequently undergoing dewetting to render MVVs. Scale bar: 100 μm.

vents molecules above 400 Da from entering [132]. This forms a basis for the size-selective chemical communication between two synthetic organelles (inner LUVs) within artificial cells (outer GUVs).

At first, the lipid composition suitable for efficient reconstitution of membrane channel protein OmpF was investigated. The inclusion of DPhPC lipids in the GUV lipid composition mix confirmed a better reconstitution of the protein OmpF (data not shown) as previously shown in the reported protocol [128]. This could be attributed to the presence of more methyl branches that provides higher bilayer stability [133]. Therefore, these literature studies confirmed that the addition of lipid DPhPC within GOx-LUVs was extremely important for better reconstitution of OmpF pores into the membranes. Furthermore, to confirm the effective incorporation of membrane protein OmpF, the labelling of the protein with fluorescamine was carried out for 2 hours at 4 °C (see section 4.1.8). This facilitated the detection of the reconstituted OmpF on the lipid membrane of the GUVs. Fig 4.9a shows the confocal images of GUVs reconstituted with OmpF protein labelled with fluorescamine as described in section 4.1.9 and the corresponding intensity plots show the increase in fluorescence intensities on the membrane (Fig 4.9b). Note that the fluorescence from the background is due to the incorporation of fluorescamine to the casein coated wells although it did not interfere with the signal from

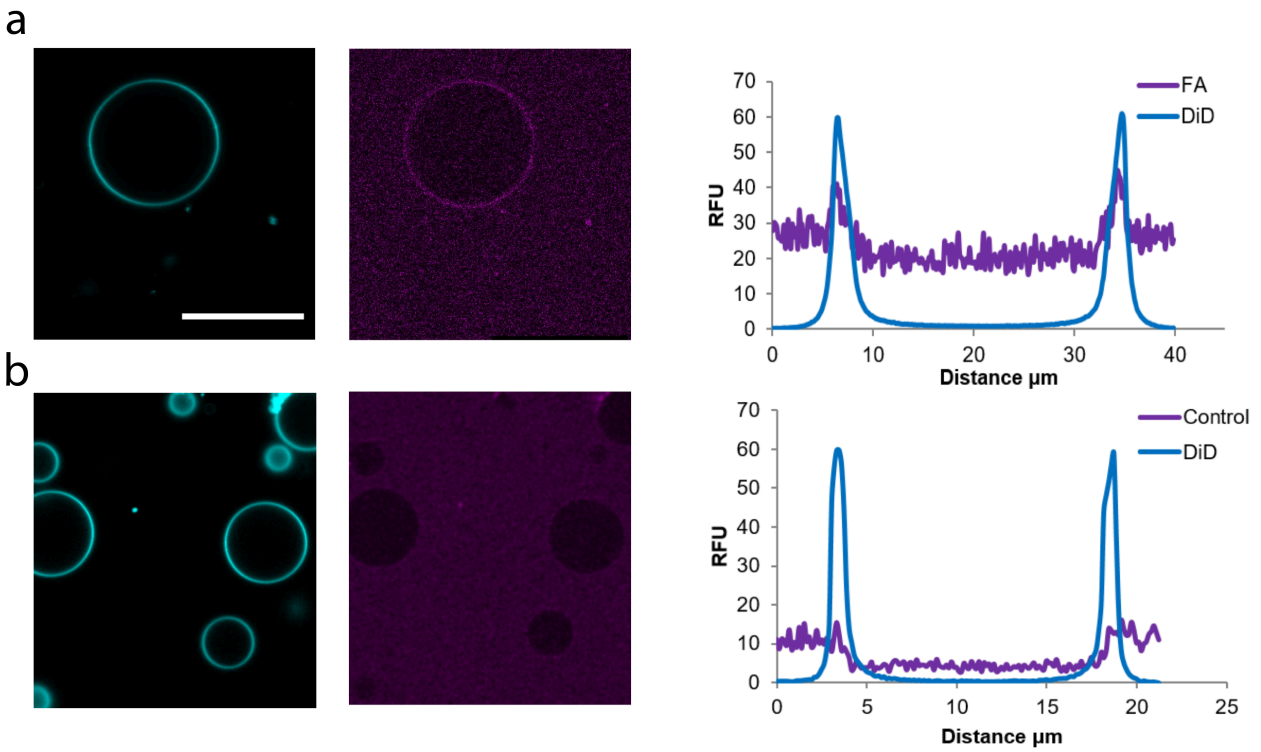

Figure 4.9: Reconstitution of fluorescamine labelled OmpF protein in electroformed GUVs (a) POPC:DPhPC GUV tagged to membrane dye DiD (cyan channel) and fluorescamine tagged to OmpF integrated into the membrane(purple channel). On the right the intensity plots of fluorescamine and DiD, fluorescamine intensity peaks present at the membrane corresponding to DiD labelled membrane. (b) Control experiments in the absence of OmpF showing GUVs (cyan) with no fluorescamine signal (purple) at the membrane and the corresponding intensity plots (on the right). Scale bar: 25 μm.

OmpF which is only detected on the membranes of GUVs. This confirmed the successful incorporation of OmpF in GUVs. The control experiments in the absence of OmpF reconstituted within GUVs was diluted in isotonic glucose solution that showed no presence of fluorescence signal on the membrane of GUVs showing that fluorescamine does not on its own integrate into the membrane.

The next step was to check the poration of the GUVs due to the reconstitution of OmpF into the membranes. 10 μM fluorescein in glucose buffer was externally added to the GUVs and the fluorescence signal was monitored inside the GUVs. The fluorescein signal was detected within the GUVs reconstituted with OmpF and the control experiments showed no fluorescence within the GUVs thereby confirming successful incorporation of protein OmpF within the membranes as shown in Fig 4.10.

Therefore, to attain a temporal control over the cascade network, the membrane pores αHL and OmpF were integrated into the system and the trigger molecule stachyose was added externally. Stachyose molecules enter the outer

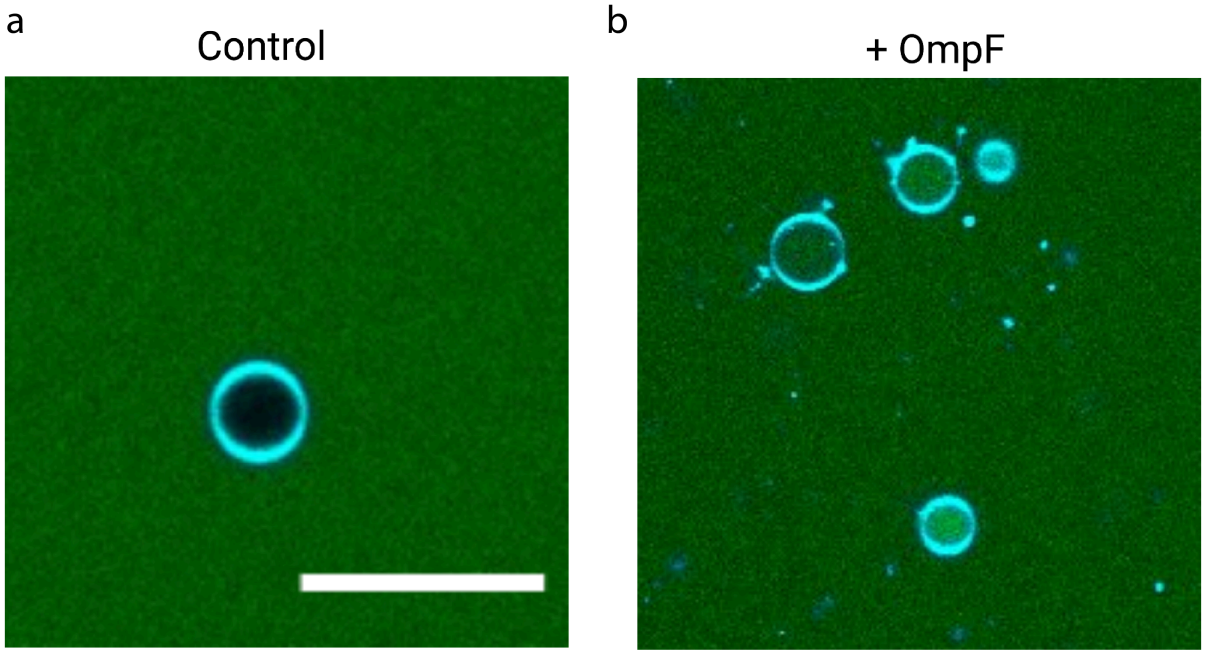

Figure 4.10: Permeability assay for OmpF integration in membranes. Confocal images of GUVs (cyan) (a) without OmpF and (b) with OmpF and fluorescein (green) added externally to check for active reconstitution of OmpF. Scale bar: 50 μm.

GUVs *via* αHL pores and subsequently enter α-Glc-LUVs where it is broken down into smaller glucose molecules, which in turn diffuses into the GUV lumen. Glucose molecules then enter the GOx-LUVs *via* OmpF pores where it is oxidized to form gluconolactone and H_2O_2. H_2O_2 can freely diffuse across LUV membranes into the lumen of GUV where the enzyme HRP converts AUR into fluorescent resorufin (Fig 4.11).

The efficient encapsulation of two sets of LUVs which are fluorescently labelled with Atto-390 DOPE for GOX-LUVs and NBD-PE for α-Glc-LUVs was achieved with the two-inlet microfluidic device. The co-encapsulation of both LUVs was uniform, and the fluorescence from the two LUV populations was detected over a period of 600 s as shown in Fig 4.12a. The time-dependent plots show the constant intensities thereby confirming that there was no bursting observed. Confocal images in Fig 4.12b show the fluorescently labelled LUVs at the time point of initiation (0 s) until the reaction duration of the experiment (600 s).

Time-lapse confocal images of GOx-LUVs (first panel), α-Glc-LUVs (second panel), outer GUVs (third panel), resorufin fluorescence observed (fourth panel), and MVVs encapsulating both sets of LUVs (fifth panel) are depicted (Fig 4.13). Following the addition of the external trigger stachyose, the corresponding images of resorufin signal (*i.e.*, red channel) show an increase in final fluorescence signal over a period of 600 s. To form three-compartment systems with a mean size diameter of 73.1 $\pm$ 7.2 μm, the pressures of 90 mbar at the

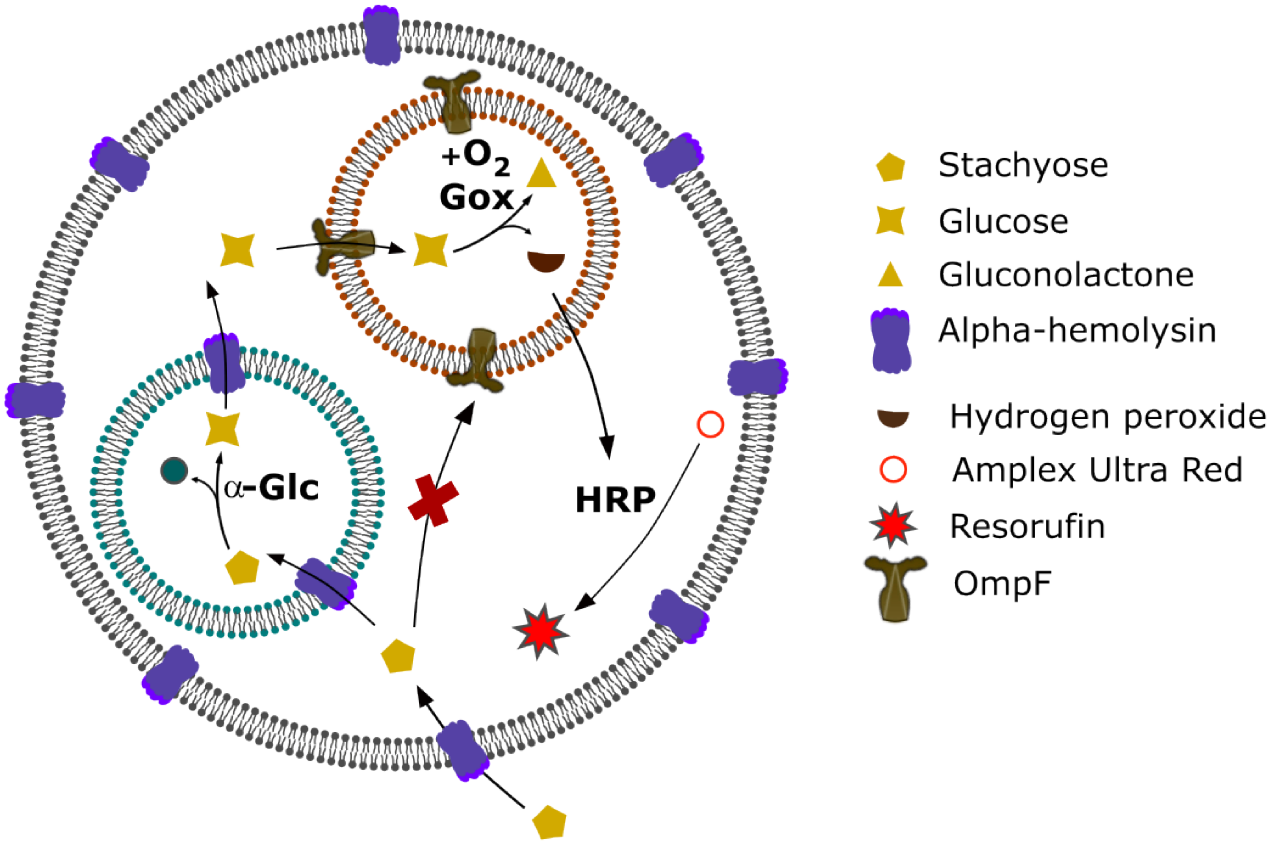

Figure 4.11: Scheme of three-compartment MVVs with an outer GUV enclosing GOx-LUVs, α-Glc-LUVs, and HRP.

IA (inlet 1), 90 mbar at the IA (inlet 2), 65 mbar at the OA and 115 mbar at the LO were applied.

The kinetics of the formed resorufin was analyzed when the entire cascade was activated within three-compartment system with trigger molecules, stachyose. An increase in formation of final product resorufin (black line) was observed in comparison with the control without stachyose (red line) and the control without α-Glc and GOx (green line) which showed no increase in fluorescence signal. This confirms that there was no spontaneous formation of resorufin due to non-specific oxidation of substrate AUR. An additional control was performed to confirm that the reaction proceeds in the desired sequence. Therefore, the reaction cascade mechanism was performed in the absence of OmpF in the GOx-LUVs (violet line). The non-formation of resorufin demonstrated that the integrity and stability of the LUVs are maintained as the membrane must be made permeable for the reaction to proceed. Endpoint analysis revealed a significant increase in resorufin fluorescence in comparison with the controls performed (Fig 4.14).

With the above observations, the successful activation of signaling cascade within the three-compartment system was achieved and furthermore the fabri-

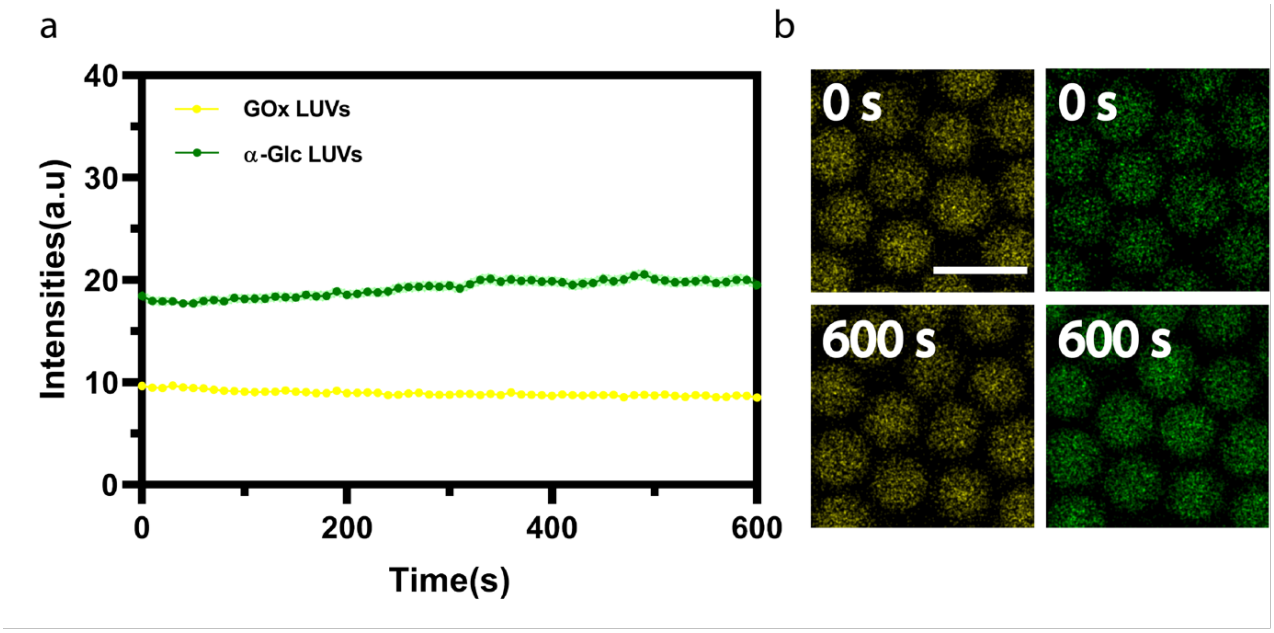

Figure 4.12: Fluorescence intensities of encapsulated inner GOX-LUVs and α-Glc-LUVs within three-compartment system. (a) Intensities of encapsulated GOx-LUVs fluorescently labeled with Atto 390 DOPE (yellow channel), and α-Glc-LUVs labeled with NBD-PE (green channel) within the three-compartment system. (b) Confocal images of fluorescently labelled LUVs at 0 s and 600 s. Error bars are taken from the standard error of the mean (n = 30). Scale bar: 100 μm.

cation of complex artificial eukaryotic cells was demonstrated using a two-inlet microfluidic device. The directed chemical pathways by incorporating size-selective channel proteins within inner LUVs and outer GUVs respectively was also described. In the next section, the effects of confinement on the entire chemical cascade and how it affects the overall rate of the reaction is discussed.

4.3.4 Effects of Confinement

After successful generation of three-compartment systems, the next focus was on understanding the significance of confinement in multi-compartment systems. Therefore, the open bulk system where enzymes are not confined were compared with one-, two- and three-compartment system wherein the enzymes are enclosed as shown in Fig 4.15. The effect of the increasing complexity of the system on the overall enzyme kinetics of the reaction network and the formation of final product resorufin was further investigated.

The open bulk-system was compared with all compartment systems as the enzyme concentrations per GUV/MVV were adjusted to be the same across all the systems. To do this, the trigger molecule stachyose and the substrate AUR was maintained at the same concentration for all systems. The same

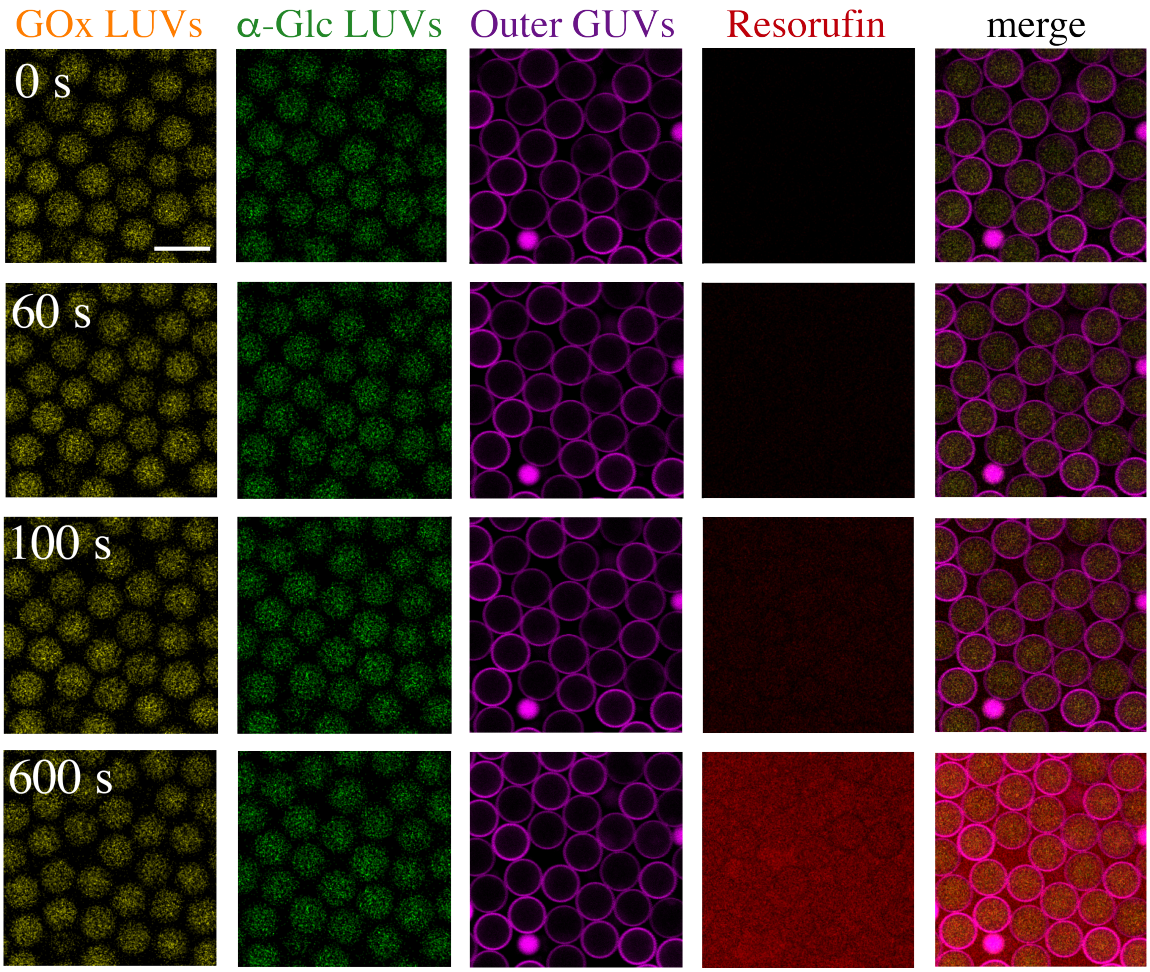

Figure 4.13: Confocal fluorescence time-series of the MVVs with a mean diameter of 73.1 ± 7.2 μm after input of the chemical trigger. GOx-LUVs tagged with Atto-390-DOPE and reconstituted with OmpF pores (yellow channel), α-Glc-LUVs tagged with NBD-PE and embedded with αHL pores, the outer microfluidic GUVs tagged with Atto-633-DOPE (purple channel) and resorufin (red channel) fluorescence over time. Scale bar: 100 μm.

concentration of enzymes was achieved by calculating the lipid concentration using Triton X solubilization assay. With the estimated lipid concentration as shown in Fig 4.16, the enzyme concentrations were calculated within MVVs using the Eq 4.1 (see section 4.1). Please note that the enzyme concentrations of the LUVs within GUVs were higher than the concentration of enzymes within one-compartment system but enzyme concentration per GUV/MVV were maintained to be equal across all systems. The estimated enzyme concentrations for HRP, GOx and α-Glc (see section 4.1) were maintained within bulk, one-, two- and three-compartment to carry out comparative analysis across the systems.

The compartmentalization affected the kinetics of the formation of final product resorufin as shown in Fig 4.17a. With the same amount of trigger molecule, stachyose and fluorescence substrate AUR, the steady state rate of the final product formed was higher in the confined systems than the open/bulk

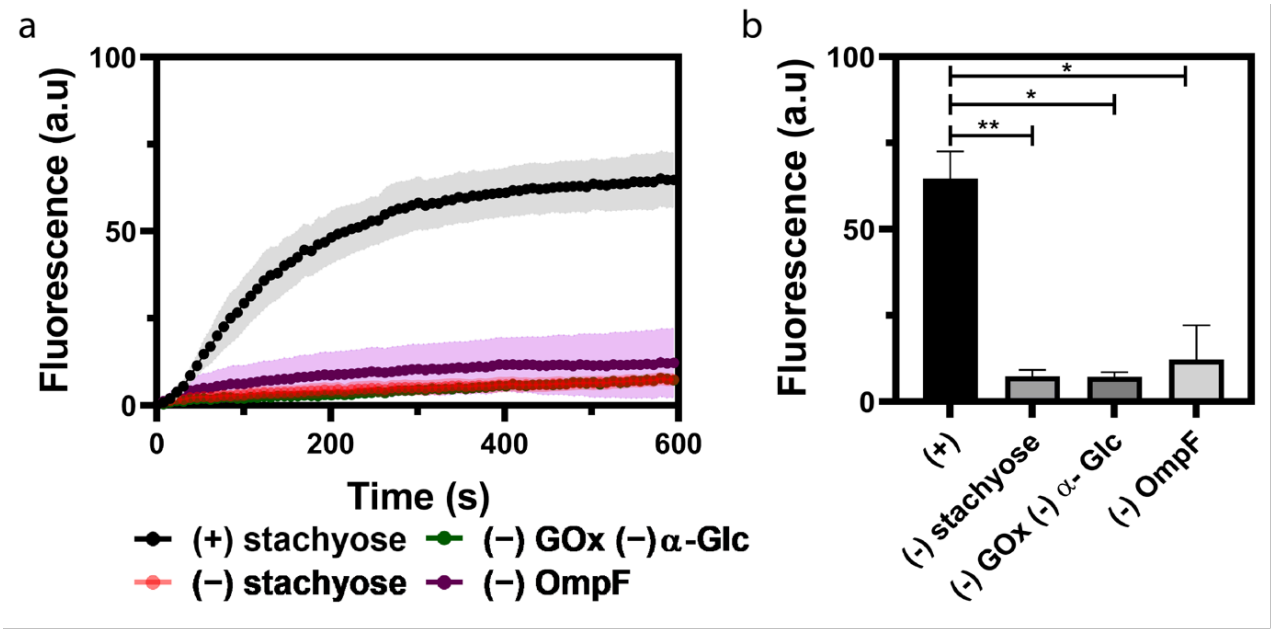

Figure 4.14: Kinetics and endpoints of reaction network in three-compartment systems. (a) Average kinetic traces (left) and (b)endpoints (right) of the fluorescent resorufin product formed as a final output of the successful initiation of the enzyme cascade. ($P < 0.005$, unpaired t-test, $N \geq 2$ for the whole system, - stachyose, - OmpF, and - GOx-α-Glc controls respectively, $n \geq 50$). Error bars are taken from the standard error of the mean.

system. The endpoints also confirmed this observation as seen in Fig 4.17b. This could be attributed to the presence of membrane surfaces, which have a significant effect on the kinetics of the cascade network [134]. However, the more likely reason is due to the greater diffusion lengths for reactants/ intermediates to reach their reaction sites in the open system compared to the bulk system [135]. Moreover, the available AUR and oxygen are consumed faster in open system due to their larger volumes and higher enzyme numbers in comparison to confined system which leads to lower endpoint values in open

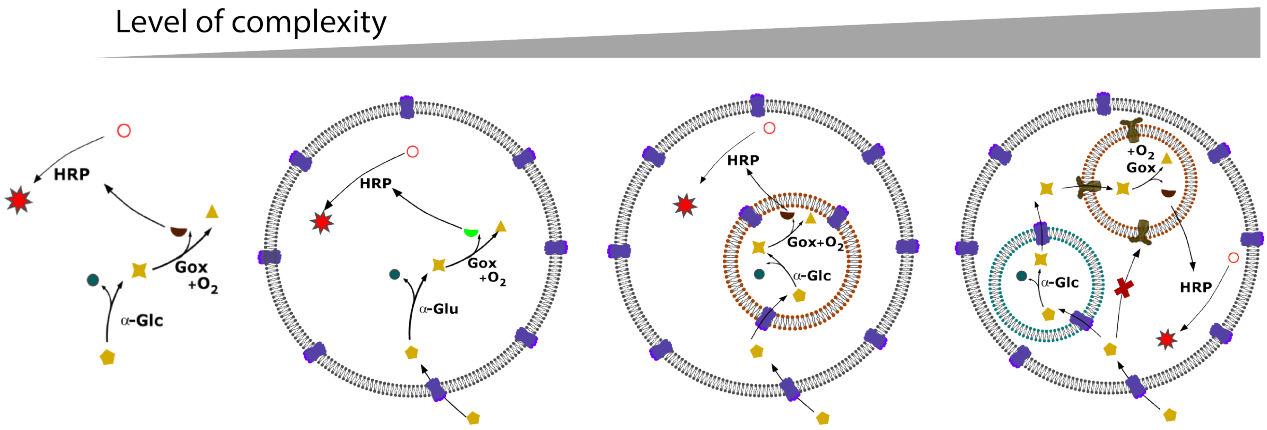

Figure 4.15: Schematic representation of the increasing levels of complexity from the bulk system to one-, two- and three- compartment systems.

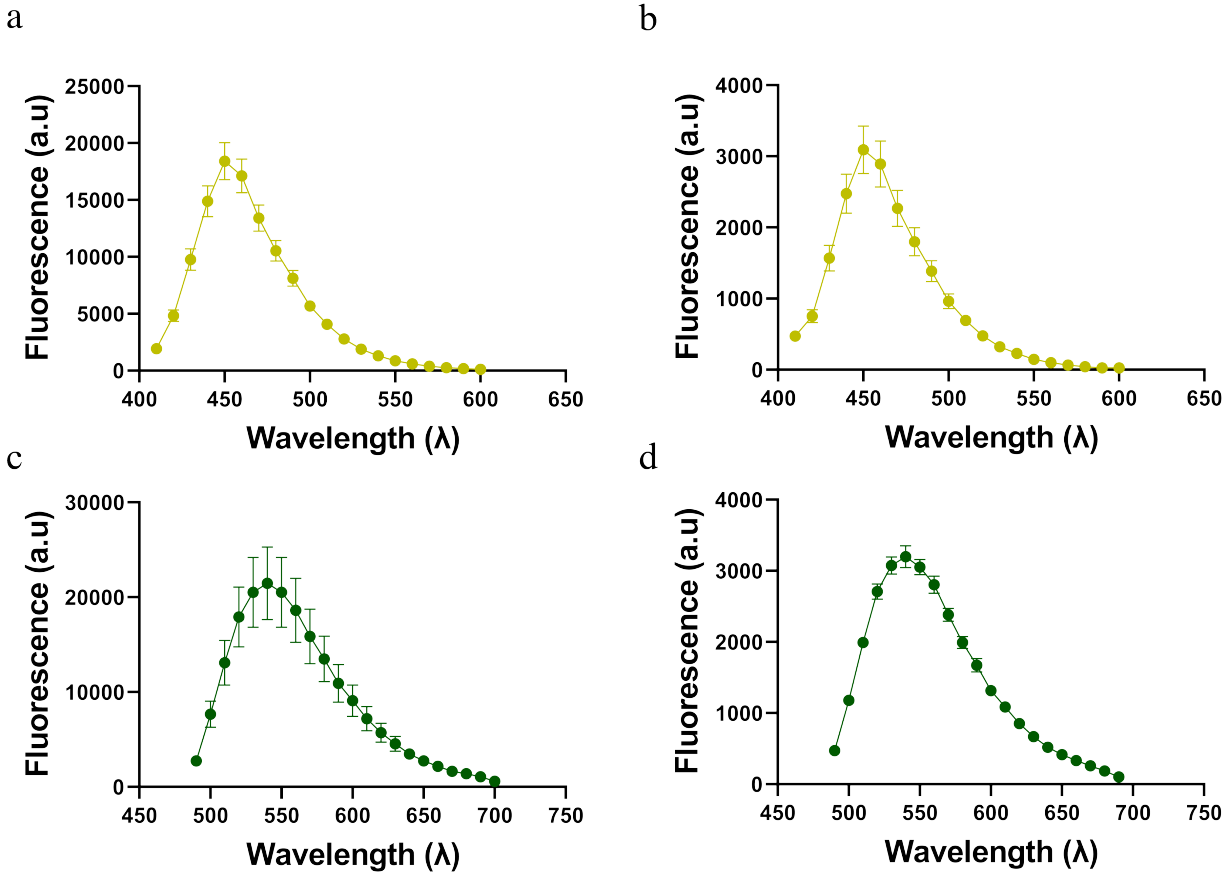

Figure 4.16: LUV lipid concentration estimation using Triton-X 100 solubilization assay. Fluorescence spectra obtained after solubilization of LUVs with (a) Atto-390, (c) NBD labelled lipids with starting lipid concentration 5 mM, and (b) Atto-390 (d) NBD labelled lipids after passing through PD-10 columns. Error bars in are taken from the standard error of the mean (n = 3).

system.

The observed reaction rate constants for the confined systems were higher than bulk system as shown in Fig 4.18a. Here the concentrations of enzymes per GUV/MVV are comparable and therefore kinetic plots were fit to a single exponential eq 4.2 below:

$$y = A(1 - e^{-t\tau}) \tag{4.2}$$

where A is the amplitude of the product signal, t is time and τ is rate constant(s^{-1})

The overall rate of product formation was higher in compartment systems when compared to bulk systems. Furthermore, the observed rate constants were lower in two- and three-compartment system compared to the one-compartment system and this could be attributed to the additional membrane barriers (*i.e.* LUV membranes) slowing down the transport of input and intermediate molecules to the reaction sites of the enzymes. Moreover,

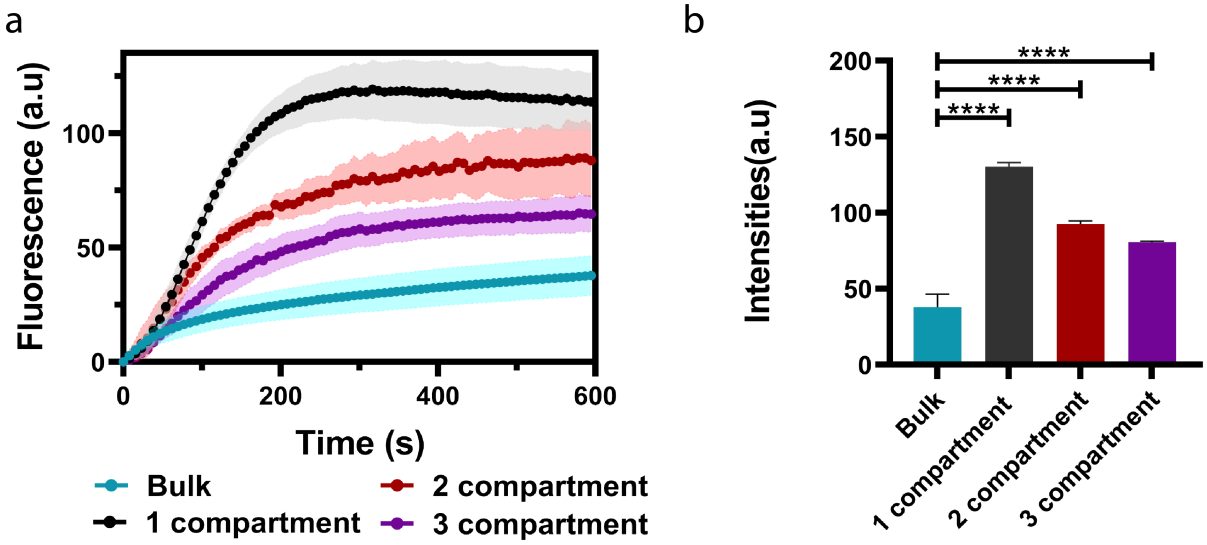

Figure 4.17: Comparison of enzyme kinetics and endpoints across all four systems. (a) Average kinetic traces of bulk, one-, two- and three-compartment systems. (b) Final resorufin intensities for bulk and compartment systems ($N \geq 2$). Error bars are taken from the standard error of the mean. ($P < 0.05$, unpaired t-test, n = 6, 85, 88, and 116 for the bulk system, single compartment, two-compartment, and three-compartment systems respectively).

one can assume that in two- and three-compartment systems with the presence of further membrane barriers, the intermediate glucose can diffuse out into the external environment before reaching the next site of reaction. This acts as a contributing factor towards product variability observed as seen in the endpoint steady-state analysis of one- and two-compartment systems.

The relative distributions of the final product resorufin is depicted using the violin plots (Fig 4.18b). The single-compartment system showed a bimodal distribution which denotes a higher variance in the product formed compared to multi-compartment systems. A narrow size distribution as seen in the case of three-compartment systems suggests an increased regulation in the cascade network when the enzymes are spatially separated in distinct compartments. Segregation of enzymes in different compartments as shown in the three-compartment system is advantageous as it avoids inactivation of the enzymes due to the presence of the intermediates formed such as hydrogen peroxide that could potentially inactivate GOx [46]. Furthermore, the enzyme-substrate equilibrium is shifted in the forward direction towards the formation of product as the formed product readily diffuses out of the compartment [136]. These two reasons could be attributed to the decline in the formation of low resorufin output whereas due to the presence of multiple membrane barriers, the intermediates have a higher chance of leakage out of the compartment rather than towards the formation of final product resorufin. This results in low probability of formation of high resorufin output. Both these effects re-

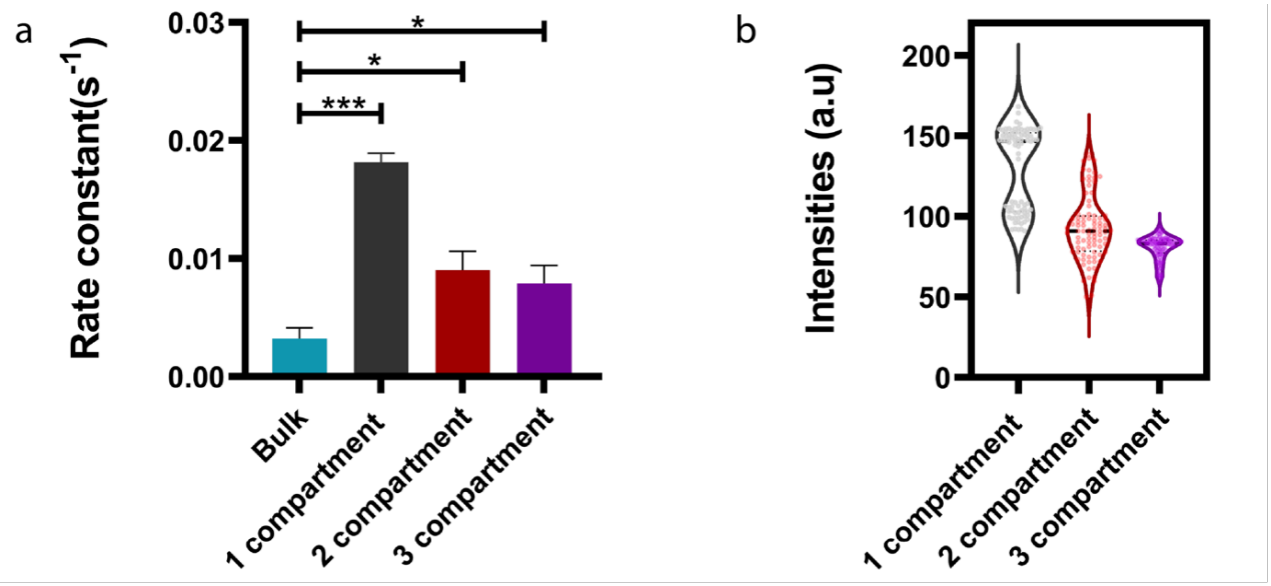

Figure 4.18: Comparison of rate constants across all systems and endpoint analysis of one-, two- and three- compartment system. (a) Apparent rate constants of bulk and compartment systems. ($N \geq 2$). Error bars are taken from the standard error of the mean. (P < 0.05, unpaired t-test, n = 6, 85, 88, and 116 for the bulk system, single compartment, two-compartment, and three-compartment systems respectively). (b) Violin plots of resorufin intensities across each of the different compartmentalized systems.

sult in tighter regulation and lowers the variability in product formation. This showed that spatially segregating enzymes in different compartments as shown in three-compartment system facilitated better control over the output which could be explored further for other multi-step biochemical processes.

Chapter 5

Induced cell-free expression of membrane proteins using PURexpress

This chapter focusses on the cell-free expression of membrane pore protein αHL in GUVs that are chemically induced with addition of transcription inducer molecules. At first, optimization of the cell-free expression system was carried out in bulk solutions followed by the integration of cell-free expressed αHL into artificial cell systems. The αHL cell-free expression was induced with a lipid membrane permeable small molecule N-(3-oxohexanoyl)-L-homoserine lactone (3OC6HSL) within and outside of GUVs. The permeability studies were also shown to determine the membrane transport activity in GUVs using fluorescence dye assay.

5.1 Cell-free expression

Gene expression can be defined as a flow of genetic information from DNA to gene product, beginning with the transcription of DNA to messenger RNA (mRNA) followed by translation of mRNA into protein [137]. Modern proteomics have facilitated various protein expression technologies to generate proteins in their natural folded state. Currently, protein expression could be divided into three categories:

1. chemical synthesis,
2. cell-based expression (*in vivo*)
3. cell free expression (*in vitro*)

Protein expression has been extensively employed in the field of biotechnology and more recently also in the field of bottom-up synthetic biology. One of the most commonly used protein expression technology is the cell-based recombinant protein expression using bacterial host *Escherichia coli* [138]. This model host organism has been well studied and well characterized to produce various heterologous proteins [139].

Membrane proteins play an integral role in biology and are involved in transport of nutrients and also act as active targets for immune response and drugs [140]. Membrane proteins can be expressed using heterologous systems by over-expression of protein of interest [141]. However, one of the disadvantages with over-expression methodology is the cellular toxicity due to expression of foreign proteins in non-physiological levels. Moreover, this methodology could result in protein aggregation and misfolding which leads to the loss of activity. An alternative approach is to reconstitute the purified protein into artificial membranes such as liposomes mediated with the addition of detergent to solubilize membrane proteins. However, the main drawbacks with this method were, firstly, the detergent extraction after reconstitution by dialysis which is time-consuming and laborious at times. Secondly, the dilution of protein detergent solution could lead to low protein concentration. To overcome these issues, another approach known as cell-free protein expression has been widely developed and first introduced in 1950s. Early cell-free expression systems (CFES) mainly contained endogenous mRNA to express the desired protein [142, 143]. Zubay and colleagues first reported the coupled transcription-translation system with DNA acting as a template for the synthesis of proteins [144]. More recently, CFES are becoming extensively popular in the field of synthetic biology for the *in vitro* expression of proteins in artificial cellular constructs [145]. One key advantage is that it offers a high degree of control over the chemical parameters governing the protein production such as plasmid concentration, quantity and type of amino acids, regeneration system *etc* [146]. It has been reported that synthesis of certain complex proteins, such as human growth factors, produced higher yields with cell-free systems compared to cell-based protein expression systems as it circumvented the issues of cell-based ones, such as metabolic regulation and homeostasis [147].

CFES mainly consists of cell extract that makes up the macromolecular components for transcription and translation, amino-acid module, tRNA synthetases, ribosomes, energy source such as adenosine 5'-triphosphate (ATP), other co-factors. Commercially available systems are used more frequently as it is a quick and simple way to synthesize proteins. The in-house protocol to formulate these systems is laborious since the preparation of cell-free extract and the other components such as energy regeneration system, amino acids and buffers is time-consuming and requires a lot of effort. The PURExpress

system, the most commonly used CFES consisted purified components of *E. Coli* [148]. These systems have an added advantage of being capable of producing toxic proteins as they are expressed outside of a cell. In this thesis, PURExpress system was employed to investigate and optimize the expression a membrane protein αHL tagged to green-fluorescent protein (GFP) in GUVs. The template DNA consisted of a gene coding for GFP-tagged αHL and a T7 promoter coupled an esaO-binding repressor protein (EsaR) which was responsive to transcription inducer molecule N-(3-oxohexanoyl)-L-homoserine lactone (3OC6HSL).

5.2 Objectives

The objective is to optimize the chemically inducible cell-free expression of membrane pore protein αHL within GUVs using the PURExpress system. Furthermore, the activity of cell-free expressed αHL is investigated using membrane permeability assay within GUVs.

5.3 Methods

5.3.1 Cell-free expression of αHL-GFP in bulk

The commercially available kit PURExpress (New England BioLabs, Ipswich, MA) was used for the cell-free expression of membrane protein αHL and red-fluorescent protein (RFP). Two DNA plasmids, one consisting of gene for a membrane porin αHL tagged to a GFP (DC061a) and the other consisting a gene coding for RFP (DC054a) and both having a T7 promoter coupled to an esaO operator expressing RFP were employed to test inducible cell-free protein expression. The template plasmid PEXP-NT/CALML3 was used for control experiments. A 25 μL reaction mix was set up for PURExpress samples using the following reagents as shown below in Table 5.1 followed by incubation at 37 °C for 2 hours at 350 rpm. The fluorescence measurements for the gene expression were carried out using 384-well plate using Cytation 5 well-plate reader. Solution A contains tRNAs and small molecules such as amino acids and rNTPs. Solution B contains ribosomes and protein components such as T7 RNA polymerase, translation factors, aminoacyl-tRNA synthetases and energy systems [149].

Reagent	Volume
Solution A	10 μL
Solution B	7.5 μL
RNAse Inhibitor	0.5 μL
Template DNA	1000 ng
Nuclease-free water	To a final volume of 25 μL

Table 5.1: PURExpress cell free expression reaction setup.

5.3.2 DNA purification for cell-free expression system

The plasmids were obtained from Dr. Dora Tang's group and were prepared as described in the previously reported protocol [40]. Further DNA purification was carried out from the overnight culture as per manufacturer's protocol (Qiagen Maxiprep Kit). Briefly, the cells were lysed by adding the lysis buffer and then the lysate was poured onto the filter cartridge to filter the cell lysate into a new 50 mL tube. The purification column was equilibrated with equilibration buffer and the filtered lysate was poured onto it and the flow-through was discarded. The column was then washed with the wash buffer and finally the elution of DNA was carried out into a clean 30 mL tube by addition of 15 mL elution buffer. A precipitation step was carried out with isopropanol followed by 5 mL ethanol to yield a purified plasmid DNA. The concentration of DNA and its purity was estimated using nano-drop spectrophotometer (NanoDrop^{TM} 2000 Spectrophotometer, Thermo fisher Inc.).

5.3.3 Preparation of lipid vesicles

Phase transfer method forming GUVs expressing GFP-tagged αHL POPC: Cholesterol GUVs in the ratio of 1:2 was formed with the emulsion phase-transfer method. 10 μL of reaction mix containing PURExpress components, a DNA plasmid (1000 ng) was used for the inner solution to create emulsion droplets thereby encapsulating the plasmid and CFES within the GUVs. The membrane-permeable inducer molecule 3OC6HSL was then added externally and the entire system was incubated for 2 hours at 37 °C to induce the cell-free expression of GFP-tagged αHL. GFP fluorescence was monitored using confocal microscopy with fluorescence spectra (λ_{exc}- 488 nm, λ_{em} - 500-600 nm).

Electroformed GUVs for CFES of GFP-tagged αHL POPC: Chol GUVs in the ratio of 1:2 was formed using electroformation. The 12.5 μL reaction mix comprising PURExpress and the DNA plasmid encoding GFP-tagged αHL was added externally to 12.5 μL solution containing GUVs. The

solution mix was then incubated for 2 hours with gentle mixing at 37°C with 10 μM inducer 3OC6HSL. Cell-free protein expression of GFP-tagged αHL was monitored using confocal microscopy.

5.3.4 Membrane-permeability assay

The expression of GFP-tagged αHL was detected using confocal microscopy and to check for its effective incorporation (and function) within GUVs, 10 μM of Alexa 647 hydrazide molecules was added externally. The signal fluorescence inside the GUVs was analyzed to check for the permeation of Alexa 647 hydrazide molecules into the GUV's lumen.

5.3.5 Confocal microscopy

$DiIC_{18}$ labelled GUVs were imaged using a confocal microscope (SP8, Leica) with laser excitation of 552 nm and emission was detected between 565 nm to 635 nm. For the cell-free expression of GFP-αHL protein, the excitation was at 488 nm and emission was detected in the range of 498 to 540 nm. Alexa-647 fluorescence was excited at 638 nm and fluorescence was detected at 650-720 nm. Sequential channel acquisitions were performed for multiple fluorophores and bright field transmission images were also obtained. Image analysis was performed using FIJI.

5.4 Results and Discussion

5.4.1 Set-up of CFES in bulk studies

In order to determine the activity of EsaR repressor switch as shown in Fig 5.1a, bulk test experiments were performed without any vesicles. A 12.5 μL reaction mix with components A and B from the PURExpress system was setup with 1000 ng of plasmid and incubated for 3 hours at 37°C. Two plasmids were tested in bulk system explained as follows, at first the plasmid DC054a encoding for RFP under EsaR switch was expressed using PURE system. The increase in the RFP fluorescence signal confirmed the protein synthesis in 3 hours at 37°C when induced with the molecule 3OC6HSL as shown in Fig 5.1c (blue line). In the absence of 3OC6HSL there was non-induced expression of RFP (Fig 5.1c, red line) observed, albeit the measured fluorescence intensities were 50% lower than the induced expression with the responsive EsaR switch. This ascertained the function of repressor switch and that it maintained its activity with the PURE system. Another control experiment was performed with

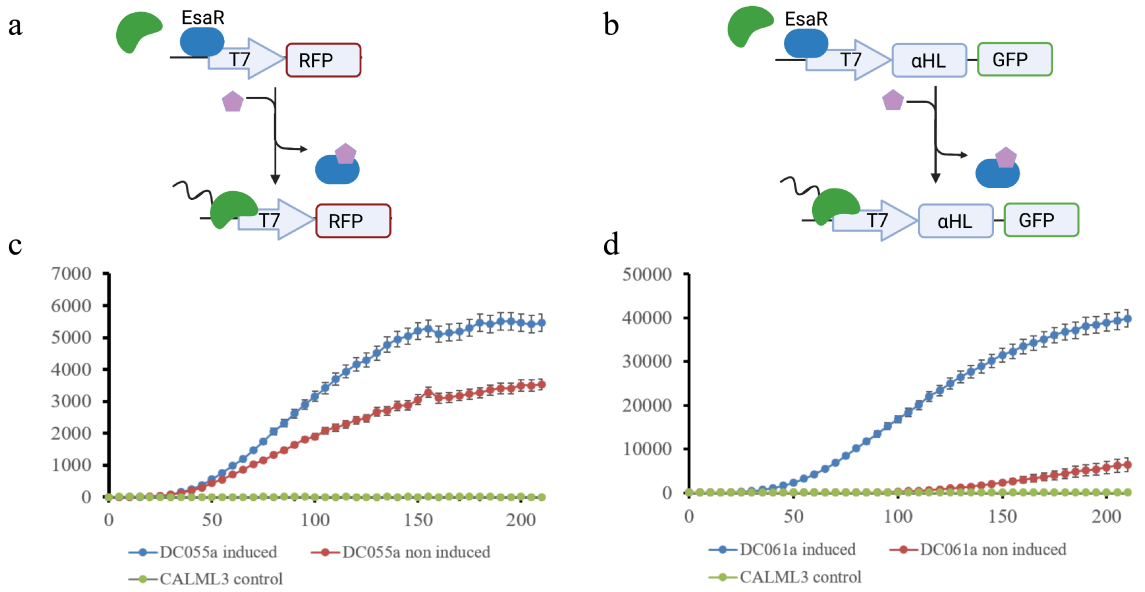

Figure 5.1: Investigating the activity of EsaR repressor switch. (a) EsaR transcription repressor protein provides negative regulation by binding to the operator sequence close to T7 promoter and thus blocking RNA polymerase binding through steric hindrance. The binding of inducer molecule (3OC6HSL) induces a conformational change that clears the promoter sequence to start gene transcription of RFP and (b) GFP-tagged αHL (c) Expression of pET21b/esaO/RFP plasmid showing time-dependent increase in fluorescence intensity at 37 °C (λ_{ex} = 565 nm, λ_{em} = 585 nm) (d) Expression of pET21b/esaO/αHL-GFP plasmid construct (DC061a) for GFP-tagged α-hemolysin showing time dependent increase in fluorescence intensity (λ_{ex} = 488 nm, λ_{em} = 510 nm). The fluorescence intensity measurements obtained from well-plate reader with transcription inducer (blue, 10 μM) or without transcription inducer (red, HEPES buffer) and control CALML3 plasmid encoding for the non-porin protein, calmodulin (green). Error bars are taken from standard error of mean.

plasmid PEXP-NT/CALML3 encoding for the non-fluorescent protein calmodulin which showed no fluorescence signal detected over time (Fig 5.1c, green line). This confirmed that PUREsystem machinery do not by itself give rise to any fluorescence signal. This showed that inducer molecule can activate the expression of fluorescent protein RFP and thereby showed the effectiveness of repressor switch. Therefore, the plasmid DC061a encoding the gene for GFP-tagged αHL protein coupled to the gene coding for an esaO-binding repressor protein (Fig 5.1b) was tested in bulk systems. An increase in GFP fluorescence was observed thereby confirming successful expression of GFP-tagged αHL in the presence of inducer molecules (Fig 5.1d, blue line) compared to control experiments (without inducer and with CALML3 plasmid) as shown in Fig 5.1d (red line, green line). This showed that the synthesis of membrane pore-protein αHL was activated with transcription inducer molecules. The next goal was to encapsulate the PURExpress system along with the plasmid DC061a in GUVs and inducing the protein expression within the GUVs along with the inducer molecules added externally.

5.4.2 Cell-free expression in GUVs

Cell-free expression of plasmid comprising gene coding for GFP-αHL was tested within the GUVs by the diffusion of inducer molecules into the lumen. GUVs were formed with emulsion phase transfer method with a 1:2 mixture of POPC: Cholesterol with the inner solution containing plasmid DNA and cell-free components. The lipid composition mix was chosen based on previous study which showed successful reconstitution of cell-free expressed αHL in LUVs [40]. GUVs were fluorescently labelled with Atto-390 and the fluorescence of GFP was monitored over the period of 2 hours to confirm the induction of cell-free synthesis with 10 μM 3OC6HSL molecules as shown in Fig 5.2.

A high localized green fluorescence was observed within the lumen of GUVs suggesting that there was a potential cleavage of protein GFP post protein synthesis. Moreover, the fluorescence signal could not be detected on the membranes of GUVs that confirmed no reconstitution of pore protein αHL. It has been shown that cholesterol is important for the integration of αHL [150]. One reason could be that the cholesterol ends up in oil phase and therefore is not integrated into the membranes of GUVs thus hindering the integration of αHL into the GUV membranes. Therefore, an alternate approach was employed with the electroformed GUVs, wherein the cell-free protein expression of GFP- αHL was induced in the outer environment of GUVs. Here, the PURE components and the template DNA were added externally and furthermore the protein expression was triggered with the transcription inducer 3OC6HSL.

To achieve this, the GUVs with a lipid composition of POPC: Cholesterol labelled with $DiIC_{18}$ (1,1'-dioctadecyl-3,3,3',3' tetramethylindocarbocyanine) were formed using electroformation method. Equal volume of GUV solution were mixed with cell-free system along with plasmid DC061a (1000 ng) and the expression was triggered with inducer 3OC6HSL at 37°C with gentle shaking at 350 rpm for 2 hours. The GUVs were then harvested and imaged on a microtiter plate using confocal microscopy. Fig 5.3a shows the images of GUVs with cell-free expression of GFP- αHL activated with transcription inducer. Merge images show that the green fluorescence is localized on the membrane of GUVs and therefore confirm the integration of αHL into GUVs. The non-induced population of GUVs showed low green fluorescence intensities, therefore low expression of GFP-αHL as seen in Fig 5.3b. Next, the permeability of GUVs was investigated with the addition of water-soluble dye Alexa 647 hydrazide when induced with 3OC6HSL, to test for the protein's functionality.

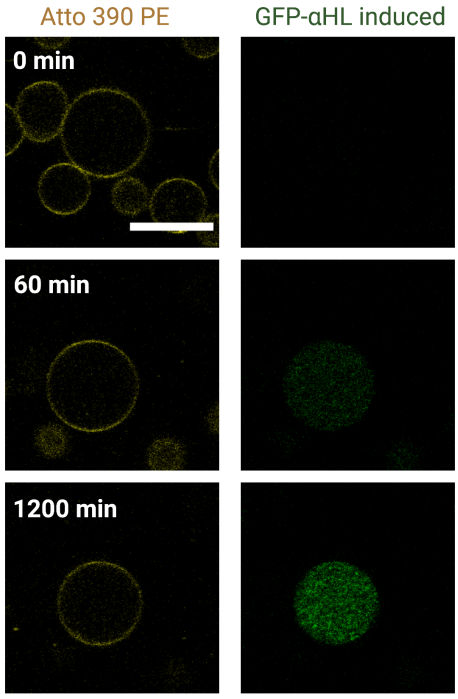

Figure 5.2: Cell-free expression of GFP-tagged αHL within GUVs. Time-lapse confocal images showing the increase in GFP fluorescence signal (right panel) within POPC:Chol GUVs labelled with Atto-390 PE lipids (left panel) over the period of 2 hours. Scale bar: 25 μm.

5.4.3 Investigating the membrane transport activity of GUVs

The incorporation of alpha-hemolysin into the electroformed GUVs was determined with a permeability assay using fluorescent dye Alexa 647 molecules. It is more commonly used for labelling aldehydes or ketones in polysaccharides and glycoproteins. This dye is brighter and more resistant to photobleaching than fluorescein making it an ideal choice for membrane transport assay [151]. To probe the permeability of GUVs, at first GUVs prepared in 900 mM sucrose with 1X HEPES buffer was incubated for 2 hours at 37 °C with cell-free system along with plasmid DNA in the outer environment of GUVs and loaded into micro-titer plate wells. Subsequently, 10 μM Alexa 647 prepared in isotonic sucrose solution was added externally and the confocal time series was acquired to determine the permeability of the membranes.

The permeation of Alexa 647 molecules (blue channel) into the lumen of GUVs was observed within the induced population of GUVs with cell-free expressed of GFP-tagged αHL. Control experiments were carried out with the non-induced population of GUVs, and another control was performed with expression of non-porin protein, calmodulin within GUVs, both experiments showed no transport of dye molecules into the GUVs as shown in Fig 5.4. Therefore, this confirmed that the permeability was achieved within the in-

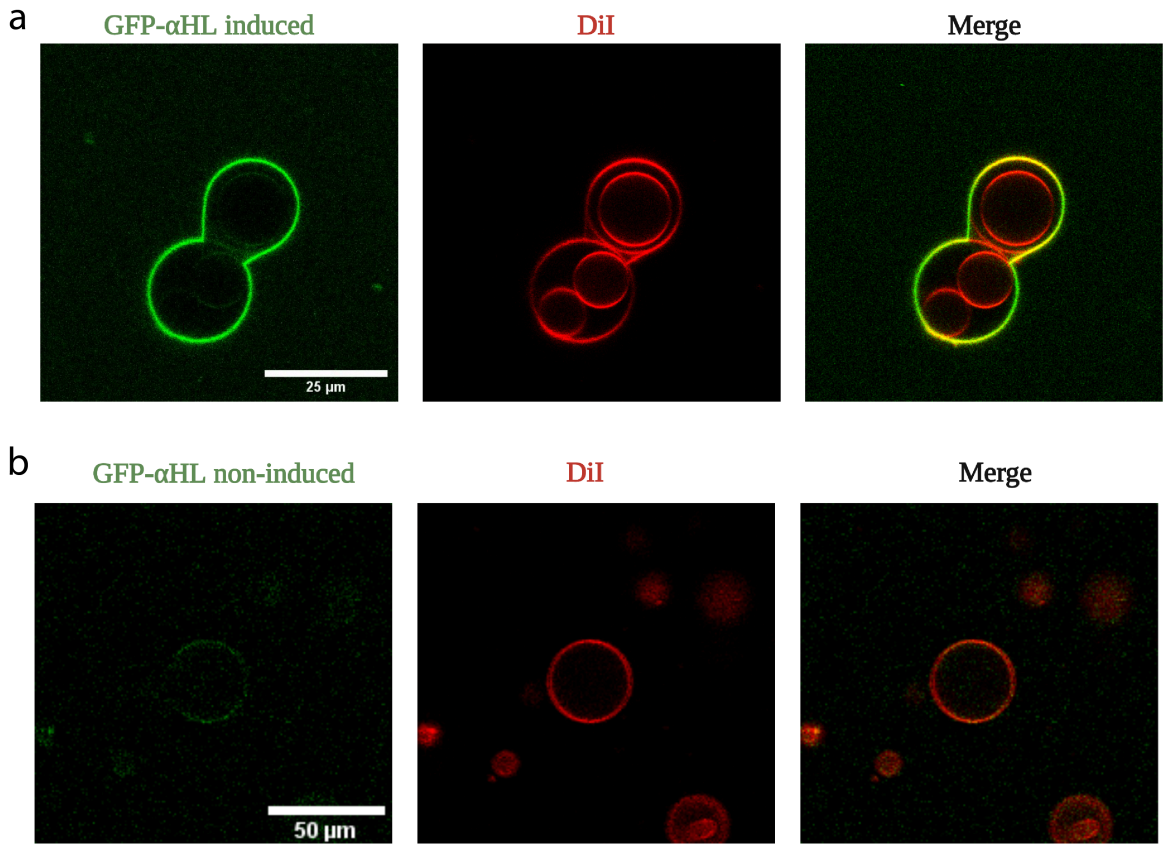

Figure 5.3: Cell-free expression of GFP-tagged αHL on the membrane of GUVs. (a) GFP expression confirmed by the fluorescence (green channel) signal on the GUV membranes (red channel) when induced. Scale bar: 25 μm. (b) GUVs with low fluorescence signal due to non-induction. Scale bar: 50 μm.

duced population of GUVs wherein the cell-free expression of GFP-tagged αHL was induced with 3OC6HSL compared to control experiments.

Furthermore, the fluorescence of Alexa 647 hydrazide molecules within a GUV when induced with the 3OC6HSL was monitored over time as shown in time-lapse confocal images (Fig 5.5, left). This showed that the membrane was indeed permeable as there was transportation of dye molecules into the aqueous lumen of GUVs. Endpoint measurements of population of GUVs which are triggered with transcription inducer molecules showed high fluorescence intensities of dye molecules within GUVs in comparison to the non-induced GUV population as shown in Fig 5.5 (right). The fluorescence of Alexa 647 was also observed in non-induced population of GUVs as there was some non-induced (leaky) expression of GFP-tagged αHL observed even in non-induced population of GUVs, probably resulting from the delay in the expression of repressor protein EsaR. This led to uninhibited αHL expression and resulting in pore formation in the non-induced population of GUVs. This could be attributed to the low fluorescence signal observed in control experiments.

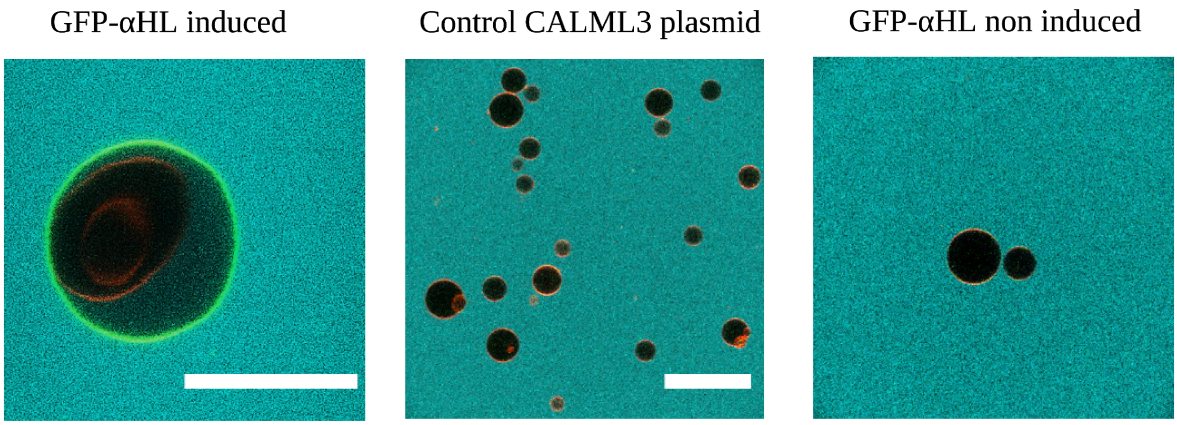

Figure 5.4: Confocal images with three channels merged to observe the localized fluorescence of GFP-tagged αHL (green channel) on the membrane of GUVs (red channel). Alexa-647 fluorescence shown inside the lumen of GUVs for induced population of GUVs (blue channel). Scale bars: 25 μm.

A more quantitative analysis revealed that only 10% of the induced population of GUVs showed expression of GFP- αHL and consequently, the membrane permeation of dye molecules in these GUVs. Although, CFES provides an advantage to control and tweak each constituent to optimize and increase the degree of complexity, still there was a stochasticity observed in the expression of pore protein within the GUV populations. This could be attributed to the dilution of PURexpress components in the outer environment leading to low plasmid numbers due to the addition of GUV solution externally. More-

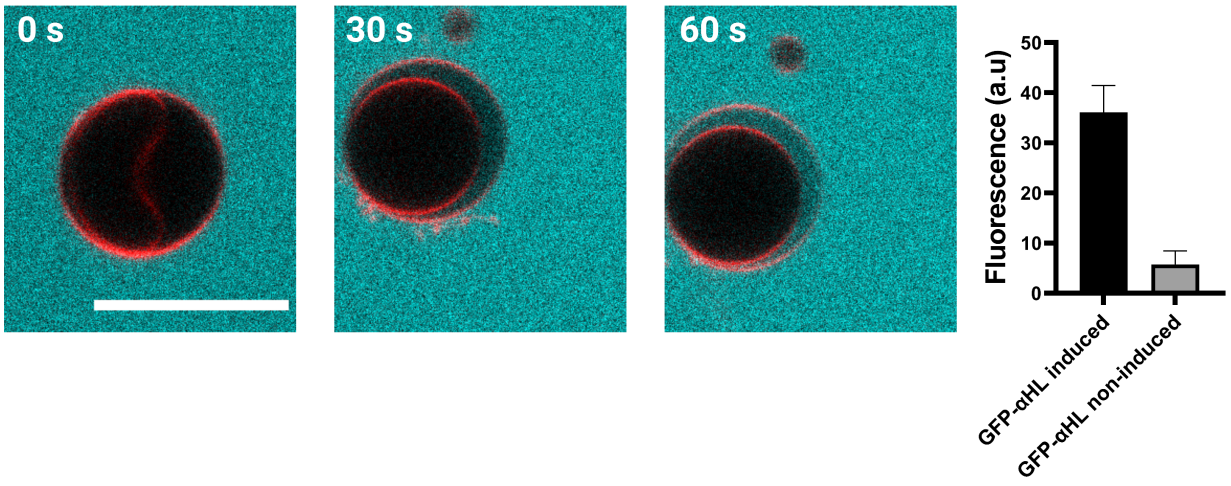

Figure 5.5: Membrane permeability assay. Time-lapse confocal images showing the permeation of Alexa-647 molecules into the lumen of GUVs wherein the cell-free expression of alpha hemolysin induced with 3OC6HSL (left panel). Scale bar: 20 μm. Endpoint fluorescence intensities of induced versus non-induced population of GUVs (right) (n = 10).

over, a high osmolarity within the GUV population was maintained to render isotonic conditions with the PURexpress system which led to unphysiological high concentrations of sugars.

In order to circumvent these issues, one could adopt microfluidic strategies to reduce the variability in the expression and furthermore it provides a platform to have higher precision and control over inner fluid volumes. This is a crucial factor as CFES could be tuned by having defined plasmid concentrations for optimum protein synthesis. Therefore, at first the optimum conditions to induce the cell-free expression of pore protein in synthetic cell population needs to be established. Following which, the gene directed communication pathways within different compartments of multi-compartment systems as previously described in Chapter 4 remains to be developed. This would facilitate a wide range of applications in the field of biotechnology as biosensors, nanocarriers and as gene circuits [87, 152]. It would further facilitate synthetic cell related research like content release [153] and multistep bioprocesses [105].

Chapter 6

Conclusion

In this thesis, different methodologies to fabricate artificial eukaryotic cells were developed and furthermore a multi-step enzyme cascade was studied within these compartment systems. In nature, communication between biological cells occur by signal transduction to regulate different biological processes. However, construction of analogous synthetic systems to mimic the cellular signaling remains challenging. Several designs that explore intercellular signaling mainly rely on either induced *in vitro* protein expression [152, 154] *via* small uncharged molecules like peroxides to initiate enzyme cascade [103, 155, 156], or using DNA oligonucleotides [157, 158]. In cells, however small molecules constitute the main class of information messengers which are secreted by cells and recognized by receptors to carry out downstream processing. The synthetic signaling cascade described in Chapter 3 operate on the same lines, as it comprises enzymes and small molecule substrates to carry out the signal transduction within artificial eukaryotic cells. Importantly, this could then be translated to integrate more complex signal transduction mechanisms that are found in eukaryotic cells. The synthetic enzyme cascade was triggered by tetrasaccharide molecule stachyose to initiate the multi-step enzyme network comprising enzymes HRP, GOx, and α-Glc to form the final fluorescent output resorufin. The final enzymatic reaction with the fluorescence output was chosen for the ease of detection and quantification purposes using fluorescence detection methods. The final intermediate H_2O_2, has been shown to cause lipid peroxidation which can result in cytotoxicity in biological cells [159]. Therefore, one needs to take into account the concentration of substrate fed into the reaction cascade to avoid high amounts of H_2O_2 formation so that it does not affect the integrity of the vesicles. Therefore, the enzyme studies were carried out in well-defined bulk or open systems to tune the parameters such as enzyme and substrate concentrations to achieve efficient signal transduction. However, these bulk aqueous systems do not fully reflect the complexity of a cellular environment and moreover enzymatic reactions occur in molecularly

crowded environment [160] and more often in confined spaces like organelles, with high surface to volume ratios, in case of eukaryotic cells. Therefore, the entire enzyme cascade network was successfully tested and optimized in single compartment systems *i.e.* GUVs formed with emulsion phase transfer method and further built up towards more complex structures.

For further construction of eukaryotic cell mimics, multi-compartmental liposomal architectures were established. At first, bulk methodologies such as two-step emulsion phase transfer method was employed for the generation of MVVs. The optimal conditions comprising raffinose and sucrose for the first set of phase transfer GUV formation and glucose as external solution for second phase transfer method was chosen to render the required density gradient. This methodology however suffered from low yields and poor control over the size of inner compartments. One of the reasons for low encapsulation efficiency, was that the large emulsion droplets formed were not being encapsulated within outer GUVs. Therefore to improve the yield, one could first extrude the first set of GUVs to obtain intermediate sized GUVs of uniform size distribution which can then be encapsulated within second set of GUVs to obtain a better encapsulation efficiency [60].

Alternatively, the encapsulation of LUVs as inner compartments instead of GUVs was carried out to overcome some of the challenges faced with the previous methodology. LUVs were formed using lipid-film hydration method followed by extrusion and then encapsulated in larger compartments such as GUVs using phase transfer method to generate MVVs. Although a good encapsulation efficiency of inner compartments was achieved, still several bursting events of inner LUVs occurred during the encapsulation process. This could be mitigated with the addition of charged lipids to both LUV and GUV composition mix to stabilize the LUVs through electrostatic repulsion and further aid in better encapsulation.

To overcome the challenges faced with bulk methodologies, microfluidic platforms were adopted to build multi-compartment systems. At first, a PDMS-based microfluidic device was introduced to encapsulate smaller compartments *i.e.* LUVs within outer larger compartments *i.e.*GUVs using a one-inlet microfluidic device. The significance of inclusion of PEGylated lipids in the lipid composition mix was highlighted. As PEGylated lipids exhibit amphiphilic properties, its inertness blocked any interaction between opposing membranes and thereby facilitated high encapsulation of inner LUVs. This resulted in uniform encapsulation of inner compartments and due to the microfluidic platforms, monodisperse populations of multi-compartment systems was achieved. Therefore, the addition of 1 mol% DSPE-PEG lipids was found to be crucial for successful encapsulation of LUVs in outer GUVs without any rupture of LUVs. However, one needs to avoid high amounts of PEGylated

lipids ($> 7 \pm 2$ mol%), as it can affect the stability of LUVs [161]. Moreover, by tuning the pressures (and hence the flow rates) required for the formation of MVVs, microfluidic platforms could also be employed for high-throughput formation of artificial cells of varying diameters. This acts as an added advantage for the applications such as constructing synthetic prototissues, to study collective response within large population of synthetic cells to mimic bacterial quorum sensing, clinical diagnostics, and drug-delivery systems wherein the size diameter could be readily tuned based on the requirements. Previously reported microfluidic stragies to build hierarchical architectures have implemented a two-step enzymatic reaction within them [90] and moreover a hybrid system by encapsulation of living cells was also shown [59]. Another approach showed generation of MVVs with a high control over the number of inner compartments along with their encapsulated content using co-flow devices [105]. Although, these approaches showed an advanced level of control in building MVVs, they do not directly compare the effects of different hierarchical levels of compartmentalization on enzymatic pathways which is reported in this thesis.

A two-inlet microfluidic design was introduced in Chapter 4 to generate three-compartment systems. The enzyme signaling cascade within the compartment systems was triggered externally to mimic simple signaling pathways occurring in eukaryotic cells. Here two key features of eukaryotic cells were addressed within the multi-compartment systems, first, by having a spatial control by segregating the enzymes within defined compartments. Second, to have a temporal control by allowing the passage of molecules such as initiator molecules within the systems *via* membrane pores. A three-enzyme reaction pathway was implemented spanning across two populations of inner LUVs with different permeability properties. This allowed for the directed pathways of reaction intermediates due to the reconstitution of size-selective membrane pores within the membranes of two LUV populations. The two inlet-design allowed the separation of two populations of LUVs to avoid any cross-contamination and cross-enzyme inhibition and it also promoted efficient co-encapsulation of the inner LUVs to yield complex MVVs.

In this work, the artificial cells were fabricated with PDMS-based microfluidic device rather than glass-capillaries, which have also been used to form multi-compartment structures [105]. PDMS-based microfluidic platforms require reagent-heavy fabrication technology, but they are easier to fabricate and handle compared to glass-capillaries with complex alignment procedures that are extremely arduous to perform [122]. Owing to the monodispersity of the formed GUVs/MVVs with the help of microfluidic platforms, direct comparisons were drawn across one-, two- and three compartment systems with open/bulk systems. These approaches also resulted in low variability across

the same MVV population and provided high reproducibility of compartment systems. The effects of confinement on enzymes within increasingly complex liposomal structures were studied and concluded that compartmentalization affects the overall kinetics of the enzyme reaction network. Previously, it has been reported that membrane surfaces have a significant effect on the enzyme activity [134]. The overall rate of formation of resorufin was higher in the confined systems compared to the open systems which was attributed to the larger diffusion lengths that the intermediates must travel to reach active reaction sites in case of bulk aqueous system. Moreover, the intermediates and the input substrate could get consumed faster in the bulk system in comparison to the compartment systems with defined enzyme numbers within smaller volumes. Furthermore, it was reported that one-compartment systems had higher reaction rate constants compared to two- and three-compartment system and this could be due to the additional membrane barriers which might slow down the diffusion of intermediates or reactants formed within the compartments [131]. Another interesting observation was the lower variance observed in the product formation within the three-compartment systems. This leads us to believe that three-compartment systems have a better regulation on the enzyme cascade network, perhaps because they are spatially segregated within distinct compartments. This could be further translated for other naturally relevant biochemical pathways to have a regulation over biochemical processes within the artificial cells similar to biological cells that control metabolism using enzymatic regulation that is essential for cellular homeostasis.

A bottom-up approach was established to construct an artificial cell with microfluidics that can uptake external trigger molecules which triggers a signaling cascade along a specific pathway. Therefore, this system could mimic the behavior of eukaryotic cells that comprise interactions between cellular machinery and the cellular environment. Cells are able to sense sugars, lipids, amino acids or metabolites in their environment and accordingly respond to any changes by reorganizing metabolic networks or modulated signal transduction downstream in specific organelles [162]. Previously reported synthetic beta cells demonstrated sensing the external environment *i.e.* the glucose levels and releasing of cargo *i.e.* insulin by exocytosis [35]. Similarly, such sense-release behaviors could be integrated into our multi-compartment systems that could be used for replacement cell therapy.

Chapter 5 encompasses the design and assembly of gene-based expression system within lipid-based compartmentalized systems using a bottom-up synthetic biology approach. The significance of cell-free expression systems for protein synthesis is outlined as it mitigates several issues that occur during cell-based expression of proteins. Moreover, membrane proteins play an integral role as a facilitator to transport molecules in several biochemical processes

and often membrane protein expression faces several issues as it is more likely to form aggregates during the purification step and therefore could lose its activity. CFES aids to overcome these challenges and is widely used as an alternative for membrane protein synthesis. In this thesis, the primary focus was to have an inducible expression of membrane protein αHL within the artificial cells. The use of repressor switch EsaR which can be activated with a transcription inducer 3OC6HSL allowed for the gene-mediated control over the expression of the proteins that was tested within GUVs formed with bulk methodologies. The permeabilities of the GUVs were further tested to determine the incorporation of pore protein and observed that only 10 % of entire GUV population showed induced protein expression and consequently permeation of dye molecules into the system. In order to increase the efficiency of protein expression in GUVs and have controlled volumes of PURexpress components and plasmid concentrations, microfluidic strategies need to be employed. This would bring us one step closer to realize the goal of gene-mediated communication system by establishing a greater control over the artificial eukaryotic cells.

Chapter 7

Outlook

The novel microfluidic platform introduced in this thesis paves the way towards new possibilities for the formation of highly tunable and controllable multi-compartment systems which have several advantages over conventional approaches. PDMS-based microfluidic chips provide high flexibility and could be easily translated in the future for subsequent capture and analysis of the produced MVVs on the same device [90, 163, 164] . A three-step synthetic signaling cascade was explored in this thesis with a primary focus on the effect of compartmentalization on overall enzyme activity. In future applications, this could be utilized to tune the rate of reactions in different compartments to yield the desired output. It also opens up a vast range of applicability for these multi-compartmentalized systems in order to understand molecular phenomenon such as the effect of crowding and potentially could be explored as synthetic models to study out-of-equilibrium behaviour [165].

The two-inlet microfluidic platform described in this thesis could be further explored in the future for applications that require the inner components to be kept segregated until encapsulation *e.g.* when the sensor liposomes and reporter liposomes need to be encapsulated within a microfluidic GUV, any unspecific interaction between them could be avoided until they are encapsulated and trapped for analysis. Moreover, the two-inlet microfluidic system has the advantage where one could vary the flow rates to obtain different ratios of encapsulated inner compartments within the MVVs.

In the complex three-compartment system presented in this work, apart from the novelty associated with reconstituting two different membrane proteins, one of the main reasons was to impart different permeabilities to the two different populations of inner LUVs. GOx-LUVs contain OmpF pores which work to block the transport of larger stachyose into their lumen and only allow the smaller glucose to enter after it is produced in the other α-Glc-LUVs. In this way, the input molecules are directed to the first population of LUVs for more efficient reaction cascade and at the same time ensure that

it does not compete with oxidative reaction of glucose by enzyme GOx. The multi-compartment system segregates the enzymes within specific compartments, and with the different permeabilities due to OmpF and αHL pores, the intermediates and input molecules would be separated within the system to increase the efficiency of the reaction cascade. Therefore, it is essential to gain deeper understanding of the reaction network encompassed within these multi-compartment systems by having theoretical models to predict parameters such as turnover rate at each step of signal transduction and feedback mechanisms. Modelling of each step of reaction network by using differential equations could enable one to simulate parameters such as concentrations of different components and optimum pore density for the desired product outflux. Although modelling of enzyme reaction networks have been shown in open or bulk systems [166, 167], confinement adds a layer of complexity due to the interactions between the components of reaction system and the compartment [168–170]. Microfluidic techniques enable a precise control over the internal fluid volumes and produce more homogeneous populations of GUVs. This would tremendously simplify the modelling to predict the complex behavior of enzyme cascades in multi-compartment architecture. Furthermore, the optimal environment for producing stable MVVs could be established and the optimum parameters to have efficient signal transduction within the MVVs could be estimated. Previously, a theoretical model was built to predict the leakage kinetics of molecules within multi-walled vesicles and was further fit with experimental data. Here they proposed a model that determined the permeability of the bilayer to small molecules (in this case glucose). They further reported that the leakage of the molecules across the membrane was slowed down proportionally depending on the number of bilayers [131]. However, this model does not fully reflect the multi-compartment system that has been described in this thesis and therefore to gain deeper insights, a detailed investigation needs to be implemented.

In this system, the size-selective communication is achieved with the incorporation of αHL (larger pores) and OmpF (smaller pores) in the two inner LUVs, the cascade network is mainly controlled by the relative cut-off sizes of the pores on the external membrane and inner LUVs. Therefore, there could be passive transport of unwanted molecules out of the system. One way to limit this is by incorporating active transporters or specific transporters such as GLUT1 [118] (specific to glucose transport) into the MVV membranes to facilitate one-way movement of molecules which would provide further control over the entire system. This would also provide an opportunity to have a wider range of biotechnological applications in the future. However, one advantage of our system is that although the internal osmotic pressure is affected by the formation of intermediates and products, the effect is minimized due to the

presence of membrane pores.

Towards the end of the thesis, the possibility of expressing a heptameric membrane protein αHL was explored with *in vitro* expression approaches. Membrane proteins play pivotal roles in a wide range of cellular processes and act as key targets for drug discovery [140]. One such example is G-protein coupled receptors (GPCRs), a class of proteins that make up 30 % of all drug targets, although few crystal structures are present in Protein Data Bank (PDB) [171]. The main challenge for advancement and acquirement of more structural information in this field is the insufficient yield of transmembrane proteins in cell-based expression system due to protein cytotoxicity, aggregation, and misfolding [172]. Alternate approaches for efficient expression of membrane proteins are the cell-free approaches [173]. This provides numerous advantages as it saves time required for the expression which essentially requires 2-3 hours in comparison with cell-based protein expression which takes few days. As an outlook, the integration of the cell-free expression system module with the multi-compartment system described in Chapter 4 to have a gene-expressed communication network is described to add to the system's complexity to mimic the complex nature of eukaryotic cells. Fig 7.1 shows the multi-compartment system with the cell-free expression module that encompasses three inner compartments within an outer GUV and could be generated using microfluidic platforms.

The MVV constructs comprise a cell-free synthetic organelle (*i.e.* LUVs) encapsulating the cascade-initiator molecules, stachyose along with cell-free components *i.e.* PURExpress along with plasmid with a T7 promoter with a repressor switch EsaR that was responsive to 3OC6HSL (transcription inducer) and a gene for GFP- tagged-αHL. The previously described enzyme cascade network spanning across two inner LUVs (GOx-LUVs and α-Glc LUVs) were co-encapsulated with the cell-free synthetic organelle in outer GUVs containing the enzyme HRP. The entire cascade could be initiated with inducer molecule 3OC6HSL which would at first initiate the cell-free expression of membrane porin αHL that results in the permeation of stachyose molecules from the inner lumen of cell-free encapsulating LUVs. Stachyose would then initiate the enzyme-cascade network with all three enzymes working in cohort to form the final fluorescence product resorufin. These artificial cell systems could be further translated to address other complex reaction cascades involving biologically relevant enzymes such as dehydrogenases, phosphatases (*etc.*) There are certain challenges that need to be dealt with while integrating the cell-free module, one issue could be the compatibility of PURExpress CFES with the microfluidic MVVs which would affect the synthesis of membrane pores. Also, the LUVs encapsulating the cell-free system are difficult to extrude and therefore the unilamellarity of vesicles remains elusive in these systems which needs

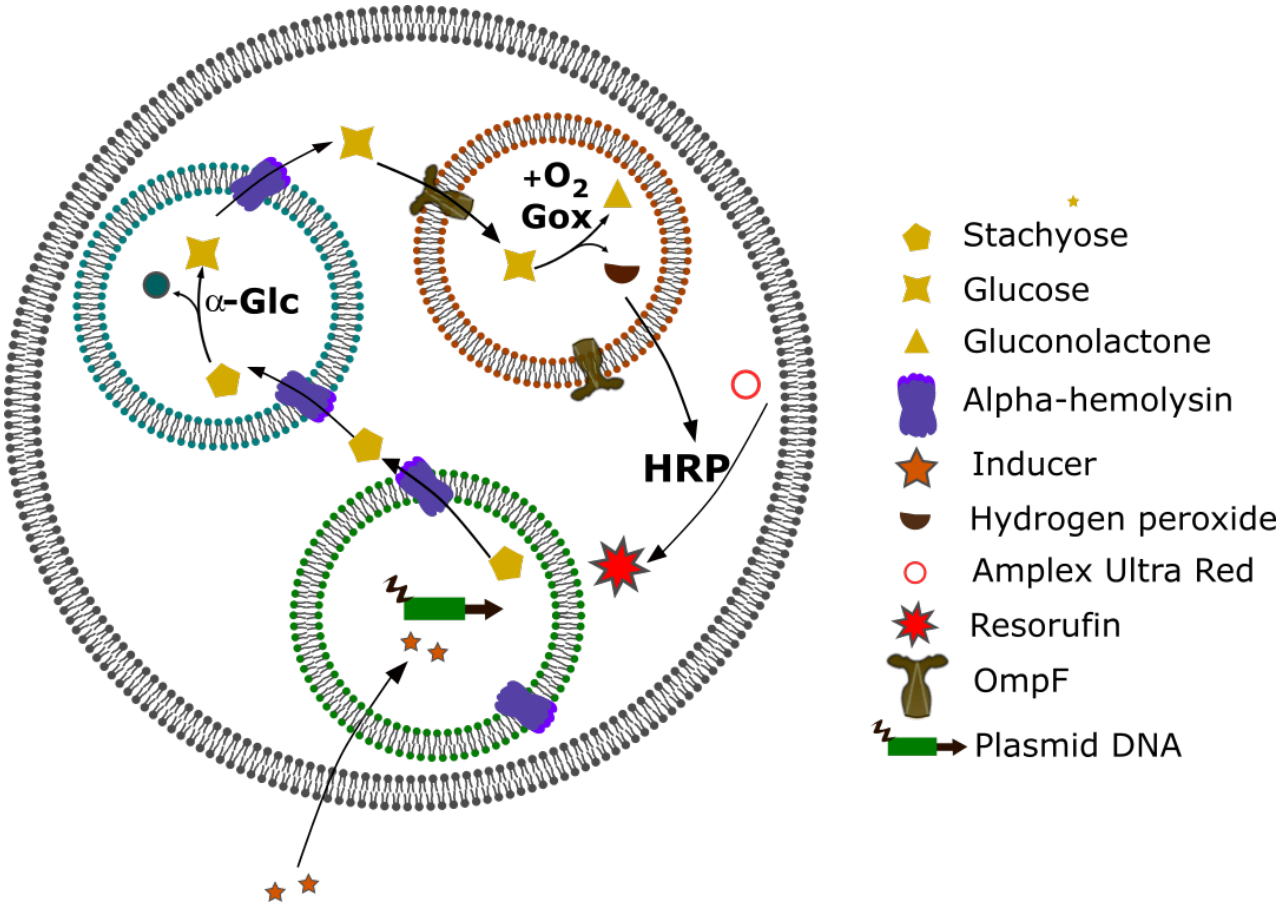

Figure 7.1: Schematic of gene-triggered communication in multi-compartment system including the enzyme cascade network and the cell-free expression module spanning across three inner LUVs and outer GUV.

to be addressed in future.

As a final word, in this thesis, a strategy to study the signaling, communication, and information processing that occur in eukaryotic cells was demonstrated. Bottom-up approaches were employed to build synthetic cellular constructs encompassing four key features of biological cells namely i) multi-compartmentalization ii) spatial control (segregation of enzymes in different compartments) iii) temporal control (transport of trigger molecules regulated *via* membrane pores) and iv) directionality. In future, artificial eukaryotic cells have the potential to be used as research tools to investigate more fundamental questions that still remain unanswered in biology.

Bibliography

(1) Gest, H. **2004**, *58*, 187–201 (cit. on p. 1).

(2) Mazzarello, P. **1999**, *1*, E13–E15 (cit. on p. 2).

(3) Maienschien, J. **1991**, *21*, 357–372 (cit. on p. 2).

(4) Vellai, T.; Vida, G. **1999**, *266*, 1571–1577 (cit. on p. 2).

(5) Battista, J. R. Against all odds: The survival strategies of Deinococcus radiodurans, 1997 (cit. on p. 2).

(6) Shiratori, T.; Suzuki, S.; Kakizawa, Y.; ichiro Ishida, K. **2019**, DOI: 10.1038/s41467-019-13499-2 (cit. on p. 2).

(7) Dacks, J. B.; Field, M. C.; Buick, R.; Eme, L.; Gribaldo, S.; Roger, A. J. **2016**, 3695–3703 (cit. on pp. 2, 4).

(8) Doolittle, W. F. **1998**, *392* (cit. on p. 2).

(9) Zaremba-Niedzwiedzka, K. et al. **2017**, *541*, 353–358 (cit. on p. 3).

(10) Gray, M. W. **2012**, *4*, 1476–1482 (cit. on p. 3).

(11) Vosseberg, J.; Hooff, J. J. E. V.; Marcet-houben, M.; Vlimmeren, A. V.; Wijk, L. M. V.; Gabaldón, T.; Snel, B. **2021**, *5*, DOI: 10.1038/s41559-020-01320-z (cit. on p. 3).

(12) Lane, N.; Martin, W. **2010**, *467*, 929–934 (cit. on p. 3).

(13) Martijn, J.; Ettema, T. J. **2013**, *41*, 451–457 (cit. on p. 3).

(14) Harold, F. M. **2005**, DOI: 10.1128/mmbr.69.4.544-564.2005 (cit. on p. 4).

(15) Szostak, J. W.; Bartel, D. P.; Luisi, P. L., 387–390 (cit. on p. 4).

(16) Chen, A. H.; Silver, P. A. Designing biological compartmentalization, 2012 (cit. on pp. 4, 5).

(17) Kerfeld, C. A.; Heinhorst, S.; Cannon, G. C. **2010**, *64*, 391–408 (cit. on p. 4).

(18) Yeates, T. O.; Kerfeld, C. A.; Heinhorst, S.; Cannon, G. C.; Shively, J. M. **2008**, *6*, 681–691 (cit. on p. 4).

(19) Penrod, J. T.; Roth, J. R. **2006**, DOI: 10.1128/JB.188.8.2865-2874.2006 (cit. on p. 4).

(20) Sampson, E. M.; Bobik, T. A. **2008**, DOI: 10.1128/JB.01925-07 (cit. on p. 5).

(21) Zhang, Y. H. Substrate channeling and enzyme complexes for biotechnological applications, 2011 (cit. on p. 5).

(22) Dunn, M. F. Allosteric regulation of substrate channeling and catalysis in the tryptophan synthase bienzyme complex, 2012 (cit. on p. 5).

(23) Tran, L.; Broadhurst, R. W.; Tosin, M.; Cavalli, A.; Weissman, K. J. **2010**, DOI: 10.1016/j.chembiol.2010.05.017 (cit. on p. 5).

(24) Fontes, C. M.; Gilbert, H. J. Cellulosomes: Highly efficient nanomachines designed to deconstruct plant cell wall complex carbohydrates, 2010 (cit. on p. 5).

(25) Gehrmann, W.; Elsner, M. **2011**, DOI: 10.3109/10715762.2011.560148 (cit. on p. 5).

(26) Fernie, A. R.; Carrari, F.; Sweetlove, L. J. **2004**, *7*, 254–261 (cit. on p. 5).

(27) Woolfson, D. N.; Bromley, E. **2011**, 19–25 (cit. on p. 5).

(28) Gibson, D. G. et al. **2010**, DOI: 10.1126/science.1190719 (cit. on p. 5).

(29) Hutchison, C. A.; Peterson, S. N.; Gill, S. R.; Cline, R. T.; White, O.; Fraser, C. M.; Smith, H. O.; Venter, J. C. **1999**, DOI: 10.1126/science.286.5447.2165 (cit. on p. 5).

(30) Luisi, P. L.; Ferri, F.; Stano, P. Approaches to semi-synthetic minimal cells: A review, 2006 (cit. on p. 6).

(31) Gil, R.; Silva, F. J.; Peretó, J.; Moya, A. **2004**, DOI: 10.1128/mmbr.68.3.518-537.2004 (cit. on p. 6).

(32) Luisi, P. L.; Walde, P.; Oberholzer, T. **1999**, DOI: 10.1016/S1359-0294(99)00012-6 (cit. on p. 6).

(33) Rasmussen, S.; Chen, L.; Nilsson, M.; Abe, S. **2003**, DOI: 10.1162/106454603322392479 (cit. on p. 6).

(34) Marguet, M.; Bonduelle, C.; Lecommandoux, S. **2013**, *42*, 512–529 (cit. on p. 6).

(35) Chen, Z.; Wang, J.; Sun, W.; Archibong, E.; Kahkoska, A. R.; Zhang, X.; Lu, Y.; Ligler, F. S.; Buse, J. B.; Gu, Z. **2017** (cit. on pp. 6, 85).

(36) Xu, C.; Hu, S.; Chen, X. Artificial cells: from basic science to applications, 2016 (cit. on p. 7).

(37) Amy Yewdall, N.; Mason, A. F.; Van Hest, J. C. The hallmarks of living systems: Towards creating artificial cells, 2018 (cit. on p. 7).

(38) Schwille, P. et al. **2018**, *57*, 13382–13392 (cit. on pp. 7, 14).

(39) Huang, X.; Li, M.; Green, D. C.; Williams, D. S.; Patil, A. J.; Mann, S. **2013**, *4*, DOI: 10.1038/ncomms3239 (cit. on p. 7).

(40) Tang, T.-Y. D.; Cecchi, D.; Fracasso, G.; Accardi, D.; Coutable-Pennarun, A.; Mansy, S. S.; Perriman, A. W.; Anderson, J. L. R.; Mann, S. **2017**, acssynbio.7b00306 (cit. on pp. 7, 74, 77).

(41) Discher, D. E.; Eisenberg, A. Polymer vesicles, 2002 (cit. on pp. 7, 8).

(42) Belluati, A.; Thamboo, S.; Najer, A.; Maffeis, V.; von Planta, C.; Craciun, I.; Palivan, C. G.; Meier, W. **2020**, DOI: 10.1002/adfm.202002949 (cit. on pp. 7, 8).

(43) Li, M.; Green, D. C.; Anderson, J. L. R.; Binks, B. P.; Mann, S. *Chemical Science*, *2*, 1739 (cit. on p. 7).

(44) Koga, S.; Williams, D. S.; Perriman, A. W.; Mann, S. **2011**, *3*, DOI: 10.1038/nchem.1110 (cit. on p. 7).

(45) Grimaldi, N.; Andrade, F.; Segovia, N.; Ferrer-Tasies, L.; Sala, S.; Veciana, J.; Ventosa, N. Lipid-based nanovesicles for nanomedicine, 2016 (cit. on p. 8).

(46) Küchler, A.; Yoshimoto, M.; Luginbühl, S.; Mavelli, F.; Walde, P. **2016**, DOI: 10.1038/nnano.2016.54 (cit. on pp. 8, 68).

(47) Nam, J.; Beales, P. A.; Vanderlick, T. K. Giant phospholipid/block copolymer hybrid vesicles: Mixing behavior and domain formation, 2011 (cit. on p. 8).

(48) Cheng, Z.; Tsourkas, A. **2008**, DOI: 10.1021/la801027q (cit. on p. 8).

(49) Lasic, D. D. The mechanism of vesicle formation. 1988 (cit. on p. 9).

(50) Angelova, M.; Dimitrov, D. S. In *Trends in Colloid and Interface Science II*, 2007 (cit. on p. 9).

(51) Schmid, E. M.; Richmond, D. L.; Fletcher, D. A. **2015**, DOI: 10.1016/bs.mcb.2015.02.004 (cit. on p. 9).

(52) Bucher, P.; Fischer, A.; Luisi, P. L.; Oberholzer, T.; Walde, P. **1998**, DOI: 10.1021/la971318g (cit. on p. 9).

(53) Pereno, V.; Carugo, D.; Bau, L.; Sezgin, E.; Bernardino De La Serna, J.; Eggeling, C.; Stride, E. **2017**, DOI: 10.1021/acsomega.6b00395 (cit. on p. 9).

(54) Ayuyan, A. G.; Cohen, F. S. **2006**, DOI: 10.1529/biophysj.106.087387 (cit. on p. 9).

(55) Le Berre, M.; Yamada, A.; Reck, L.; Chen, Y.; Baigl, D. **2008**, DOI: 10.1021/la703391q (cit. on p. 9).

(56) Politano, T. J.; Froude, V. E.; Jing, B.; Zhu, Y. **2010**, *79*, DOI: 10.1016/j.colsurfb.2010.03.032 (cit. on p. 9).

(57) Moga, A.; Yandrapalli, N.; Dimova, R.; Robinson, T. **2019**, DOI: 10.1002/cbic.201900529 (cit. on p. 9).

(58) Litschel, T.; Ganzinger, K. A.; Movinkel, T.; Heymann, M.; Robinson, T.; Mutschler, H.; Schwille, P. **2018**, DOI: 10.1088/1367-2630/aabb96 (cit. on p. 10).

(59) Elani, Y.; Trantidou, T.; Wylie, D.; Dekker, L.; Polizzi, K.; Law, R. V.; Ces, O. **2018**, *8*, 4564 (cit. on pp. 10, 15, 84).

(60) Hadorn, M.; Boenzli, E.; Eggenberger Hotz, P.; Hanczyc, M. M. **2012**, *7*, 1–7 (cit. on pp. 10, 14, 83).

(61) Qin, D.; Xia, Y.; Rogers, J. A.; Jackman, R. J.; Zhao, X.-M.; Whitesides, G. M. In 1998 (cit. on p. 10).

(62) Terry, S. C.; Herman, J. H.; Angell, J. B. **1979**, DOI: 10.1109/T-ED.1979.19791 (cit. on p. 10).

(63) Manz, A.; Graber, N.; Widmer, H. M. **1990**, DOI: 10.1016/0925-4005(90)80209-I (cit. on p. 10).

(64) Brouzes, E.; Medkova, M.; Savenelli, N.; Marran, D.; Twardowski, M.; Hutchison, J. B.; Rothberg, J. M.; Link, D. R.; Perrimon, N.; Samuels, M. L. **2009**, DOI: 10.1073/pnas.0903542106 (cit. on p. 10).

(65) Markey, A. L.; Mohr, S.; Day, P. J. **2010**, DOI: 10.1016/j.ymeth.2010.01.030 (cit. on p. 10).

(66) Kitson, P. J.; Rosnes, M. H.; Sans, V.; Dragone, V.; Cronin, L. **2012**, DOI: 10.1039/c2lc40761b (cit. on p. 10).

(67) Sjostrom, S. L.; Bai, Y.; Huang, M.; Liu, Z.; Nielsen, J.; Joensson, H. N.; Andersson Svahn, H. **2014**, DOI: 10.1039/c3lc51202a (cit. on p. 10).

(68) Huang, C. J.; Chen, Y. H.; Wang, C. H.; Chou, T. C.; Lee, G. B. **2007**, DOI: 10.1016/j.snb.2006.06.015 (cit. on p. 10).

(69) Whitesides, G. M. The origins and the future of microfluidics, 2006 (cit. on p. 10).

(70) Reynolds, O. **1883**, *174*, DOI: 10.1098/rstl.1883.0029 (cit. on p. 10).

(71) Avila, K.; Moxey, D.; De Lozar, A.; Avila, M.; Barkley, D.; Hof, B. The onset of turbulence in pipe flow, 2011 (cit. on p. 11).

(72) Squires, T. M.; Quake, S. R. **2005**, *77*, DOI: 10.1103/RevModPhys.77.977 (cit. on p. 11).

(73) Convery, N.; Gadegaard, N. **2019**, *2*, 76–91 (cit. on p. 11).

(74) Ai, Y.; Xie, R.; Xiong, J.; Liang, Q. **2020**, *16*, 1–24 (cit. on pp. 12, 13, 15, 41).

(75) Zhu, P.; Wang, L. **2017**, *17*, DOI: 10.1039/C6LC01018K (cit. on p. 12).

(76) Collins, D. J.; Neild, A.; DeMello, A.; Liu, A. Q.; Ai, Y. The Poisson distribution and beyond: Methods for microfluidic droplet production and single cell encapsulation, 2015 (cit. on p. 12).

(77) Thorsen, T.; Roberts, R. W.; Arnold, F. H.; Quake, S. R. **2001**, *86*, DOI: 10.1103/PhysRevLett.86.4163 (cit. on p. 12).

(78) Abate, A. R.; Poitzsch, A.; Hwang, Y.; Lee, J.; Czerwinska, J.; Weitz, D. A. **2009**, *80*, DOI: 10.1103/PhysRevE.80.026310 (cit. on p. 12).

(79) Zhou, C.; Yue, P.; Feng, J. J. **2006**, *18*, DOI: 10.1063/1.2353116 (cit. on p. 13).

(80) Chen, Z.; Han, J. Y.; Shumate, L.; Fedak, R.; DeVoe, D. L. **2019**, *4*, DOI: 10.1002/admt.201800511 (cit. on p. 13).

(81) Umbanhowar, P. B.; Prasad, V.; Weitz, D. A. **2000**, *16*, DOI: 10.1021/la990101e (cit. on p. 13).

(82) Osaki, T.; Takeuchi, S. **2017**, *89*, 216–231 (cit. on p. 13).

(83) Schrader, M.; Costello, J.; Godinho, L. F.; Islinger, M. **2015**, *38*, 681–702 (cit. on p. 13).

(84) Pagano, R. E. **1990**, *2*, 652–663 (cit. on p. 13).

(85) Satori, C. P.; Henderson, M. M.; Krautkramer, E. A.; Kostal, V.; Distefano, M. M.; Arriaga, E. A. Bioanalysis of eukaryotic organelles, 2013 (cit. on p. 13).

(86) Walde, P. Building artificial cells and protocell models: Experimental approaches with lipid vesicles, 2010 (cit. on p. 13).

(87) Lentini, R.; Martín, N. Y.; Forlin, M.; Belmonte, L.; Fontana, J.; Cornella, M.; Martini, L.; Tamburini, S.; Bentley, W. E.; Jousson, O.; Mansy, S. S. **2017**, *3*, DOI: 10.1021/acscentsci.6b00330 (cit. on pp. 13, 81).

(88) Bayoumi, M.; Bayley, H.; Maglia, G.; Sapra, K. T. **2017**, *7*, DOI: 10.1038/srep45167 (cit. on p. 13).

(89) Hindley, J. W.; Zheleva, D. G.; Elani, Y.; Charalambous, K.; Barter, L. M.; Booth, P. J.; Bevan, C. L.; Law, R. V.; Ces, O. **2019**, DOI: 10.1073/pnas.1903500116 (cit. on pp. 13, 14).

(90) Nuti, N.; Verboket, P. E.; Dittrich, P. S. **2017**, *17*, 3112–3119 (cit. on pp. 13, 15, 84, 87).

(91) Elani, Y.; Law, R. V.; Ces, O. **2014**, *5*, 1–5 (cit. on p. 13).

(92) Peters, R. J. R. W.; Marguet, M.; Marais, S.; Fraaije, M. W.; Van Hest, J. C. M.; Lecommandoux, S. **2014**, *53*, DOI: 10.1002/anie.201308141 (cit. on p. 14).

(93) Städler, B.; Chandrawati, R.; Goldie, K.; Caruso, F. **2009**, *25*, DOI: 10.1021/la900213a (cit. on p. 14).

(94) Chandrawati, R.; Caruso, F. **2012**, *28*, 13798–13807 (cit. on p. 14).

(95) Boyer, C.; Zasadzinski, J. A. **2007**, *1*, 176–182 (cit. on p. 14).

(96) Okumura, Y.; Ohmiya, T.; Yamazaki, T. **2011**, DOI: 10.3390/membranes1040265 (cit. on p. 14).

(97) Walker, S. A.; Kennedy, M. T.; Zasadzinski, J. A., 61–64 (cit. on p. 14).

(98) Papahadjopoulos, D.; Vail, W. J.; Jacobson, K.; Poste, G. **1975**, *394*, DOI: 10.1016/0005-2736(75)90299-0 (cit. on p. 14).

(99) Kisak, E. T.; Coldren, B.; Zasadzinski, J. A. **2002**, *18*, DOI: 10.1021/la0156053 (cit. on p. 14).

(100) Bolinger, P.-Y.; Stamou, D.; Vogel, H. **2004**, *126*, 8594–8595 (cit. on p. 14).

(101) Berhanu, S.; Ueda, T.; Kuruma, Y. **2019**, *10*, 1325 (cit. on p. 14).

(102) Ip, T.; Li, Q.; Brooks, N.; Elani, Y. **2021**, DOI: 10.1002/cbic.202100072 (cit. on p. 14).

(103) Li, S.; Wang, X.; Mu, W.; Han, X. **2019**, *91*, 6859–6864 (cit. on pp. 14, 82).

(104) Bolinger, P. Y.; Stamou, D.; Vogel, H. **2008**, *47*, 5544–5549 (cit. on p. 14).

(105) Deng, N.-N.; Yelleswarapu, M.; Zheng, L.; Huck, W. T. S. **2017**, *139*, 587–590 (cit. on pp. 15, 42, 81, 84).

(106) Bagatolli, L. A. In 2012 (cit. on p. 15).

(107) Jabłoństski, A. Efficiency of anti-stokes fluorescence in dyes [6], 1933 (cit. on p. 16).

(108) Conchello, J. A.; Lichtman, J. W. Optical sectioning microscopy, 2005 (cit. on p. 17).

(109) Lira, R. B.; Robinson, T.; Dimova, R.; Riske, K. A. **2019**, *116*, DOI: 10.1016/j.bpj.2018.11.3128 (cit. on p. 27).

(110) Süel, G. **2011**, *497*, DOI: 10.1016/B978-0-12-385075-100013-5 (cit. on p. 28).

(111) Rhee, S. G.; Chang, T. S.; Jeong, W.; Kang, D. Methods for detection and measurement of hydrogen peroxide inside and outside of cells, 2010 (cit. on p. 32).

(112) Liebherr, R. B.; Gorris, H. H. Enzyme molecules in solitary confinement, 2014 (cit. on p. 32).

(113) Zhu, A.; Romero, R.; Petty, H. R. **2010**, *403*, DOI: 10.1016/j.ab.2010.04.008 (cit. on p. 32).

(114) Pautot, S.; Frisken, B. J.; Weitz, D. A. **2003**, *19*, DOI: 10.1021/la026100v (cit. on p. 32).

(115) Tsumoto, K.; Hayashi, Y.; Tabata, J.; Tomita, M. **2018**, *546*, DOI: 10.1016/j.colsurfa.2018.02.060 (cit. on p. 32).

(116) Yandrapalli, N.; Petit, J.; Bäumchen, O.; Robinson, T. **2021**, *4*, 100 (cit. on pp. 33, 43, 47, 50).

(117) Towne, V.; Will, M.; Oswald, B.; Zhao, Q. **2004**, *334*, DOI: 10.1016/j.ab.2004.07.037 (cit. on p. 36).

(118) Hansen, J. S.; Elbing, K.; Thompson, J. R.; Malmstadt, N.; Lindkvist-Petersson, K. **2015**, *51*, DOI: 10.1039/c4cc08838g (cit. on pp. 37, 88).

(119) Elani, Y. **2016**, *44*, 723–730 (cit. on p. 41).

(120) Sato, Y.; Takinoue, M. **2019**, *10*, DOI: 10.3390/MI10040216 (cit. on p. 41).

(121) Weibel, D. B.; Whitesides, G. M. **2006**, *10*, 584–591 (cit. on p. 41).

(122) Trantidou, T.; Friddin, M. S.; Salehi-Reyhani, A.; Ces, O.; Elani, Y. **2018**, *18*, 2488–2509 (cit. on pp. 41, 84).

(123) Mata, A.; Fleischman, A. J.; Roy, S. **2005**, *7*, DOI: 10.1007/s10544-005-6070-2 (cit. on p. 41).

(124) FORTI, S.; MENESTRINA, G. **1989**, *181*, DOI: 10.1111/j.1432-1033.1989.tb14791.x (cit. on p. 44).

(125) Woodle, M. C.; Lasic, D. D. **1992**, *1113*, 171–199 (cit. on p. 45).

(126) Mori, A.; Chonn, A.; Choi, L. S.; Israels, A.; Monck, M. A.; Cullis, P. R. **1998**, *8*, 195–211 (cit. on p. 45).

(127) Yavlovich, A.; Singh, A.; Tarasov, S.; Capala, J.; Blumenthal, R.; Puri, A. **2009**, DOI: 10.1007/s10973-009-0228-8 (cit. on p. 45).

(128) Cama, J.; Bajaj, H.; Pagliara, S.; Maier, T.; Braun, Y.; Winterhalter, M.; Keyser, U. F. **2015**, 1–5 (cit. on pp. 49, 60).

(129) Blin, G.; Margeat, E.; Carvalho, K.; Royer, C. A.; Roy, C.; Picart, C. **2008**, *94*, DOI: 10.1529/biophysj.107.110213 (cit. on p. 51).

(130) Song, L.; Hobaugh, M. R.; Shustak, C.; Cheley, S.; Bayley, H.; Gouaux, J. E. **1996**, *274*, 1859–1866 (cit. on p. 53).

(131) Faure, C.; Nallet, F.; Roux, D.; Milner, S. T.; Gauffre, F.; Olea, D.; Lambert, O. **2006**, *91*, DOI: 10.1529/biophysj.106.088401 (cit. on pp. 58, 85, 88).

(132) Lout, K. L.; Saint, N.; Prilipov, A.; Rummel, G.; Benson, S. A.; Rosenbusch, J. P.; Schirmer, T. *Journal of Biological Chemistry*, *271*, 20669–20675 (cit. on p. 60).

(133) Kara, S.; Afonin, S.; Babii, O.; Tkachenko, A. N.; Komarov, I. V.; Ulrich, A. S. **2017**, *1859*, 1828–1837 (cit. on p. 60).

(134) Kato, A.; Yanagisawa, M.; Sato, Y. T.; Fujiwara, K.; Yoshikawa, K. **2012**, *2*, 1–5 (cit. on pp. 66, 85).

(135) Chen, Q.; Schönherr, H.; Vancso, G. J. **2009**, *5*, 1436–1445 (cit. on p. 66).

(136) Minten, I. J.; Claessen, V. I.; Blank, K.; Rowan, A. E.; Nolte, R. J.; Cornelissen, J. J. **2011**, *2*, 358–362 (cit. on p. 68).

(137) O'Connor, C. M. and Adams, J. U., *Essentials of Cell Biology*, 2010 (cit. on p. 71).

(138) Baneyx, F. Recombinant protein expression in Escherichia coli, 1999 (cit. on p. 72).

(139) Cronan, J. E. In *eLS*, 2014 (cit. on p. 72).

(140) Pandey, A.; Shin, K.; Patterson, R. E.; Liu, X. Q.; Rainey, J. K. Current strategies for protein production and purification enabling membrane protein structural biology1, 2016 (cit. on pp. 72, 89).

(141) Mathieu, K.; Javed, W.; Vallet, S.; Lesterlin, C.; Candusso, M. P.; Ding, F.; Xu, X. N.; Ebel, C.; Jault, J. M.; Orelle, C. **2019**, *9*, DOI: 10.1038/s41598-019-39382-0 (cit. on p. 72).

(142) NIRENBERG, M. W.; MATTHAEI, J. H. **1961**, *47*, DOI: 10.1073/pnas.47.10.1588 (cit. on p. 72).

(143) Lamborg, M. R.; Zamecnik, P. C. **1960**, *42*, DOI: 10.1016/0006-3002(60)90782-4 (cit. on p. 72).

(144) Zubay, G. In vitro synthesis of protein in microbial systems. 1973 (cit. on p. 72).

(145) Strychalski, E. A.; Freemont, P., DOI: 10.1038/s43586-021-00046-x (cit. on p. 72).

(146) Endo, Y.; Sawasaki, T. **2006**, *17*, 373–380 (cit. on p. 72).

(147) Jérôme, V.; Thoring, L.; Salzig, D.; Kubick, S.; Freitag, R. **2017**, *17*, DOI: 10.1002/elsc.201700005 (cit. on p. 72).

(148) Shimizu, Y.; Inoue, a.; Tomari, Y.; Suzuki, T.; Yokogawa, T.; Nishikawa, K.; Ueda, T. **2001**, *19*, 751–5 (cit. on p. 73).

(149) Tuckey, C.; Asahara, H.; Zhou, Y.; Chong, S. **2014**, *2014*, DOI: 10.1002/0471142727.mb1631s108 (cit. on p. 73).

(150) Watanabe, M.; Tomita, T.; Yasuda, T. **1987**, *898*, DOI: 10.1016/0005-2736(87)90065-4 (cit. on p. 77).

(151) Shuma, M. L.; Moghal, M. M. R.; Yamazaki, M. **2020**, *59*, DOI: 10.1021/acs.biochem.0c00102 (cit. on p. 78).

(152) Adamala, K. P.; Martin-Alarcon, D. A.; Guthrie-Honea, K. R.; Boyden, E. S. **2017**, *9*, DOI: 10.1038/nchem.2644 (cit. on pp. 81, 82).

(153) Hilburger, C. E.; Jacobs, M. L.; Lewis, K. R.; Peruzzi, J. A.; Kamat, N. P. **2019**, *8*, DOI: 10.1021/acssynbio.8b00435 (cit. on p. 81).

(154) Dupin, A.; Simmel, F. C. **2019**, *11*, DOI: 10.1038/s41557-018-0174-9 (cit. on p. 82).

(155) Sun, S.; Li, M.; Dong, F.; Wang, S.; Tian, L.; Mann, S. **2016**, DOI: 10.1002/smll.201600243 (cit. on p. 82).

(156) Mason, A. F.; Buddingh, B. C.; Williams, D. S.; Van Hest, J. C. **2017**, *139*, DOI: 10.1021/jacs.7b10846 (cit. on p. 82).

(157) Joesaar, A.; Yang, S.; Bögels, B.; Linden, A. V. D.; Kumar, B. V. V. S. P.; Dalchau, N. **2019**, 1–18 (cit. on p. 82).

(158) Gines, G.; Zadorin, A. S.; Galas, J. C.; Fujii, T.; Estevez-Torres, A.; Rondelez, Y. **2017**, *12*, DOI: 10.1038/nnano.2016.299 (cit. on p. 82).

(159) Sheridan, A. M.; Fitzpatrick, S.; Wang, C.; Wheeler, D. C.; Lieberthal, W. *Kidney International*, *49*, DOI: 10.1038/ki.1996.12 (cit. on p. 82).

(160) Ellis, R. J. Macromolecular crowding: Obvious but underappreciated, 2001 (cit. on p. 83).

(161) Garbuzenko, O.; Barenholz, Y.; Priev, A. **2005**, *135*, DOI: 10.1016/j.chemphyslip.2005.02.003 (cit. on p. 84).

(162) Wang, Y. P.; Lei, Q. Y. **2018**, *3*, 1–9 (cit. on p. 85).

(163) Matosevic, S. **2012**, *34*, DOI: 10.1002/bies.201200105 (cit. on p. 87).

(164) Yandrapalli, N.; Seemann, T.; Robinson, T. **2020**, *11*, DOI: 10.3390/mi11030285 (cit. on p. 87).

(165) Beneyton, T.; Love, C.; Girault, M.; Tang, T.-Y. D.; Baret, J.-C. **2020**, *2*, DOI: 10.1002/syst.202000022 (cit. on p. 87).

(166) Hold, C.; Billerbeck, S.; Panke, S. **2016**, *7*, DOI: 10.1038/ncomms12971 (cit. on p. 88).

(167) Semenov, S. N.; Wong, A. S.; Van Der Made, R. M.; Postma, S. G.; Groen, J.; Van Roekel, H. W.; De Greef, T. F.; Huck, W. T. **2015**, *7*, DOI: 10.1038/nchem.2142 (cit. on p. 88).

(168) Idan, O.; Hess, H. Engineering enzymatic cascades on nanoscale scaffolds, 2013 (cit. on p. 88).

(169) Tsitkov, S.; Hess, H. **2019**, *9*, 2432–2439 (cit. on p. 88).

(170) Sunami, T.; Ichihashi, N.; Nishikawa, T.; Kazuta, Y.; Yomo, T. **2016**, 1282–1289 (cit. on p. 88).

(171) Lluis, M. W.; Godfroy, J. I.; Yin, H. Protein engineering methods applied to membrane protein targets, 2013 (cit. on p. 89).

(172) Katzen, F.; Peterson, T. C.; Kudlicki, W. Membrane protein expression: no cells required, 2009 (cit. on p. 89).

(173) Kögler, L. M.; Stichel, J.; Beck-Sickinger, A. G. Structural investigations of cell-free expressed G protein-coupled receptors, 2019 (cit. on p. 89).